Alma Mater Studiorum ·
Università di Bologna

SECOND FACULTY OF ENGINEERING
Master Degree in Aerospace Engineering

A Numerical Study of Temperature Effects on Hot Wires Measurements in Turbulent Channel Flows

Master thesis in Applied Aerodynamic

Supervisor:
Prof. A. Talamelli

Assistant supervisors:
Dr. A. Cimarelli
Dr. P. Schlatter

Student:
Fabio Malizia

Session:III
2011/2012

A coloro con
cui ho scritto le
pagine della mia vita

A coloro che mi
daranno una mano
a dipingere le prossime

Abstract (English)

Turbulence is a physical phenomena that can be experienced everywhere and for more than one century it has been object of study. Despite this, many issues are still unresolved and many efforts are made by the scientific community in order to understand its dynamic.

A way to investigate turbulence is through experiments where hot wire measurements are performed. Analysis of the influence of a temperature gradient on hot wire measurements is the aim of this thesis work. Actually - to author's knowledge - this investigation is the first attempt to document, understand and ultimately correct the effect of temperature gradients on turbulence statistics.

However a numerical approach is used since instantaneous temperature and streamwise velocity fields are required to evaluate this effect. A channel flow simulation at $Re_\tau = 180$ is analyzed to make a first evaluation of the amount of error introduced by temperature gradient inside the domain. Hot wire data field is obtained processing the numerical flow field through the application of a proper version of the King's law, which connect voltage, velocity and temperature. A drift in mean streamwise velocity profile and rms is observed when temperature correction is performed by means of centerline temperature. A correct mean velocity profile is achieved correcting temperature through its mean value at each wall normal position, but a not negligible error is still present into rms. The key point to correct properly the sensed velocity from the hot wire is the knowledge of the instantaneous temperature field. For this purpose three correction methods are proposed.

At the end a numerical simulation at Re_τ =590 is also evaluated in order to confirm the results discussed earlier.

Abstract (Italiano)

La turbolenza è un fenomeno fisico comune che può essere facilmente osservato in natura e per più di un secolo è stato oggetto di studi. Nonostante ciò, molte delle sue caratteristiche non sono ancora completamente conosciute e molti sforzi sono compiuti dalla comunità scientifica al fine di comprendere la sua dinamica.
Uno dei modi con cui viene studiata la turbolenza è attraverso esperimenti in laboratorio, dove vengono effettuate misure con sonde a filo caldo. Lo scopo di questa tesi è quello di investigare gli effetti dei gradienti di temperatura sulle misurazioni con sonde a filo caldo. Effettivamente - a conoscenza dell'autore - questo studio è il primo tentativo di documentare, comprendere e infine correggere l'effetto del gradiente di temperatura sulle misure statistiche dei fluidi in regime turbolento.
Vista la necessità di conoscere instantaneamente i campi di temperatura e la velocità, un approccio numerico è stato necessario per analizzare questo effetto. Una simulazione del flusso in un canale, a $Re_\tau = 180$ è stata analizzata allo scopo di effettuare una prima valutazione della percentuale di errore introdotto dalla presenza del gradiente di temperatura all'interno del dominio. La velocità misurata dalla sonda a filo caldo è stata riprodotta attraverso l'elaborazione dei dati numerici effettuata per mezzo della legge di King, la quale mette in relazione il potenziale elettrico del filo caldo e la velocità e temperatura del flusso che investe la sonda. Uno scostamento nel profilo medio della velocità longitudinale e nella deviazione standard può essere osservato quando la correzione della temperatura è effettuata tramite la temperatura al centro del canale. Utilizzando la temperatura media per correggere l'equazione di King, si ottiene un profilo medio di velocità longitudinale corretto, ma un errore non trascurabile è presente nella deviazione standard. Il punto chiave per correggere in modo efficace la velocità misurata dalla sonda a

filo caldo, è quello di conoscere instantaneamente il campo di temperatura sulla sonda. A questo proposito tre metodi correttivi sono proposti. Infine, al fine di confermare le osservazioni fatte e i risultati raggiunti, un'ulteriore simulazione di un canale a $Re_\tau = 590$ è stata effettuata.

Contents

Tesi - Versione Italiana

La turbolenza è un comune fenomeno fisico che può essere facilmente osservato e vissuto in maniera diretta. I fluidi come acqua ed aria, infatti, sono ovunque in natura e interagiscono continuamente con i corpi che vi si trovano immersi. Con il movimento di questi fluidi, si creano dei flussi che possono trovarsi in vari regimi: fra questi quello turbolento è molto comune, ed individuabile dalla contemporanea presenza di specifici comportamenti che caratterizzano questo tipo di flusso. Inoltre si possono distinguere flussi a turbolenza libera, quando non sono presenti pareti o corpi con il quale il flusso può interagire, e flussi di parete, dove l'interazione fra parete e flusso genera dinamiche, nei pressi della parete, differenti rispetto a quelle tipiche dei flussi a turbolenza libera.
La turbolenza di parete è stata largamente investigata, vista la sua importanza in applicazioni ingegneristiche. Flussi in condotti, resistenza generata su oggetti in movimento come palle, automobili, aeroplani, etc. sono solo alcuni esempi di interazione flusso - parete, dove spesso il flusso si trova in regime turbolento.
Dal punto di vista matematico, le equazioni che descrivono la dinamica dei fluidi sono conosciute da circa due secoli: le equazioni di Navier Stokes sono state formulate per la prima volta nel 1821. Nonostante ciò la loro soluzione è limitata esclusivamente a casi semplificati [1].
Questa complessità ha spinto all'utilizzo di altri metodi di analisi dei flussi turbolenti, come test sperimentali in gallerie del vento e analisi numeriche. Entrambi i metodi presentano vantaggi e svantaggi che si necessita di conoscere se si vuole comprendere quale metodo usare per lo specifico problema in esame.
L'analisi numerica si è sviluppata largamente solo negli ultimi decenni, grazie allo sviluppo esponenziale delle potenze di calcolo, rendendo accessibili analisi sempre più complesse. Esistono differenti tipi di analisi che possono essere effettuate, come analisi numeriche dirette (DNS), simulazioni a grandi vortici (LES) e simulazioni delle equazioni di Navier Stokes mediate alla Reynolds. Il

[1] Clay Mathematics Institution ha inserito le equazioni di Navier - Stokes come uno dei sette problemi del millennio ("Millennium Prize Problems"), mancando ancora una teoria matematica che consenta di comprenderle appieno ed analizzarle. Il premio è di un milione di dollari.

primo metodo (DNS) si basa sulla soluzione completa delle equazioni di Navier Stokes. Questo approccio è computazionalmente molto dispendioso dato che tutte le scale del moto vengono risolte. Ciò significa che tutte le variabili del moto vengono fornite in uscita, il che permette di effettuare molte analisi statistiche che altrimenti non potrebbero essere svolte. Simulazioni a grandi numeri di Reynolds non sono tuttavia ancora realizzabili. Se invece la dinamica di piccola scala non viene risolta direttamente ma attraverso l'utilizzo di un modello, si ottiene un metodo denominato LES - simulazioni a grand vortici. Questo metodo rimane, seppur in modo inferiore rispetto ad una DNS, molto costoso computazionalmente, il che non permette analisi su casi ad alti numeri di Reynolds. I risultati ottenuti rimangono di buona qualità sebbene la validità del modello utilizzato deve essere verificata. Metodi RANS vengono per lo più utilizzati a livello industriale, vista la necessità di analizzare flussi ad elevati numeri di Reynolds. Questo approccio fornisce solamente il campo medio delle varie variabili. Tuttavia, questo sistema di equazioni non è risolvibile in maniera diretta data la presenza di più incognite che equazioni. Infatti, mediando alla Reynolds le equazioni di Navier Stokes, si ottiene un nuovo sistema di equazioni al cui interno compare una nuova variabile, che prende il nome di tensore degli sforzi di Reynolds. Un modello deve essere quindi introdotto al fine di rendere risolvibile il sistema. Ciò fa si che sebbene le equazioni RANS permettano l'analisi di flussi ad elevati numeri di Reynolds, la qualità della soluzione dipende fortemente dal tipo di modello utilizzato per lo specifico problema fluidodinamico.
Tutto questo fa si che l'unico metodo per analizzare flussi ad elevati numeri di Reynolds sia un approccio sperimentale. Questo metodo è utilizzato da più di un secolo, e notevoli progressi nelle gallerie del vento e nei sistemi di misura sono stati raggiunti. Nonostante ciò rimane ancora una sfida ottenere contemporaneamente alti numeri di Reynolds, alta risoluzione spaziale e convergenza delle statistiche. Questa è la ragione della necessità della costruzione di nuove strutture e sistemi di misura che rispondano a tali obiettivi. A questo scopo l'università di Bologna è impegnata in prima linea con la creazione del "*Center for International Cooperation in Long Pipe Experiments, CICLoPE"* [Talamelli et al., 2009].
Durante i test sperimentali, diversi tipi di misura possono essere effettuati, fra cui il più utilizzato per conoscere il campo di velocità è la misura a filo caldo. La ragione è l'elevata risoluzione frequenziale di questo strumento e la sua accuratezza. Tuttavia diversi errori caratterizzano le misure di questo strumento: il più influente risulta l'effetto di filtraggio dovuto all'eccessiva lunghezza del filo rispetto alle piccole scale del moto. Infatti la temperatura avvertita dallo strumento è solo una media di quella lungo il filo, vista la presenza di zone del filo a diverse temperatura dovuta alle diverse fluttuazioni che si generano lungo

di esso.
Inoltre un nuovo problema è stato supposto in recenti esperimenti su condotti [Sattarzadeh et al., 2013], cioè l'effetto della presenza di gradienti di temperatura all'interno del flusso, i quali possono modificare la temperatura vista dal filo caldo dovuta alla sola convezione forzata. Infatti una non uniforme temperatura all'interno del condotto genera fluttuazioni di temperatura - le quali sono altamente correlate con quelle di velocità - che influenzano così la temperatura del filo [2].
In questa tesi magistrale l'effetto del gradiente di temperatura sulla sonda a filo caldo è investigata. L'approccio usato è numerico, dato che l'analisi richiede la conoscenza istantanea di diverse variabili.

Risultati I principali risultati sono stati ottenuti analizzando la simulazione numerica di un canale a $Re_\tau = 180$ e $Pr = 0.71$, realizzata tramite un codice spettrale. La prima analisi è stata effettuata sulle statistiche classiche della turbolenza, cioè profili di velocità media e deviazione standard, le quali hanno mostrato la bontà della simulazione numerica realizzata. Successivamente la presenza di una correlazione fra velocità longitudinale e temperatura è stata verificata. Tale correlazione è maggiore vicino alla parete e minore avvicinandosi al centro del canale. Il risultato raggiunto è di notevole importanza, poiché permette di comprendere la fisica dietro all'influenza della temperatura sulla sonda a filo caldo: fluttuazioni positive della velocità longitudinale generano fluttuazioni positive delle fluttuazioni di temperatura, le quali generano un innalzamento della temperatura della sonda. Questa maggiore temperatura non permette allo strumento di percepire tutta la quantità di calore dispersa dal flusso d'aria, così che una minore velocità viene misurata. Viceversa una fluttuazione negativa fa si che la temperatura del filo venga diminuita, generando una misura di velocità maggiore: in definitiva la velocità misurata istante per istante viene smorzata da quella reale, come si può verificare dalla figura 5.2.
La successiva analisi è stata realizzata cercando di riprodurre a posteriori il voltaggio generato da una sonda a filo caldo immersa virtualmente all'interno del flusso: tale procedimento è stato realizzato attraverso l'utilizzo della legge di King, che relaziona il voltaggio della sonda con la temperatura e velocità istantanea. Due versioni della legge di King sono state analizzate, le quali generano gli stessi risultati se opportunamente relazionate. Una volta ottenuto il campo di tensione, la velocità misurata è stata riprodotta attraverso un ulteriore utilizzo della legge di King, dove però il campo istantaneo di temperatura,

[2] La temperatura del filo è influenzata, da una parte, dal calore prodotto dal circuito elettrico, mentre dall'altra dal calore disperso dalla convezione naturale e forzata, dalla radiazione e dalla conduzione sui supporti. Tuttavia l'effetto principale è quello della convezione forzata dovuta al flusso che investe la sonda

che non è noto, è stato sostituito da due diverse temperature di correzione: la temperatura media al centro del condotto e il profilo di temperatura medio [3].
Il primo caso genera diversi tipi di errore. Il profilo di velocità presenta un discostamento dal valore reale soprattutto vicino alla parete, dove è presente una maggiore differenza fra la temperatura media di correzione, cioè quella alla mezzeria, e la temperatura media locale. Inoltre anche la deviazione standard presenta errori non trascurabili. Utilizzando invece il profilo medio di temperatura come temperatura di correzione, un corretto profilo di velocità viene misurato. Ciononostante, la deviazione standard della fluttuazione di velocità longitudinale risulta sottostimata: questo comportamento risulta accentuato innalzando la differenza di temperatura fra parete e mezzeria, o equivalentemente, innalzando il gradiente di temperatura a parete.
Successivamente, l'effetto dei parametri sperimentali all'interno dell'equazione di King sono stati analizzati. Innalzando il rapporto di surriscaldamento del filo, il valore della deviazione standard viene innalzato, mentre aumentando il valore del coefficiente di temperatura della resistività, la deviazione standard subisce una decrescita. In entrambi i casi, la variazione di questi due parametri non mostra influenze sensibili nel profilo medio di velocità.
A questo punto l'effetto della temperatura sulle misure effettuate con la sonda a filo caldo, è stato paragonato agli effetti dovuti al filtraggio spaziale dovuto alla lunghezza del filo. Innanzitutto il singolo effetto del filtraggio spaziale è considerato. Esso non influenza il profilo medio di velocità, mentre genera una minore deviazione standard. Combinando gli effetti di questi due errori, si può osservare come la percentuale di errore dovuta all'influenza di temperatura rispetto all'errore totale, sia maggiore per sonde piccole e in presenza di una maggiore differenza di temperatura fra parete e mezzeria all'interno del canale. Seguendo le linee guida presenti in Ligrani and Bradshaw [1987], per diminuire l'errore dovuto al filtraggio spaziale un filo dovrebbe possedere una lunghezza inferiore a venti lunghezze viscose: con questi valori di lunghezza del filo l'errore dovuto alla temperatura non è trascurabile, soprattutto se alte differenze di temperatura fra parete e mezzeria sono presenti.
La quantificazione di questo errore ha permesso di ipotizzare alcuni metodi correttivi per la misura della velocità e la formulazione di metodi indiretti per la misura della temperatura istantanea. Il primo metodo analizzato è l'utilizzo di due sonde, le quali forniscono gli ingressi necessari per risolvere il sistema composto da due equazioni di King. I risultati generati sono ottimi se virtualmente le due sonde fossero piazzate nello stesso punto, mentre divergono con l'allontanamento delle due sonde fra loro. Questo fa si che questo metodo non

[3] La temperatura è una variabile di cui non si riesce ad avere accesso istantaneamente attraverso strumenti di misura durante prove sperimentali.

sia praticamente utilizzabile.
Un altro metodo è quello di ipotizzare - vista l'alta correlazione fra fluttuazioni di velocità longitudinale e temperatura - che le fluttuazioni di temperatura possano essere sostituite da quelle di velocità, opportunamente scalate. Innanzitutto un profilo di velocità viene ottenuto correggendo l'equazione di King con il solo profilo medio di temperatura: ciò permette di trovare un valore approssimato della velocità dal quale ricavare le fluttuazioni di velocità. Quest'ultime vengono utilizzate per una nuova misura della velocità misurata dalla sonda, dove la correzione della temperatura nell'equazione di King, viene effettuata tramite la somma fra il profilo medio di temperatura e la fluttuazione della velocità, ottenuta precedentemente, opportunamente scalata. I risultati ottenuti da questo metodo sono incoraggianti, soprattutto se un coefficiente aggiuntivo viene introdotto per diminuire il valore delle fluttuazioni di velocità, all'interno della variabile di correzione, lontano dalla parete. Ciò è dovuto alla minore correlazione fra velocità e temperatura in prossimità della mezzeria.
Infine un metodo per la misura approssimata di un profilo medio di temperatura è proposto: invece di misurare la temperatura media in molti punti lungo la direzione normale alla parete, la misura può essere effettuata solo in pochi punti, ricostruendo il profilo medio tramite l'interpolazione di questi punti con l'utilizzo di una legge lineare vicino alla parete e della legge logaritmica lontano dalla parete. Il problema di questo metodo può risultare nella corretta misura della temperatura viscosa a parete.
L'ultimo capitolo della tesi vuole invece verificare i risultati raggiunti su un'ulteriore simulazione numerica dove il numero di Reynolds è stato incrementato a $Re_\tau = 590$. Risultati simili al caso precedente sono stati ottenuti, verificando inoltre la bontà del metodo correttivo utilizzato. Tuttavia un'ulteriore miglioramento di questo metodo è stato proposto, ma non verificato, riguardante la modifica del coefficiente utilizzato per smorzare le fluttuazioni di velocità all'interno del fattore correttivo. L'idea è di utilizzare non più un valore lineare da parete a mezzeria, ma un coefficiente che agisca con maggiore forza vicino alla parete per poi smorzarsi allontanandosi da essa.

Struttura Questa tesi è composta da sette capitoli, redatti in lingua inglese. I primi tre si concentrano su alcuni concetti teorici, che spaziano dalla turbolenza (capitolo primo), alle equazioni della fluidodinamica e termodinamica (capitolo secondo) fino alla descrizione della sonda a filo caldo (capitolo terzo). Successivamente la simulazione numerica a $Re_\tau = 180$ e $Pr = 0.71$ viene descritta del capitolo quarto e i risultati ottenuti nel capitolo cinque. Il capitolo sesto si concentra sui metodi correttivi mentre il settimo ed ultimo capitolo descrive la simulazione numerica a $Re_\tau = 590$ e $Pr = 0.71$, insieme ai risultati ottenuti

su questa simulazione prima e dopo aver applicato uno dei metodi correttivi proposti.

Chapter 1

Introduction

Even though turbulent flows can be frequently observed in everyday life, turbulence is still a physical phenomenon, which is not completely known. Turbulent flow can be free (jets, wakes) or may interact with surfaces (ducts or boundary layers). In this case we will talk about wall bounded turbulence. Wall turbulent flows have been deeply investigated, due to their importance in engineering applications, e.g. flow in ducts, on aerodynamic surfaces, which in most of the industrial applications are in turbulent regime.
The fundamental equations of fluid dynamics are known since almost two centuries. When they are written for Newtonian fluids they are called Navier Stokes equations. Even though they are well known, an analytical solution for these equations is achievable only for simplified cases [1].
The complexity of these equations forces us to use other approaches to give insight into this problem. Investigations are performed through experimental wind tunnel tests or numerical simulations. Both methods have their advantages and disadvantages that need to be known in order to chose the best approach for each specific flow problem.
Numerical simulations have become an affordable method only in the last decades, with the increasing of computer performances. Different type of simulations can be performed using numerical methods. The most used nowadays are the Direct Numerical Simulations (DNS), the Large Eddy Simulations (LES) and the Reynolds Averaged Navier - Stokes equations (RANS). The first one is based on the numerical solution of the complete Navier - Stokes equations. This approach is computational expensive since all details of flow movements are solved. A complete data flow field is provided by this method, for each time field and

[1] Clay Mathematics Institution inserts Navier - Stokes existence and smoothness problem in the list of the seven "Millennium Prize Problems". The prize to the scientist who will solve this problem is of one million dollars.

for every point of the domain. Its weakness is that only low Reynolds number cases can be actually solved.
Turbulent flow is characterized by the simultaneous presence of scales of different size. If the small scale behavior is modeled, Navier - Stokes equations can be filtered in order to reduce its computational cost (LES). However, this method remains computationally expensive and high Reynolds number are still not affordable. Moreover, the accuracy of the model introduced must be proven.
Due to the Reynolds number limit of previous methods, industrial applications are typically solved by means of RANS method, where the Navier - Stokes equations are averaged in time. In this way only mean values are fully simulated (even though unsteady flows can be solved by introducing the variable time in the model). However, this set of equation, due to the presence of more unknowns than equations, is not directly solvable. The term that arises after the averaging operation, is called Reynolds stress tensor, which needs to be modeled. High Reynolds number simulations become computationally affordable through this method, but the quality of the solution is highly dependent on the model used.
In many applications, these limits make experimental tests the only way to investigate high Reynolds number problems. Despite the enormous progresses made by the facilities and measurements instruments from the beginning of turbulence investigation - around one century ago - nowadays is still challenging to obtain at the same time high Reynolds number, high spatial resolution and well converged statistics. For this reason, new facilities are currently designed and realized in order to achieve these goals. With this purpose at the University of Bologna is, for instance, created the Center for International Cooperation in Long Pipe Experiments, CICLoPE [Talamelli et al., 2009].
In these turbulence experiments, velocity is mainly measured through hot wire anemometry. The reason lie on the high frequency resolution and its accuracy. However, some weaknesses characterizes hot wires, like the spatial averaging effect along the wire of the probe, which basically has the effect to filter small turbulent scales.
A new problem arose in recent experiments [Sattarzadeh et al., 2013], i.e. the temperature gradient influence on hot wire measurements. Indeed, if a non uniform temperature is present inside the pipe, the wire temperature is subjected to an influence made by temperature fluctuations - which are highly correlated with velocity ones - besides the main influence made by the forced convection [2].
In this thesis, the temperature gradient influence on hot wire measurements is investigated. To assess this phenomenon a numerical approach is used, since

[2] Wire temperature is also influenced by natural convection, conduction to the prongs and radiation. However the strongest influence is the forced convection made by the air moving against the probe.

it can easily provide at each time in the entire domain all the flow parameters needed. The presence of a correlation between velocity and temperature is verified. This means that positive fluctuation of temperature are associated with positive fluctuations of velocity, thus wire senses a smaller temperature difference compared to the one achievable considering the only forced convection. After that, the velocity sensed by the hot wire is estimated through King's law equation - a law that relates flow velocity and wire voltage - and compared with the numerical original results. Finally, the quantification of the error introduced by temperature gradient allows the formulation of some correction methods.

This thesis is composed by first three chapters focusing on theoretical issues, as turbulence (1^{st} chapter), fluid dynamic equations and thermodynamics (2^{nd} chapter) and hot wire (3^{rd} chapter). Numerical simulation of a channel flow at $Re_\tau = 180$ and $Pr = 0.71$ is described in 4^{th} chapter and its results are discussed in 5^{th} chapter. Correction methods of temperature influence are discussed in 6^{th}) chapter; meanwhile a turbulent channel flow at $Re_\tau = 590$ and $Pr = 0.71$ is analyzed in the 7^{th}) chapter, where a similar analysis to the one in 5^{th} chapter is performed together with correction of the results achieved.

Chapter 2

Turbulence

2.1 Introduction to turbulence

The name turbulence derives from the old Greek "$\tau\upsilon\rho\beta\eta$" which means disorder, chaos. Those are two of the main characteristics of this phenomena.
However a proper definition of turbulence is not given yet, due to its complex behavior. In fact as Richard Feynman says: "*there is a physical problem that is common to many fields, that is very old, and that has not been solved. [...] Nobody in physics has really been able to analyze it mathematically satisfactorily in spite of its importance to the sister sciences. It is the analysis of circulating or turbulent fluids*" [Feynman et al., 1966, pag.3-9]. Thus only a description of the main features of turbulence can be provided.
Turbulence can be described as a flow regime, characterized by irregularity, diffusivity, large Reynolds numbers, three dimensional velocity fluctuations and dissipation [Tennekes and Lumley, 1972, pagg.1-3]. Moreover is a continuum phenomena that occurs at many flow scales, which are always larger enough than molecular scales.
In spite of its complexity, turbulence is a very common phenomena. Even in a house's kitchen the presence of turbulence can be experienced: from the plumes of the stove to the tap water, from the boiling water to the diffusion of food's smell.

2.1.1 Turbulence features

In this paragraph the turbulence features listed in the paragraph 2.1 are discussed.
First of all turbulence characterizes flows and not fluids. It means that different

fluids have a similar turbulence dynamic, since this phenomena is not depending on molecular properties of the particular fluid [Tennekes and Lumley, 1972, pag.3]

Irregularity is one of the fundamental characteristics of a turbulent flow. This is well empathized by Hinze through his definition of turbulence: "*turbulent fluid motion is an irregular condition of flow in which the various quantities show a random variation with time and space coordinates, so that statistically distinct average values can be discerned*" [Hinze, 1975]. This definition points out the chaotic motion of the flow, where each particle seems behave differently instant by instant. However, this chaotic behavior is only apparent, since flows are described by Navier-Stokes equations, which are deterministic.

The apparent discrepancy by deterministic equations and irregular motion, is explained by Lorentz in 1963. He discovered a high dependence from initial conditions of certain non linear equations [Lorenz, 1973]. The deterministic side of turbulence is recovered inside statistical analysis. In fact statistical quantities, such as mean values, root mean squares, etc, can be compared among different experiments, meanwhile different behaviors characterize the signal instantaneously in different experiments.

However irregularity itself is not a sufficient condition to determine if a flow is turbulent or not. In fact, considering the contrails of jet aircrafts, they show high irregular motion, but, except for the closest region to the airplane, these contrails are not turbulent. In fact their diameter is almost constant, starting from a distance to the airplane of some chords and ending several kilometers after the aircraft. The missing ingredient for this flow, in order to be considered turbulent, is the diffusivity [Tennekes and Lumley, 1972, pag.2]. In fact turbulent flows are always characterized by high mix of momentum, mass and heat.

This example shows that flows can experience not only turbulent condition, but they behave in different ways. The first intensive study of different flow regimes is made by Reynolds during 1883. Observing the motion of an ink jet inside a pipe flow, he notices different behaviors for different velocity of the flow. When the flow velocity is small he notices that the ink follows a straight line. Increasing the velocity the ink starts to oscillate and mixing with the surrounding water, coloring it. Using Reynolds own words: "*As the velocity was increased by small stages, at some point in the tube, always at a considerable distance from the trumpet or intake, the colour band would all at once mix up with the surrounding water, and fill the rest of the tube with a mass of coloured water. Any increase in the velocity caused the point of break down to approach the trumpet, but with no velocities that were tried did it reach this. On viewing the tube by the light of an electric spark, the mass of colour resolved itself into a mass of more or less distinct curls, showing eddies*" [Reynolds, 1883, pag.942]. Thus

Reynolds observes how the flow evolves from laminar condition (straight ink line) to turbulent one (all water colored), passing through instability (breaking point of laminar condition and first oscillations).
Moreover he understands that velocity and distance has a similar role on breaking the laminar condition. In fact he realizes the importance of the not dimensional number $\frac{\rho LU}{\mu}$ on the break down of the laminar condition. Thus a turbulent flow is characterized by a high value of this number, that is called Reynolds number [1]. Sommerfeld [1908] is the first scientific paper where this quantity is referred as Reynolds number.
Reynolds figures out also the presence of eddies into a turbulent flow. These structures are three dimensional. This is very important in order to self maintain the vorticity in the flow, through the vortex stretching mechanism [Tennekes and Lumley, 1972].
Another characteristic of turbulent flows is dissipation. This means that energy has to be continuously supplied to a flow to keep it turbulent, otherwise kinetic energy is dissipated into heat. The latter process is performed at small scales due to the viscosity.

Another characteristic is the simultaneous presence of a wide number of scales. As Richardson states: *"Big whirls have little whirls that feed on their velocity, and little whirls have lesser whirls and so on to viscosity"* [Richardson, 1922, pag.66].

2.2 The statistical approach to turbulence

As introduced in paragraph 2.1.1, turbulence is a chaotic phenomena, since equations that describe fluid flows are highly dependent on initial conditions. Thus a statistical approach is the only one available to recover the deterministic side of turbulence and make possible flow analysis.
The starting point is to consider different parameters, e.g. velocity, pressure, as composed by an average and a fluctuating part:

$$u = \overline{u} + u' = U + u'$$

[1] The Reynolds number has also several interpretations and its role in fluid dynamic is fundamental. A way to look on it, is to think to the ratio between inertial (mass times acceleration) and viscous forces $\frac{(\rho L^3)(u_0/t)}{\mu L^2/t} = \frac{\rho L u_0}{\mu}$. Moreover the Reynolds number is the only parameter appearing in the not dimensional Navier-Stokes equations. Thus the Reynolds number is the only independent variable in these equations. This reduces the number of experiments needed to analyze different flow cases. From the Kolmogorov theory is also the only factor who rules the scale separation in the flow, between integral scales and Kolmogorov scales, see also paragraph 2.3.

where u is the instantaneous signal, meanwhile U and u' are the mean and the fluctuation. This decomposition is well known as Reynolds decomposition.
An important property is that the average of the fluctuating part is equal to zero

$$\frac{1}{T}\int_t udt = U \rightarrow \int_t u'dt = 0 \tag{2.1}$$

since the fluctuation indicates the signal deviation from its mean value.
An useful function built from the signal quantity is the probability density function $B(u)$. This function represents the probability to find the signal u inside a certain range of values Δu around u, hence it gives informations about the relative time spent by the instantaneous signal on that range:

$$B(u)\Delta u = \lim_{t\to\infty} \frac{1}{t}\sum \Delta t$$

where $\sum \Delta t$ is the sum of each time interval the signal u spends inside the range $[u, u + \Delta u]$.
According to the probability theory, the integral of the probability density function, between $[-\infty, +\infty]$, is equals to 1. Thus inside the range of the probability density function, the event is certainly happening:

$$B(u) \geq 0;\ \int_{-\infty}^{\infty} B(u)du = 1$$

Starting from these quantities, several statistics values can be constructed.

2.2.1 Statistical moments

Moment is the name used to indicate the mean value of the powers of the signal u. A general definition of a moment of $k-$order is

$$\overline{u^k} = \int_{-\infty}^{\infty} u^k B(u)du \tag{2.2}$$

Another moment often used is the central moment, that is the mean value of the powers of the fluctuation.

$$\overline{u'^k} = \int_{-\infty}^{\infty} u'^k B(u')du' \tag{2.3}$$

From these definitions is possible to see how the mean value, equation 2.1 can be represented through equation 2.2, thus the moment of first order is equal to

$$U = \int_{-\infty}^{\infty} uB(u)du$$

and it represents also the "center of gravity" of the probability density function. The property of the zero value of the fluctuation average is expressed also using the central moment of first order. Other moments often used are the variance, the skewness and the flatness, all of them are central moments. The variance is the central moment of second order

$$\sigma^2 = \overline{u'^2} = \int_{-\infty}^{\infty} u'^2 B(u) du = \int_{-\infty}^{\infty} u'^2 B(u') du'$$

The square root of the variance, σ, is called as standard deviation, or root mean square (rms). This quantity represents the average distance of the signal from its mean value and its an useful to represent the width of the probability density function of the fluctuating signal $B(u')$.
A similar quantity to the variance, is the co-variance, which is a central second moment where two different signals are averaged:

$$\sigma_1 \sigma_2 = \overline{u'v'} = \iint_{-\infty}^{\infty} u'v' B(u'v') du' dv' \tag{2.4}$$

The skewness is the nondimensional central moment of third order

$$S = \frac{\overline{u'^3}}{\sigma^3} = \frac{\int_{-\infty}^{\infty} u'^3 B(u') du'}{\sigma^3}$$

It gives information about the asymmetry of $B(u')$ about the mean value. If the signal is symmetric with respect to the mean, the skewness is zero.
The flatness, or kurtosis, is the nondimensional central moment of fourth order:

$$F = \frac{\overline{u'^4}}{\sigma^4} = \frac{\int_{-\infty}^{\infty} u'^4 B(u') du'}{\sigma^4}$$

It also gives information about the shape of the probability density function $B(u')$. In particular a large flatness means, as it is possible to understand from the meaning of the word flatness, that peak values, both positive or negative, have a larger probability than the case where the flatness value is small, that means that the probability density function is more flat.

2.2.2 Two point statistic: correlations

One of the main statistic quantity which describe the turbulence is the correlation function. It is used for the first time to describe turbulent flows by Taylor [1935].
Informations about the relation between two different signals are provided by correlation and autocorrelation function.
The covariance, expressed in equation 2.4, is an example of correlation, since it

is not a pure moment but a joint moment, that is a moment that combines the information of two different signals.
In particular the correlation provides information about how two different signals, e.g. shifted in time, space or having different orientation, are related each other.
If the correlation is equals to 0, it means that the two variables are not correlated. However this not mean they are independent each other. In fact considering two sine waves shifted in phase of $\pi/2$, they are not correlated

$$\frac{1}{2\pi}\int_0^{2\pi} sin(x)sin(x+\pi/2)dx = \frac{1}{2\pi}\int_0^{2\pi} sin(x)cos(x)dx = -\frac{1}{4\pi}[cos(2x)]_0^{2\pi} = 0$$

but it can be noticed they are represented by the same curve but shifted along x-axis, thus they are not independent.
Statistical independence is obtained only if the the probability density of one variable is not influenced by the probability density function of the other one

$$\text{if } B(u',v') = B(u')B(v') \rightarrow u'v' \text{ are statistical independent}$$

In general a correlation function is a 9 degree tensor:

$$R(\boldsymbol{x},\boldsymbol{r}) = \overline{u'(\boldsymbol{x})u'(\boldsymbol{x}+\boldsymbol{r})}$$

where $\mathbf{x}$ is the spatial position and $\mathbf{r}$ is the separation vector between the two signals. When $\mathbf{r}$ is equals to 0, the correlation is equal to the variance.
The most common correlation are the longitudinal one, i.e. the separation vector is orientated along the direction of the vectors under analysis, and the transverse one, i.e. the separation vector is orientated perpendicular to the vectors.
Non dimensionalizing this quantity through the variance, the correlation coefficient is obtained:

$$\zeta(\boldsymbol{x},\boldsymbol{r}) = \frac{R(\boldsymbol{x},\boldsymbol{r})}{\overline{u'^2}}$$

If this coefficient is equals to 1, the two signals are perfectly correlated, meanwhile when it is equal to -1 they are anti-correlated. No-correlation is obtained when the coefficient is equal to 0. When the separation vector is 0, the coefficient is equal to 1.
When two different signals are analyzed with this method, e.g. longitudinal and normal to wall velocity components, cross correlation are obtained. Similar relation as above can be written for this quantity.
The last kind of correlation analyzed is the auto-correlation. This function is a correlation between the same signal in different time instants, i.e. the same

signal shifted in time:

$$C = \overline{u'(t)u'(t')} = \frac{1}{T}\int_0^T u'(t)u'(t')dt = \frac{1}{T}\int_0^T u'(t)u'(t+\tau)dt$$

Since the signals considered in turbulence are statistically stationary [2], the auto-correlation is not function of the two different time instants, but only of their difference $\tau = t - t'$.
An auto-correlation coefficient is obtained dividing the auto-correlation function with the variance of the signal

$$\frac{\overline{u'(t)u'(t')}}{\overline{u'^2}} = \rho(\tau) = \rho(-\tau)$$

2.2.3 Spectral analysis

Fourier [1808], introduces the idea to split up a signal in a series of harmonics, each one with a different weight, in order to reproduce the signal itself. Thus signal domain is moved from temporal to frequency.
Considering a periodic signal $u(t)$, Fourier series is a signal decomposition made through different harmonics, each one with a different weight:

$$u(t) = \sum_{n=-\infty}^{+\infty} (a_n + ib_n)\, e^{i\omega_n t} = A_n e^{i\omega_n t} \tag{2.5}$$

where A_n is a complex coefficient. This is the spectral representation of the signal $u(t)$.
Averaging the multiplication between eq. 2.5 and the $-m$-th mode, Fourier coefficients are obtained [Pope, 2000], i.e. they are the product of the correlation between the signal and the harmonics:

$$\begin{aligned}\overline{(e^{-i\omega_m t}u(t))}_T &= \overline{\left(\sum_{n=-\infty}^{+\infty} A_n e^{i\omega_n t}e^{i\omega_m t}\right)}_T \\ &= \sum_{n=-\infty}^{+\infty} A_n \delta_{n,m} = A_m\end{aligned}$$

Fourier transform operator is now introduced as:

$$F_{\omega_n}(u_t) = \overline{(u(t)e^{-i\omega_n t})}_T = \frac{1}{T}\int_0^T u(t)e^{-i\omega_n t}dt \tag{2.6}$$

[2] For statistical stationarity is meant that statistic are time independent.

This decomposition is allowed only when the original signal is periodic. However assuming an infinite period for the signal, Fourier series can be applied to every signal. Thus the signal is represented as the integral of different harmonics, each one with a different weight $A(f)$:

$$u(t) = F_t(A(f)) = \int_{-\infty}^{\infty} A(f)e^{i2\pi ft}df \tag{2.7}$$

The latter formula is the Fourier transform of the weight $A(f)$. It is known also as Fourier anti-transformation or plus-i Fourier transform. The weight $A(f)$ is obtained using the Fourier transform on the signal $u(t)$ (or minus-i Fourier transform):

$$A(f) = F_f(u(t)) \int_{-\infty}^{+\infty} u(t)e^{-i2\pi ft}dt \tag{2.8}$$

that means the weight is given by the correlation between the temporal signal and the specific harmonic, i.e. how much that harmonic weights on the signal history.
Often the term $2\pi f$ is renamed as the frequency $\omega = 2\pi f$. This transformation yields to a new way to represent equations 2.7 and 2.8, i.e. Fourier antitransform and Fourier transform [Bracewell, 2000, pag.23]

$$\begin{cases} u(t) = F_t(A(\omega)) = \frac{1}{2\pi}\int_{-\infty}^{\infty} A(\omega)e^{i\omega t}d\omega \\ A(\omega) = F_\omega(u(t)) = \int_{-\infty}^{+\infty} u(t)e^{-i\omega t}dt \end{cases} \tag{2.9}$$

2.2.4 Discrete analysis

In spite of the beauty of continuous systems, both data from experiments and computations are obtained in a discrete domain. Fourier transforms has to be adapted to this different kind of domain, i.e. discrete instead of continuous domain. First of all a time step Δt is defined as:

$$\Delta t = \frac{T}{N}$$

where T represents the finite period time and N the number of samples. Thus a certain instant t_j is defined as $t_j = n \cdot \Delta t$, with $n = 0, \ldots, N-1$. Moreover $u(t_j) = u_j$, i.e. the discrete signal is equal to the real one at the same sampled time.
A signal can be decomposed using discrete Fourier series as follow:

$$u(t_j) = a_0 + \sum_{n=1}^{T-1} a_n \cos(2\pi f_n t_j) + ib_n \sin(2\pi f_n t_j)$$

where n determines the frequency of each harmonic. The Fourier coefficients are equal to:

$$a_0 = \frac{1}{T}\sum_{t_j=0}^{T-\Delta t} u(t_j);$$
$$a_n = \frac{1}{T}\sum_{t_j=0}^{T-\Delta t} u(t_j)cos(2\pi f_n t_j);$$
$$b_n = \frac{1}{T}\sum_{t_j=0}^{T-\Delta t} u(t_j)sin(2\pi f_n t_j)$$

This decomposition is allowed only when the original signal is periodic. However, as before, assuming an infinite period, the Fourier series can be applied to every signal.
Fourier transform can also be adapted to a discrete domain, obtaining the discrete Fourier transform, DFT. Using symmetry properties, different strategies to speed up DFT can be obtained: these methods are called fast Fourier transform, FFT.

2.2.5 Energy relations

Spectra analysis is important during turbulence analysis thanks to several properties they are characterized by.
One of the main interesting aspect of spectra analysis can be investigated starting from Fourier transform of autocorrelation function $C(t,\tau)$. Assuming statistical independence, autocorrelation function depends only on time spacing of the two signals, τ. Thus the Fourier transform of autocorrelation coefficient can be written as:

$$S(\omega) = \frac{1}{2\pi}\int_{-\infty}^{+\infty} \rho(\tau)e^{-i\omega\tau}\, d\tau \tag{2.10}$$

meanwhile the anti Fourier transform is:

$$\rho(\tau) = \int_{-\infty}^{+\infty} S(\omega)e^{+i\omega\tau}\, d\omega \tag{2.11}$$

The quantity $S(\omega)$ is known as power spectral density (PSD) or spectrum Tennekes and Lumley [1972].
Spectrum is related with signal energy. In order to show this correspondence, Parseval's theorem is introduced. It establishes that energy contain of a signal in temporal domain is the same in frequency domain, i.e. applying Fourier

transform to a squared signal its energy is not modified

$$\int_{-\infty}^{+\infty} |u(t)u^*(t)|\, dt = \frac{1}{2\pi}\int_{-\infty}^{+\infty} |A(\omega)A^*(\omega)|\ d\omega$$

where $A(\omega) = \int_{-\infty}^{+\infty} u(t)e^{-i\omega t}\ dt$. In order to avoid convergence problem [3] a finite time can be considered:

$$A_T(\omega) = \int_{-T/2}^{+T/2} u(t)e^{-i\omega t}\ dt$$

then the multiplication between the Fourier transform of a signal and its complex conjugate becomes

$$A_T(\omega)A_T^*(\omega) = \left[\int_{-T/2}^{+T/2} u(t)e^{-i\omega t}\ dt\right]\left[\int_{-T/2}^{+T/2} u(t')e^{i\omega t'}\ dt'\right]$$

Assuming $t' = t + \tau$, the equation above becomes

$$A_T(\omega)A_T^*(\omega) = \int_{-T/2}^{+T/2}\int_{-T/2}^{+T/2} u(t)u(t+\tau)e^{-i\omega\tau}\ dt\ dt' \tag{2.12}$$

Averaging equation 2.12 the autocorrelation function appears

$$\overline{A_T(\omega)A_T^*(\omega)} = \int_{-T/2}^{+T/2}\int_{-T/2}^{+T/2} C(\tau)e^{-i\omega\tau}\ dt\ dt' \tag{2.13}$$

Using some multi-variable calculus and considering an infinite period T through the use of a limit, equation 2.13 becomes:

$$\lim_{T\to\infty} \overline{A_T(\omega)A_T^*(\omega)} = \lim_{T\to\infty} T\int_{-T}^{+T} C(\tau)e^{-i\omega\tau}\ d\tau =$$
$$\lim_{T\to\infty} \frac{1}{T}\overline{A_T(\omega)A_T^*(\omega)} = \int_{-\infty}^{+\infty} C(\tau)e^{-i\omega\tau}\ d\tau = S(\omega) \tag{2.14}$$

This is the same result inside the Wiener–Khinchin theorem. The $S(\omega)$ unity of measure is equal to the square of the signal unit over frequency.

[3] Many signals do not have a finite value of their integral over an infinite time.

Integrating PSD over all the frequencies, the total amount of energy is obtained:

$$\begin{aligned}\int_{-\infty}^{+\infty} S(\omega)\ d\omega &= \int_{-\infty}^{+\infty}\int_{-\infty}^{+\infty} C(\tau)e^{-i\omega\tau}\ d\tau\ d\omega = \\ &= \lim_{T\to\infty}\frac{1}{T}\int_{-T/2}^{+T/2}\overline{A_T(\omega)A_T^*(\omega)}\ d\omega = \\ &= \lim_{T\to\infty}\frac{2\pi}{T}\int_{-T/2}^{+T/2}\overline{u(t)u^*(t)}dt \end{aligned} \tag{2.15}$$

Thus from equation 2.14, it can established that Fourier transform of autocorrelation function is equal to the power spectrum, i.e. the square of the Fourier transform of the signal.
In turbulence, the kinetic energy distribution among different wave numbers is described by the energy spectrum [4]. Thanks to the above results, this energy distribution is equal to the correlation between two velocities [Batchelor, 1959]. Also this concept is introduced for the first time by Taylor [1938].
However, considering spatial correlation of velocity, the wavenumber becomes a three component vector, such that Fourier transform has to be rewritten as:

$$F(u(\mathbf{x})) = A(\boldsymbol{\kappa}) = \iiint u(\mathbf{x})e^{-i\boldsymbol{\kappa}\cdot\mathbf{x}}dx_1dx_2dx_3 \tag{2.16}$$

Thus the energy associated of each wave, or eddies, is the information provided by the spectrum at a given frequency. From it, several conclusions about spectral dynamic and how energy is transfered from large scale to smaller scaler can be achieved.
Similar results to the ones obtained considering the autocorrelation function can be achieved. Fourier wave number spectrum is defined as:

$$\begin{aligned}\Phi_{i,j}(\boldsymbol{\kappa}) &= \frac{1}{(2\pi)^3}\iiint_{\infty}^{+\infty}\overline{u_i'(\mathbf{x},t)u_j'(\mathbf{x}+\mathbf{r},t)}e^{-i\boldsymbol{\kappa}\cdot\mathbf{x}}d\mathbf{r} = \\ &= \frac{1}{(2\pi)^3}\iiint_{\infty}^{+\infty}R_{i,j}(\mathbf{r})e^{-i\boldsymbol{\kappa}\cdot\mathbf{x}}d\mathbf{r}\end{aligned} \tag{2.17}$$

where κ is the wave number vector defined as $\kappa = 2\pi/\lambda$ with λ defined as wavelength.

2.3 The scales of turbulence

Turbulent fluid flows are characterized by simultaneous presence of structures of different sizes. Thus several length scales can be defined inside a flow field.

[4] The difference between power and energy spectrum is that the former is integrates on an infinite domain meanwhile the latter is integrated on a finite range of values.

The larger scales are defined by the geometric dimension of domain meanwhile the smallest scale is defined using Kolmogorov scales. In between these scales, an energy cascade process takes place.
Thus energy is produced at larger scales. Eddies are both characterized by a certain life time and subjected to instability process which make possible the breaking down of the structure in smaller ones [Verzicco, 2002]. The eddy evolution is depending on the faster event: eddies are breaking into smaller ones if the instability amplification process is faster than the life time of the eddies, otherwise their energy is dissipated into heat before creating new sub-vortices. The breaking down process usually is interrupted at small scales where viscosity effects are high, hence the structure life time is smaller than the time needed to instabilities to grow.
This theory is known as cascade process and it is elaborated by Kolmogorov [1991] under the assumptions of homogeneous and isotropic flow.
The scales where energy dissipation takes place are known as Kolmogorov scales. Assuming that at small scales, eddies are independent by geometric conditions and only a dependence on viscosity ν and viscous dissipation $\epsilon([m^2/s^3])$ is present, using a dimensional analysis the following results can be achieved:

$$\begin{aligned} \eta &= (\nu^3/\epsilon)^{1/4} && \text{Kolmogorov length scale} \\ t_\eta &= (\nu/\epsilon)^{1/2} && \text{Kolmogorov time scale} \\ v_\eta &= (\nu\epsilon)^{1/4} && \text{Kolmogorov velocity scale} \end{aligned}$$

Integral scales are dependent by outer geometric conditions. From the Kolmogorov theory is at these scales that energy is inserted. An approximation of the length over the signal is correlated with itself, is given by the integral length scale, defined as:

$$L = \int_0^{+\infty} \frac{R(\mathbf{r})}{R(0)}\, d\mathbf{r}$$

Integral time scale is defined through autocorrelation coefficient ρ:

$$\Lambda = \int_0^{+\infty} \rho(\tau)\, d\tau$$

Another important turbulent scale is the Taylor micro scale, introduced by Taylor [1935]. It is defined from the second derivative of the correlation coefficient when the distance between the two signals is zero. In the longitudinal case is:

$$\lambda_x(t) = \left[-\frac{1}{2}\zeta_x''(0,t)\right]^{-1/2} = \left[-\frac{1}{2}\left(\frac{\partial^2\zeta}{\partial r_x^2}\right)\Big|_{r_x=0}\right]^{-1/2} \tag{2.18}$$

From a graphical point of view, the value of Taylor micro scale is the intersection between the parabola tangent at the origin of the correlation function, $\zeta_x(0,t)$, and the abscissa axes, i.e. r_x. From this point of view, it can be understood that over Taylor micro scale signal is still strongly correlated.
Moreover Taylor micro scale can be related to velocity derivatives using eq. 2.18:

$$\begin{aligned}
-u'^2\zeta_x''(0,t) &= -u'^2 \lim_{r\to 0} \frac{\partial^2}{\partial r_x^2}\zeta_x(r_x,t) = \\
&= -\lim_{r\to 0} \frac{\partial^2}{\partial r_x^2}\overline{(u'(x+r_x,y,z,t)u'(x,y,z,t))} = \\
&= -\lim_{r\to 0} \overline{\left(\left(\frac{\partial^2 u'}{\partial x^2}\right)\Big|_{x+r_x} u'(x,y,z,t)\right)} = \\
&= -\overline{\left(\frac{\partial^2 u'}{\partial x^2}u'\right)} = -\overline{\left(\frac{\partial}{\partial x}\left(u'\frac{\partial u'}{\partial x}\right) - \left(\frac{\partial u'}{\partial x}\right)^2\right)} = \\
&= \overline{\left(\frac{\partial u'}{\partial x}\right)^2}
\end{aligned}$$

Thus

$$\overline{\left(\frac{\partial u'}{\partial x}\right)^2} = \frac{2u'^2}{\lambda_x^2} \tag{2.19}$$

Using ζ_z, transverse Taylor micro-scale can be computed. Longitudinal and transverse Taylor micro-scales are related by $\lambda_z(t) = \lambda_x(t)/\sqrt{2}$.
With the assumptions of homogeneous and isotropic turbulence, dissipation ϵ can be related with Taylor micro-scales as:

$$\epsilon = 15\nu\overline{\left(\frac{\partial u'}{\partial x}\right)^2} = 15\nu\frac{u'^2}{\lambda_z^2}$$

Taylor micro scale is an intermediate scale between integral and Kolmogorov one.
Recent papers, as Segalini et al. [2011b], empathizes the role of Taylor micro scale in turbulence.

2.4 Leonardo da Vinci

As introduced in the first paragraph, a proper definition of turbulence does not exist, but usually it is described through its behavior and characteristics, e.g. irregularity, three dimensional, diffusivity, presence of eddies etc.
Deep investigation and analysis started mainly during the twentieth century. However some of typical characteristics of a turbulent flow were already observed by Leonardo da Vinci, during his hydrodynamic studies made in between 1508

- 1510.
This is what he wrote referring to his drawing in picture 2.1 [5] (translation by [Richter, 1883, ref. to drapery 389]) In "Codex "This is the translation of his words , about his drawing in picture

Observe the motion of the surface of the water which resembles that of hair, and has two motions, of which one goes on with the flow of the surface, the other forms the lines of the eddies; thus the water forms eddying whirlpools one part of which are due to the impetus of the principal current and the other to the incidental motion and return flow.

Figure 2.1: Leonardo da Vinci: *Left* An Old Man Seated *Right* Water studies, flow after a vertical plate perpendicular to it. (ca. 1508-10). Windsor, Royal Library

This is not the only drawing from Leonardo da Vinci, where he shows a great power of observation about flow movements. In fact flow behavior is also well represented in picture 2.2. Where it is possible to observe the accuracy with he reproduced flow patterns, e.g. showing the different behavior of the water when it flows around a plate positioned in different ways with respect to flow direction. Concept of turbulence was not known by Leonardo, but observing nature, he got many of the features that characterize certain flow regime.
Moreover, Leonardo was the first to understand what today is called "the principle of aerodynamic reciprocity". Following the translation found in Johnson [1998], Leonardo states: "As it is to move the object against the motionless air so it is to move the air against the motionless object" and "The same force as is made by the thing against air, is made by air against the thing".

[5] Original version from *Codex Atlanticus*: *"Il moto del vello dell'acqua, il quale fa a uso de' capelli, che hanno due moti, de' quali l'uno attende al peso del vello, l'altro al liniamento delle sue volte; così l'acqua ha le sue volte revertiginose, delle quali una parte attende a l'impeto del corso principale, l'altra attende al moto incidente e refresso."*

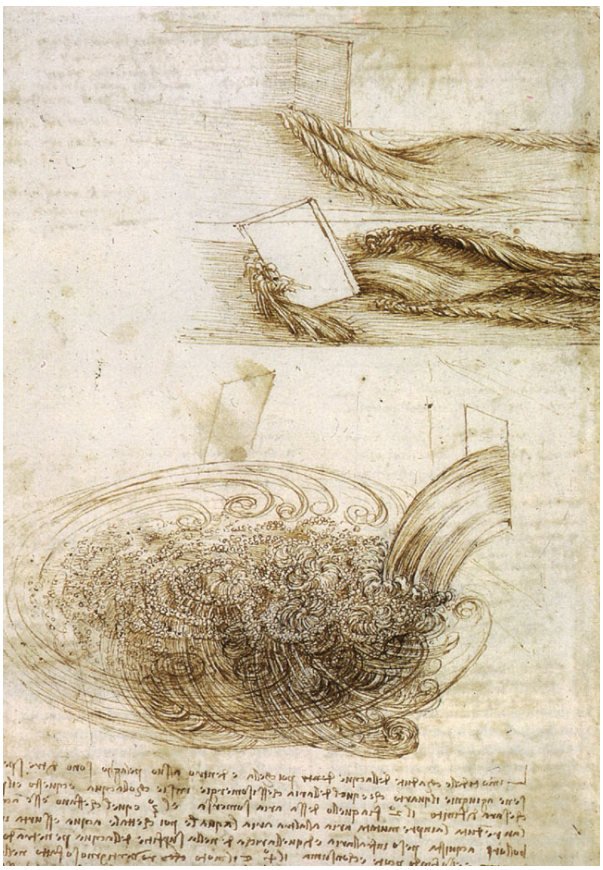

Figure 2.2: Leonardo Da Vinci: *Up* Water flowing against plates positioned in different positions with respect to flow direction *Down* Water falling into a pool. (ca. 1508-09).

Other contributions to fluid dynamic are made by Leonardo, regarding conservation of mass for a low speed flow and qualitative pressure distribution over a lifting airfoil Anderson [1999].

Chapter 3

Equations

3.1 Fluid dynamic equations

In the first chapter, turbulence is introduced as a flow characteristic. The study of fluid movements and their interaction with bodies is the main subject of fluid dynamic.

3.1.1 Continuity equation

Considering a volume $V(t)$ constituted by the same particles at each time instant, i.e. a material volume, the mass inside that volume is time invariant. In a mathematical point of view, the mass conservation is written as

$$\frac{D}{Dt}\int_{V(t)} \rho dV = 0 \tag{3.1}$$

In order to consider the material rate of each particle instead of the entire volume, Reynolds transport theorem [Reynolds, 1903] has to be used, since the volume is time depending. This theorem states that to "transport" the material derivative inside the integral sign, a correction term has to be added. The correction term is made up by the multiplication of the quantity under integration, density, and the velocity flux:

$$\frac{D}{Dt}\int_{V(t)} \rho dV = \int_{V(t)} \frac{D\rho}{Dt} + \rho\nabla\cdot\mathbf{u}\; dV = 0$$

Since this equation holds for any control volumes, the integrand vanishes and the latter equation becomes

$$\frac{D\rho}{Dt} + \rho\nabla\cdot\mathbf{u} = 0 \tag{3.2}$$

Another way to look on this formula is

$$\frac{D\rho}{Dt} + \rho\nabla\cdot\mathbf{u} = \frac{\partial\rho}{\partial t} + \mathbf{u}\cdot\nabla\rho + \rho\nabla\cdot\mathbf{u} = \frac{\partial\rho}{\partial t} + \nabla\cdot(\rho\mathbf{u}) = 0$$

In non compressible flow, density does not vary in space and time then

$$\nabla\cdot\mathbf{u} = 0 \tag{3.3}$$

3.1.2 Momentum conservation

Momentum is conserved inside a closed system in time. This conservation law can be derived from second Newton's law

$$F = \dot{q} = \frac{d}{dt}(m\mathbf{u}) = m\frac{d\mathbf{u}}{dt} \tag{3.4}$$

Considering a material volume, and using the Reynolds transport theorem and the continuity equation 3.2, the right hand side of equation 3.4 becomes

$$\begin{aligned}\frac{D}{Dt}\int_{V(t)}\rho\mathbf{u}\;dV &= \int_V \frac{D(\rho\mathbf{u})}{Dt} + \rho\mathbf{u}\nabla\cdot(\mathbf{u})\;dV = \\ &= \int_V \mathbf{u}\underbrace{\left(\frac{\partial\rho}{\partial t} + \mathbf{u}\nabla\rho + \rho\mathbf{u}\nabla\cdot\mathbf{u}\right)}_{=0} + \rho\frac{\partial u}{\partial t} + \rho\mathbf{u}\nabla\cdot\mathbf{u}\;dV \\ &= \int_V \rho\frac{D\mathbf{u}}{Dt}\;dV\end{aligned} \tag{3.5}$$

The left hand side of equation 3.4, is made by the sum of two different forces, volume and superficial forces

$$F = \int_V \rho\mathbf{f}dV + \int_S \mathbf{t}dS \tag{3.6}$$

where $\mathbf{t}$ are the superficial stresses. Those are function of time, position, surface orientation and geometrical derivatives. Through the Cauchy tensor, $\underline{\mathbf{T}}$, the surface stresses becomes function of only surface orientation, time and position. This simplification allows to develop equation 3.6 as

$$\int_V \rho\mathbf{f}dV + \int_S \mathbf{t}dS = \int_V \rho\mathbf{f}dV + \int_S \underline{\mathbf{T}}\cdot\mathbf{n}dS = \int_V (\rho\mathbf{f} + \nabla\cdot\underline{\mathbf{T}})\;dV \tag{3.7}$$

Moreover, Cauchy tensor can be split in isotropic, $\underline{-\mathbf{p}}$, and anisotropic $\underline{\boldsymbol{\tau}}$ components. Under Newton-Stokes fluid condition, the anisotropic component is

assumed to behave as

$$\underline{\boldsymbol{\tau}} = -\frac{2}{3}\mu(\nabla \cdot \mathbf{u})\delta_{i,j} + \mu\left(\frac{\partial u_i}{\partial x_j}\frac{\partial u_j}{\partial x_i}\right) \tag{3.8}$$

Using the results into equations 3.5,3.7,3.8, and mass conservation (eq.3.2); equation 3.4 can be rewritten as

$$\begin{aligned}\int_V \rho\frac{D\mathbf{u}}{Dt}\, dV = \\ &= \int_V \left(\rho\mathbf{f} + \nabla\cdot\left(-\underline{\mathbf{p}} + \mu\left(\frac{\partial u_i}{\partial x_j}\frac{\partial u_j}{\partial x_i}\right)\right)\right)\, dV = \\ &= \int_V \left(\rho\mathbf{f} - \nabla p + \mu\nabla^2\mathbf{u}\right)\, dV\end{aligned} \tag{3.9}$$

Like continuum equation, momentum equation has to be valid for any control volume, hence integrand vanishes, then:

$$\frac{D\mathbf{u}}{Dt} = \mathbf{f} - \frac{\nabla p}{\rho} + \nu\nabla^2\mathbf{u} \tag{3.10}$$

Equation 3.10 is the conservation of momentum for non compressible flow, with fluid behavior described by Newton-Stokes model.

3.2 Thermodynamics equations

The main subject of thermodynamics is to relate the various property of materials without considering their internal structure [Feynman et al., 1966, pag.44-1]. The most important relations are introduced in this chapter, as a basis of the other demonstrations present in the following chapters.

3.2.1 Fundamental laws of thermodynamics

The zeroth law affirms that if two systems are in thermal equilibrium with a third one, all of them are are each other in thermal equilibrium [Dugdale, 1996, pag.24].

$$if A \xrightarrow{T.E.} C, B \xrightarrow{T.E} C \Longrightarrow A \xrightarrow{T.E.} B \tag{3.11}$$

The first law is known also as the conservation of energy. It states that the changing in the internal energy function inside a system is due to the work done on it and the heat entering in it [1].

[1] In Dudgale book [Dugdale, 1996, pag.21] an example is present to explain in a simple way the internal energy function. Let say that the internal energy function is like a bank account. The possible ways to modify the amount of money is drawing/deposit money and pay/receive

This can be summarized using the classical notation:

$$\Delta U = \Delta Q + \Delta W \tag{3.12}$$

where U is the internal energy function, Q is the heat [2] and W is the work.
Hence the first law states that energy cannot be created by machines, but it does not state any limit of conversion of energy from one form to another one. This limit is expressed by the second law of thermodynamics [Fermi, 1956, pag.29].
The second law of thermodynamics expresses that heat is spontaneously moving from a hot body to a cold one, when they are thermally in contact. This idea is firstly originated by Carnot, years before the discovering of the first law of thermodynamics. Carnot states "partout où il existe une différence de température, il peut y avoir production de puissance motrice" [Carnot, 1872, pag.401] (Wherever a temperature difference exists, work can be produced). Generalizing this statement, work can be produced whenever thermodynamic equilibrium is not present [3], that means when, for example, a temperature, pressure, chemical potential difference is present.
Moreover Carnot understands that the heat is moving from the body with higher temperature to the one with lower temperature, when they are thermally in contact, until they reach a thermal equilibrium. However Carnot uses the caloric theory, since the first principle of thermodynamic was not available at his time. The concept of heat moving from the hotter to the colder body is postulated by the second law of thermodynamic. There are two versions of it, one from Clausius:"Heat can never pass from a colder to a warmer body without some other change, connected therewith, occurring at the same time." [Clausius, 1854, pag.86] [4] and one from Kelvin: "It is impossible, by means of inanimate material agency, to derive mechanical effect from any portion of matter by cooling it below the temperature of the coldest of the surrounding objects" [Kelvin), 1851, pag.13].
It can be proven that the two statements are the same.

cheque. The final amount of money do not distinguish between the different kind of money moving, but it is the sum of both. Thus the internal energy function do not distinguish between work and heat, but only their sum is important.

[2] Q is positive if the heat is entering the system.

[3] Thermodynamic equilibrium is achieved if thermodynamic properties, e.g. pressure, volume, mass, are not varying in time and not large scale flow are present [Dugdale, 1996, pag.12]

[4] This statement is present into Clausius work [Clausius, 1854] in German, 1854 and in English 1856. However the first demonstration by Clausius is dated 1850 in German and 1851 in English [Clausius, 1850].

3.2.2 The entropy

In order to define the entropy, the Clausius' theorem is firstly introduced. Given a system T, subjected to a cyclic transformation, which is split in several infinitesimal steps, the Clausius' theorem states:

$$\oint \frac{dq}{T} \leq 0 \tag{3.13}$$

where dq is an infinitesimal quantity given to the system from a source at temperature T [5], and $\oint$ represents an integration over a cycle. The equality is achieved only for reversible cycles. If the integral is taken from a state A to a state B, it can be demonstrated that the integral quantity depends only by the initial state and the final one, and not by the intermediate ones.
Finally the entropy S can be defined as:

$$S(A) = \int_0^A \frac{dq}{T} \tag{3.14}$$

where 0 is a fixed state, and A is a general equilibrium state and a reversible transformation move the system from the state 0 to the state A (thus T is equal to the system temperature). There is not dependence on the particular reversible transformation but only on the state A since the state 0 is fixed [Fermi, 1956, pagg.46-76].
When a infinitesimal reversible transformation is considered, the infinitesimal rate of entropy can be written, from equation 3.14, as:

$$dS = \frac{dQ}{T} \tag{3.15}$$

3.2.3 State equation

The operating fluid under consideration is considered as an ideal gas. Ideal gas is a theoretical gas made by particles which move randomly and not interact each other, and this gas obeys to a specific state equation. In general form the state equation expresses the dependence of the pressure to the density ad temperature, $P = f(\rho, T)$, meanwhile for ideal gases can be specified as:

$$\frac{P}{\rho} = RT \tag{3.16}$$

[5] T is the temperature of the source, that can be different from the temperature of the system, however when the transformation is reversible the source and system temperatures are the same.

where ρ is the density and R is the universal gas constant [6].

3.2.4 The entropy equation

The entropy equation is a particular form of the energy equation. The energy equation rewritten for the internal energy e [7] is equals to:

$$\rho\frac{De}{Dt} = -p\frac{\partial u_j}{\partial x_j} + \frac{\partial}{\partial x_j}\left(\kappa\frac{\partial T}{\partial x_j}\right) + \mu\left(\frac{\partial u_k}{\partial x_j} + \frac{\partial u_j}{\partial x_k} - \frac{2}{3}\frac{\partial u_s}{\partial x_s}\delta_{kj}\right)\frac{\partial u_k}{\partial x_j} \tag{3.17}$$

This equation is an important starting point to develop the entropy equation. In fact from equation 3.15 and the first law of thermodynamic, equation 3.12, the following result is achieved:

$$Tds = dQ = de + pd(1/\rho) = de - \frac{p}{\rho^2}d\rho \tag{3.18}$$

where $s = S/m$ is the entropy per unit mass and T, e, p, ρ are the temperature, inner energy, pressure and density respectively.
Differentiating equation 3.18, the following result is achieved:

$$T\frac{Ds}{Dt} = \frac{De}{Dt} - \frac{p}{\rho^2}\frac{D\rho}{Dt} \tag{3.19}$$

The first term on the left hand side is obtained by equation 3.17, meanwhile the right hand side can be obtained by the mass conservation equation written in convective form:

$$\frac{D\rho}{Dt} + \rho\frac{Du_j}{Dx_j} = 0 \tag{3.20}$$

Inserting equations 3.17 and 3.20 into 3.19 the entropy equation is obtained:

$$\rho T\frac{Ds}{Dt} = \frac{\partial}{\partial x_j}\left(\kappa\frac{\partial T}{\partial x_j}\right) + \mu\left(\frac{\partial u_k}{\partial x_j} + \frac{\partial u_j}{\partial x_k} - \frac{2}{3}\frac{\partial u_s}{\partial x_s}\delta_{kj}\right)\frac{\partial u_k}{\partial x_j} \tag{3.21}$$

3.2.5 Temperature equation

The temperature equation is another form of the energy equation. It can be easily found from the entropy equation 3.21 [Zuccher, 2012], where the entropy term is opportunely developed.
Since the entropy is a function of temperature and pressure, it can be expanded

[6] $R = nR'$ that is the product of moles and the universal gas constant per mole, equals to $R' = 8.314\frac{J}{molK}$. For dry air $R = 287.06\frac{J}{kgK}$.

[7] Internal energy is connected with the total energy by the following formula $e_{tot} = e + \frac{|u|^2}{2}$. Moreover from now the internal energy is indicated as e and not U

as:

$$ds = dp\left(\frac{\partial s}{\partial p}\right)\Big|_T + dT\left(\frac{\partial s}{\partial T}\right)\Big|_p = dp\left(\frac{\partial s}{\partial p}\right)\Big|_T + \frac{dT}{T}\left(T\frac{\partial s}{\partial T}\right)\Big|_p \tag{3.22}$$

Using the definition of specific heat at constant pressure and using equation 3.15,the second term of equation 3.22 can be related with c_p: The second term of equation 3.22 can be found using :

$$c_p = \left(\frac{dQ}{dT}\right)_p = T\left(\frac{ds}{dT}\right)_p \tag{3.23}$$

The first term of equation 3.22, can be derived starting from Maxwell's thermodynamics relations

$$\left(\frac{\partial s}{\partial p}\right)\Big|_T = -\left(\frac{\partial v}{\partial T}\right)\Big|_p \tag{3.24}$$

and using the definition of the thermal expansion coefficient

$$\beta = \frac{1}{v}\left(\frac{\partial v}{\partial T}\right)_p \tag{3.25}$$

thus

$$\left(\frac{\partial s}{\partial p}\right)\Big|_T = -\left(\frac{\partial v}{\partial T}\right)\Big|_p = -\beta v = -\frac{\beta}{\rho} \tag{3.26}$$

Joining results of relations 3.26 and 3.23 with 3.22, and considering its material rate, a relation for the entropy dynamic can be achieved:

$$\frac{Ds}{Dt} = \frac{c_p}{T}\frac{DT}{Dt} - \frac{\beta}{\rho}\frac{D\rho}{Dt} \tag{3.27}$$

Inserting this equation inside the entropy equation 3.21, the only variable left is the temperature, thus temperature equation is obtained:

$$\begin{aligned}\rho c_p\frac{DT}{Dt} &= \beta T\frac{Dp}{Dt} + \frac{\partial}{\partial x_j}\left(\kappa\frac{\partial T}{\partial x_j}\right) + \mu\left(\frac{\partial u_k}{\partial x_j} + \frac{\partial u_j}{\partial x_k} - \frac{2}{3}\frac{\partial u_s}{\partial x_s}\delta_{kj}\right)\frac{\partial u_k}{\partial x_j}\\ \rho c_p\frac{DT}{Dt} &= \beta T\frac{Dp}{Dt} + \frac{\partial}{\partial x_j}\left(\kappa\frac{\partial T}{\partial x_j}\right) + \Phi\end{aligned} \tag{3.28}$$

where:

$$\Phi = \mu\left(\frac{\partial u_k}{\partial x_j} + \frac{\partial u_j}{\partial x_k} - \frac{2}{3}\frac{\partial u_s}{\partial x_s}\delta_{kj}\right)\frac{\partial u_k}{\partial x_j}$$

is the rate of work spent by the stresses to distort fluid particles. This energy is transformed into heat, i.e. dissipation of mechanical energy.
The other mechanical energy term is the pressure one, $\beta T(Dp/Dt)$. It is derived by the isotropic component of the stress tensor, thus it is the work done by the

stresses in order to compress the fluid [Kay and Nedderman, 1974].
Considering low fluid velocity, heat transfer generated by the mechanical energy terms Dp/Dt and Φ, are usually small. This lead to write the temperature equation for a fluid element as:

$$\frac{DT}{Dt} = \frac{\kappa}{\rho c_p}\nabla^2 T \tag{3.29}$$

3.3 Scalar equation

In this section the passive scalar equation for the temperature is derived. Considering a control volume, the scalar can move inside or outside of it by two different kind of process: convection or diffusion.
Considering the scalar quantity T in a fixed point, its value is function of

$$T_1 = T(t_1, x_1, y_1, z_1) = T(t, \boldsymbol{\chi_1})$$

Moving on a trajectory the scalar quantity is function of the point $\boldsymbol{\chi_2}$, that is:

$$T_2 = T(t_2, x_2, y_2, z_2) = T(t + \Delta t, \boldsymbol{\chi_1} + \boldsymbol{\Delta\chi})$$

If $\boldsymbol{\Delta\chi}$ is small, Taylor expansion can be used:

$$T_2 = T_1 + \Delta T = T_1 + \Delta x\frac{\partial T}{\partial x} + \Delta y\frac{\partial T}{\partial y} + \Delta z\frac{\partial T}{\partial z} + \Delta t\frac{\partial T}{\partial t}$$

Considering an infinitesimal time step and infinitesimal length size, temperature difference between states 1 and 2 becomes infinitesimal, $\Delta t = \delta t$. Thus the ratio between $T_2 - T_1$ and infinitesimal time step dt provides a relation for the temperature convection

$$\frac{T_2 - T_1}{dt} = \frac{dT}{dt} = u\frac{\partial T}{\partial x} + v\frac{\partial T}{\partial y} + w\frac{\partial T}{\partial z} + \frac{\partial T}{\partial t} = \frac{\partial T}{\partial t} + \mathbf{u}\cdot\nabla T \tag{3.30}$$

These quantities represent the variation of the scalar in time and space due to the velocity.
Another mechanism for the scalar to vary is through the diffusion. Let say that the scalar is not uniformly distributed. This not equilibrium affects the scalar motion, since it tries to restore an equilibrium state. This means that the diffusion can be seen as a flux of the scalar acting in the opposite direction of the scalar gradient [Kirby, 2010].
Thus the diffusivity of the scalar is equal to:

$$\dot{q} = -\kappa\nabla T$$

where κ is the thermal conductivity of the material. Considering a control volume, the integral effect of diffusion, i.e. net transfer of scalar towards the boundaries of the volume, is

$$\int_A \dot{q} \cdot \mathbf{n} dA = GaussGreen = \int_V \nabla \cdot \dot{q} dV = -\kappa \int_V \nabla^2 T dV \tag{3.31}$$

Integrating over the control volume V the equation 3.30 and adding the diffusion relation above, equation 3.31, the integral scalar conservation equation is obtained

$$\int_V \left(\frac{\partial T}{\partial t} + \mathbf{u} \cdot \nabla T \right) dV - \kappa \int_V \nabla^2 T dV = 0$$

Since the function is continuous and the control volume is arbitrary, the equation is satisfied also by the terms under integration, then the scalar equation becomes

$$\begin{aligned} \frac{\partial T}{\partial t} + \mathbf{u} \cdot \nabla T &= \kappa \nabla^2 T \\ \frac{DT}{Dt} &= \frac{\kappa}{\rho c_p} \nabla^2 T \end{aligned} \tag{3.32}$$

Equation 3.32, obtained considering scalar dynamic as composed by convection and diffusion, is equal to the temperature equation 3.29 derived from energetic considerations.

Chapter 4

Hot wire anemometry

4.1 Introduction to hot wire

Fluid dynamic experiments are usually performed inside facilities called wind tunnels. Several different kind of measurement can be performed, depending on the quantity under analysis, geometric aspects, frequency resolution, etc.. Considering turbulent flows, measurements are often performed using hot wire anemometers.
The working principle of this instrument is based on the cooling of a heated wire made by the moving flow surrounding the probe. Electrical current is used to heat the wire, thus the wire becomes a resistance for the current passage. This resistance is temperature depending, this means that the surrounding flow can cause variations on the resistance values through convection and diffusion mechanisms. Moreover the wire is subjected to heat conduction to wire supports and to radiation.
This working principle is the basing idea of different kind of hot wires. The most common are the constant temperature anemometry (CTA) and the constant current (CCA) [1].

4.2 Heating on a cylinder

According to King [1915], since the beginning of the XX century, the idea that a heated wire could be used to measure fluid velocity was known and several papers about this topic were circulating inside the scientific community. The first works were made, according to King, by Shakespear, at Birmingham from 1902, but his work was discontinuous for the lack of suitable whirling table

[1] Other different kind of hot wires exist, however they are not treated in this thesis.

for the calibration of the wires. Few years later, many other scientists start to investigate the convection on a hot wire immersed in a moving flow, as Kennelly et al. [1909], Bordoni [1912] and Morris [1912]. However, the first milestone about hot wire anemometry is the King's work in 1914 [King, 1914].
Here a general overview on the basic equilibrium energy equation along a heated wire is provided.
The main hypothesis is to assume a thermal equilibrium condition over the wire, i.e. the heat generated per unit time by the current passing through the wire is equal to the heat losses. Thus, considering an infinitesimal length of the wire dx, several phenomenas influence the heat equilibrium:

$$d\dot{Q}_e = d\dot{Q}_{fc} + d\dot{Q}_{cond} + d\dot{Q}_{rad} + d\dot{Q}_{stor} \tag{4.1}$$

- $d\dot{Q}_e = \frac{I^2 \chi_w}{A_w} dx$ is the heat rate produced by Joule's effect;
- $d\dot{Q}_{fc} = \pi dh(T_w - Ta)dx$ is the heat loss rate due to forced convection;
- $d\dot{Q}_c$ is the heat transfer rate due to conduction to the supports;
- $d\dot{Q}_r$ is the radiative heat transfer rate;
- $d\dot{Q}_s$ is the heat storage rate;

where I is the current passing through a wire with cross sectional area A_w and resistivity χ_w, meanwhile d, h, T_w, T_a are respectively the wire diameter, the heat-transfer coefficient, the wire temperature and the fluid temperature.
Considering the forced convection as the main source of heat loss [2], the equilibrium equation 4.1 can be rewritten as:

$$\frac{I^2 \chi_w}{A_w} dx = \pi h d(T_w - T_a)dx = \pi \kappa_g (T_w - T_a) Nu dx \tag{4.2}$$

where κ_g is heat conductivity of the fluid at temperature T_a, and Nu is the not dimensional Nusselt number.

4.2.1 The Nusselt number

The Nusselt number is defined as:

$$Nu = \frac{hd}{\kappa_g}$$

[2] In first papers the heat conduction rate was neglected since an infinite wire was considered. However, with a finite length of the wire, heat loss due to conduction to supports can not be neglected, thus the final formula will be slightly modified to take in account also this phenomena. Anyway, in literature, several authors studied this effect on hot wire measurements.

and it can be expressed as a function of

$$Nu = f\left[Re, Pr, Gr, \frac{T_w - T_a}{T_a}, Ec, \frac{l}{d}, \phi\right]$$

i.e. the Nusselt number is function of Reynolds number, Prandtl number, Grashof number, overheat ratio $\frac{T_w - T_a}{T_a}$, Eckert number, length to diameter ratio and angle between wire axis and flow direction ϕ. The overheat ratio [3] dependence is due to the modification of fluid property closed to the wire due to the non uniform distribution of temperature, meanwhile Eckert number becomes important when dynamic flow effects cause temperature differences comparable with the temperature difference $T_w - T_a$ (this number is also related to Mach number) [Hinze, 1975].
However a simplification of this formula is needed in order to be used for practical reasons in hot wire anemometry. King proposes a relation where the Nusselt number has a square root dependence with Péclet number:

$$Nu = 1 + \sqrt{2\pi Pé}$$

that can be generalized as

$$Nu = C_1(Pr) + C_2(Pr)Re^{1/2} \tag{4.3}$$

where the most important result is the square root dependence on the Reynolds number.

4.2.2 The wire resistance

The wire resistance is a function of the resistivity, cross sectional area and length of the wire. However, if a not uniform temperature characterizes the wire, resistivity becomes also not uniform along the wire. In order to know the real wire resistance, resistivity has to be integrated over the wire length:

$$R_w = \int_{-L/2}^{+L/2} \frac{\chi_w}{A_W} dx \tag{4.4}$$

The wire resistivity can be expressed by the temperature depending formula

$$\chi_w = \chi_0 \left[1 + \alpha_0(T_w - T_0) + \beta_0(T_w - T_0)^2\right] \tag{4.5}$$

[3] Two different kind of overheat ratio can be defined: · temperature overheat ratio, $a_T = (T_w - T_{ref})/T_{ref}$; · resistance overheat ratio, $a_R = [R(T_w) - R(T_{ref})/R(T_{ref})]$, where T_{ref} is a reference temperature, that can be the fluid one. These two overheat ratio are related through the formula $a_r = \alpha_{el} T_{ref} a_T$, where α_{el} is the temperature coefficient of electrical resistivity.

where the subscript 0 means at a temperature of $0°C$ and α and β are temperature coefficient. Usually the quadratic term is neglected when velocity measures are considered. Inserting equation 4.5 into 4.4, integrating and averaging (same subscript w is used now to indicate the averaged case) the following result is achieved

$$R_w = R_0 \left[1 + \alpha_0 (T_w - T_0)\right] \tag{4.6}$$

However for hot wire measurements usually the temperature of $293.15K$ $(20°C)$ is used as reference temperature, and not the $273.15K$ $(0°C)$.

4.2.3 King's law

Considering a length l segment of an infinite wire (thus the conductive end losses can be neglected), the equation 4.2 can be re-written, using relations 4.3 and 4.6, as

$$I^2 R_{w,\infty} = \pi l \kappa_g \left(\frac{R_{w\infty} - R_a}{\alpha_0 R_0} \right) \left(C_1(Pr) + C_2(Pr) Re^{1/2} \right)$$

Considering hot wire applications, several parameters can be merged, and the following formula is obtained:

$$\frac{I^2 R_{w,\infty}}{R_{w\infty} - R_a} = A_\infty + B_\infty U^{0.50} \tag{4.7}$$

The equation 4.7 can be modified to take in account conductive end loss for the case of a finite wire, i.e. it becomes

$$\frac{I^2 R_w}{R_w - R_a} = A + B U^n \tag{4.8}$$

The three unknowns A, B, n can be determined for each hot wire using a proper calibration method, thus the only unknown becomes the instantaneous velocity U.
Moreover, using the equation 4.6 and merging α_0 and R_0 into the calibration constants A and B, the equation 4.8 becomes:

$$\frac{E_w^2}{R_w} = \left(A + B u^n\right) \left(T_w - T_a\right) \tag{4.9}$$

where the wire voltage E_w is equal to $E_w = I R_w$. This is slightly different then the original King's law but it is still referred as King's law.
It is also often used the shortest version of this formula:

$$E_w^2 = A + B u^n$$

4.3 CCA and CTA

Two of the most used operating mode for hot wire anemometers are the CCA, constant current mode, see figure 4.1, and CTA, constant temperature mode, see figure 4.2.

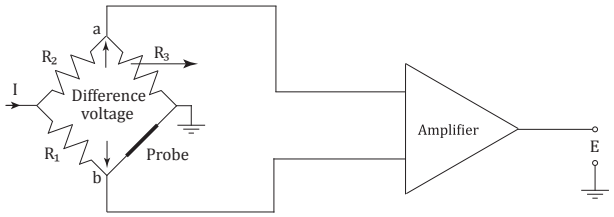

Figure 4.1: Constant current anemometry scheme [courteously M.Ferro]

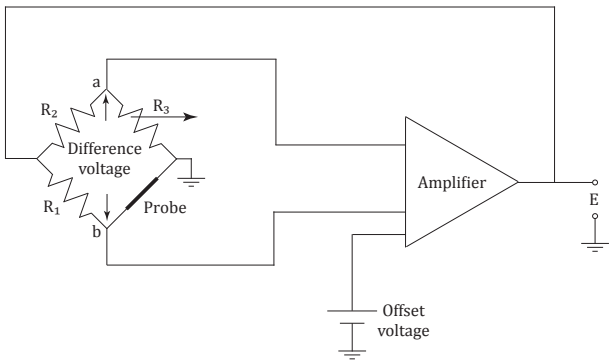

Figure 4.2: Constant temperature anemometry scheme [courteously M.Ferro]

In both cases, the wire is placed inside a Wheatstone bridge. This electronical circuit is usually used in order to compute one of the four resistance that compose it. In hot wire anemometry, one of the four resistance is the wire itself, which vary its resistance value due to the forced convection of the flow on the heated wire itself.
Using a CCA, the current passing through the wire is kept constant, thus flow fluctuations cause variations on the wire temperature, hence the wire resistance. This fluctuation creates variations on the voltage measured on the two sides of the bridge, since

$$E = IR(T)$$

This bridge voltage is related with wire voltage and then with the flow velocity. This operating method is the first one developed for hot wires anemometry, it is easy to build but its frequency resolution is lower than a CTA. Its use during the first experiments was due to a technological lack about the stabilization of the CTA operating mode.
In fact CTA mode is based on feedback control system, where the resistance, thus, the temperature of the wire, is kept constant. This system is inherently unstable, thus feedback control is needed to keep the system stable. Since this issue is not a problem anymore, CTA is widely used nowadays.
In order to keep constant the resistance, the heat produced by the wire through Joule's effect, $P = I^2R$, should change accordingly to the flow fluctuations, thus the current along the wire fluctuates.

4.4 Spatial averaging

One of the main characteristics of a turbulent flow is the the presence of numerous structures with a wide range of length scales. In order to make correct measurements, the length of the wire should be smaller than the smallest structure, otherwise a different forced convection, thus velocity, can be experienced in different points of the wire. This leads to an average measure of the effective velocity along the wire. This phenomena is called spatial averaging and it is one of the main source of error in hot wire measurements.
This effect is well known since the first era of hot wire. Dryden in 1937 studied the effects of a not complete homogeneity of velocity fluctuations along the wire on measurements of velocity fluctuation correlation, which are connected with the scales of turbulence [Dryden et al., 1936]. Theoretical approach, combined with homogeneous and isotropic turbulence assumption, is also kept Frenkiel [1949].
However, for wall turbulence, the isotropy hypothesis is not guaranteed near the wall, where high velocity gradients are experienced. Higher effects of spatial averaging on measurements are achieved in this region.
The spatial resolution effect in anisotropic turbulence starts to be investigated intensively only since eighties, using different measurements made with wires of various length. Johansson and Alfredsson [1983] investigate how spatial averaging effects turbulence statistics as turbulence intensity peak, zero crossing of skewness factor, pdf, number of bursting events etc. using two hot wire of different length.
A deeper investigation, using several hot wire of different lengths, is made by Ligrani and Bradshaw [1987]. They provide also two guidelines about hot wire dimensions: in order to reduce conductive end loss, the length to diameter

should be larger than 200, meanwhile to reduce spatial averaging effect, the length of the wire should be kept smaller than 20 viscous units.
Hutchins et al. [2009], finds a Reynolds number effect on near wall peak measurements besides the spatial averaging. Moreover the spatial averaging influences even beyond the near wall region.
Several correction schemes are developed in order to compensate, from the measurement performed, the spatial averaging error. Empirical versions are made by Chin et al. [2009], Chin et al. [2011], Smits et al. [2011] and Monkewitz et al. [2008]. Dryden approach is rediscovered and improved Segalini et al. [2011a].

4.5 Temperature correction

Wind tunnel experiments are performed at various ambient condition, e.g. with different laboratory temperature. Moreover the fan inside the facility, heat the flow, increasing its temperature. In order to obtain comparable results among several experiments, velocity measurements should be corrected for different temperature values.
In order to compensate changes in temperature values, formula 4.9 can be used as starting point

$$\frac{E_w^2}{R_w} = (A + Bu^n)\,(T_w - T_a) \rightarrow E_w^2(T_a) = f(u)(T_w - T_a) \tag{4.10}$$

During the calibration procedure, equation 4.10 can be rewritten as follow:

$$E_w^2(T_{ref}) = f(u)(T_w - T_{ref}) \tag{4.11}$$

where here T_{ref} is reference temperature during the calibration procedure, thus $E_w(T_{ref})$ is the voltage output that hot wire should measures if it is surrounded by a fluid at the calibration temperature T_{ref} instead that T_a.
Since temperature is considered a passive scalar, it not influences flow dynamics, hence velocity dependence for both equations is supposed to be equal. The ratio between equations 4.10 and 4.11 becomes:

$$\begin{aligned} \frac{E_w^2(T_a)}{E_w^2(T_{ref})} &= \frac{T_w - T_a}{T_w - T_{ref}} \\ E_w^2(T_{ref}) &= E_w^2(T_a)\left(\frac{T_w - T_a}{T_w - T_{ref}}\right)^{-1} \end{aligned} \tag{4.12}$$

Using the resistance overheat ratio formulation

$$a_r = \alpha_{el} T_{ref} a_T = \alpha_{el}\,(T_w - T_{ref})$$

equation 4.12 can be rewritten as

$$E_w^2(T_{ref}) = E_w^2(T_a)\left(1 - \frac{T_a - T_{ref}}{T_w - T_{ref}}\right)^{-1} = E_w^2(T_a)\left(1 - \frac{T_a - T_{ref}}{a_T T_{ref}}\right)^{-1} = \\ = E_w^2(T_a)\left(1 - \frac{T_a - T_{ref}}{a_R/\alpha_{el}}\right)^{-1} \tag{4.13}$$

Two experimental parameters as overheat ratio and α_{el} are present. Between them, only α_{el} is unknown, since the fluid temperature T_a can be measured with a cold wire and the overheat ratio is fixed by the user.
In fact the tabulated values of electrical resistivity α_{el} are slightly different compared to the ones found during experiments [Dijk and Nieuwstadt, 2004, Örlü, 2009], thus iterative process has to conducted to characterize α_{el} for each probe.

Chapter 5

Simulation details

5.1 General idea

The General idea of this work is to investigate how a thermal gradient inside a channel can effect hot wire measurements. Sattarzadeh et al. [2013], introduces the idea of temperature fluctuations influence on the velocity measured by a hot wire. This is due to the high correlation between streamwise velocity and temperature fluctuations [Kim et al., 1987], above all close to the wall. An idea of this interaction magnitude between temperature and streamwise velocity is given by figure 5.1, where cross moment coefficient has a value close to 1 near the wall. After around 10 viscous lengths its value starts to decrease.

Thus, when hot wire is invested by a not constant temperature, scalar fluctuations modify the quantity of heat transferred by convection from the wire to the flow. A positive velocity fluctuation is associated with a positive scalar fluctuation, which increases the temperature of the wire, i.e. a smaller heat flux from the wire is sensed by the instrument thus the resulting velocity is smaller. On the contrary, negative temperature fluctuations leads to a larger sensed velocity. The overall effect is to reduce instantaneously the fluctuations intensity of sensed velocity from the real averaged one.
This can be observed from figure 5.2, where sensed velocity by the hot wire (blue dot line) is smaller than simulated velocity (blue solid line) when temperature (red solid line) exceeds mean temperature value (dash red line) and viceversa. These instantaneous quantities are referred to a single snapshot at wall normal position $y^+ \approx 15$.

In order to evaluate and quantify temperature influence, a numerical approach is preferred. In fact, experimentally, temperature can be measured through a cold wire, however this instrument does not provide a sufficient frequency resolution, yielding to difficult analysis.

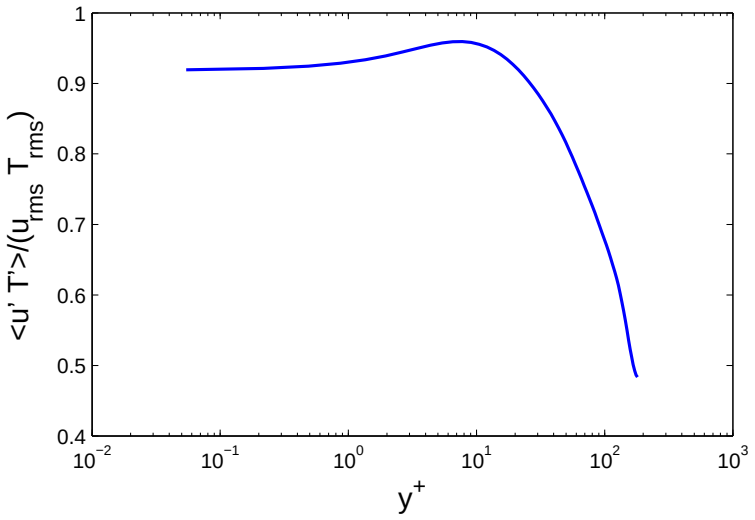

Figure 5.1: Cross moment between temperature and velocity, not dimesionalized by the product between temperature rms and velocity rms

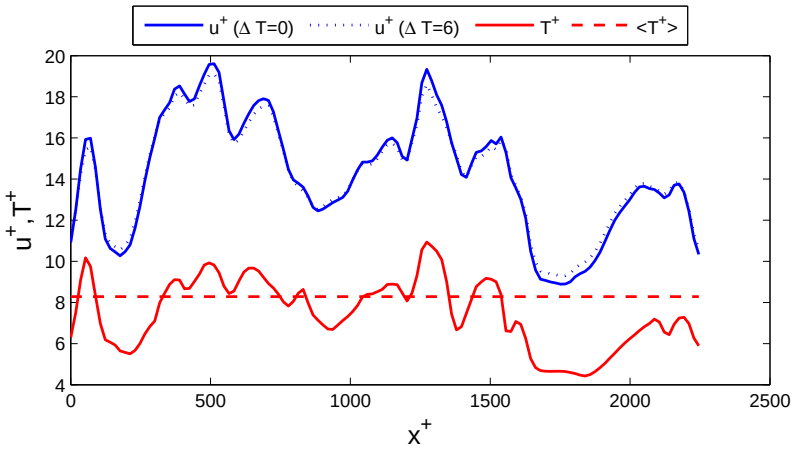

Figure 5.2: Instantaneous quantities along the streamwise axis: · blue solid line is u^+ from simulation, · blue dot line is u^+ sensed by the hot wire with a $\Delta T =$ 6K, · red solid line is T^+ and · red dash line is the mean temperature at $y^+ =$15

5.2 Simulation characteristics

Turbulent channel flow at $Re_\tau = u_\tau h/\nu = 180$ is simulated through the pseudo-spectral code Simson. No-slip condition is assumed at walls and the flow is initialized through a parabolic profile with a certain amount of noise to speed-up the turbulence development. Mass flow rate condition is used in order to keep the Re_τ value while simulation is advancing in time. Sketch of the channel is showed in figure 5.3.
Temperature is considered as a passive scalar, thus it can be solved using scalar equation. Prandtl number is fixed to 0.71. Thermal boundary conditions are set as Dirichlet condition at wall, i.e. $T|_{wall} = 0$. This kind of boundary condition fix the wall temperature to zero, but allows a heat flux through the walls. This heat loss has to be balanced by a heat source in order to preserve the temperature profile inside the channel.
The temperature source is chosen as an uniform heat inside the domain, i.e. all the domain is warmed in same way. However in order to satisfy the temperature bcs, a flux through top and bottom walls diffuse the scalar outside the domain and the temperature assumes an averaged profile similar to the velocity one.
The balance between heat flux and heat loss is an important feature to be achieved in order to know if passive scalar has reached statistically steady state. Its formulation is introduced into paragraph 5.3.1.

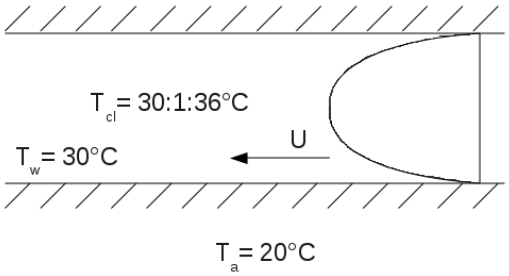

Figure 5.3: Sketch of the channel

5.3 Numerical procedure

Unsteady Navier-Stokes equation are solved using the pseudo spectral code Simson [Chevalier et al., 2007]. Velocity field is solved through the computation of not dimensional incompressible Navier-Stokes equations written using a velocity-vorticity formulation. Once velocity field is obtained, scalar field is

Direction	Box size	#Nodes/Modes	Grid spacing
x	4π	128	17.67 l^+
y	2	129	min: 0.055 l^+
z	2π	128	8.84 l^+

Table 5.1: Number of nodes/modes of channel domain and spacing in viscous units $l^+ = \nu/u_\tau = Re_\tau$ since the semi channel height h is equal to 1. Note that wall normal nodes distribution is made using Chebyshev polynomial then spacing is smaller close to walls and larger far from it.

computed solving not dimensional version of scalar equation 3.32:

$$\frac{\partial T^*}{\partial t^*} + \mathbf{u}^* \cdot \nabla T^* = \frac{1}{Re_\tau Pr} \nabla^2 T^* + Q^* \tag{5.1}$$

where * is used now to represent not dimensional variables and $Q^* = \frac{Qh}{T_\tau u_\tau}$ is a not dimensional heat source term, i.e. the one used to introduce heat into the domain.

The box dimensions are 4πx2x2π, where the first dimension is referred to streamwise direction, the second to wall normal direction and the third to spanwise direction. The number of grid points is around $2\text{x}10^6$, i.e. 128 modes are used both in streamwise and spanwise directions, and 129 nodes in wall normal direction. Domain characteristics are summarized into table 5.1. Spatial derivatives are computed with Fourier series in the periodic directions, streamwise and spanwise, meanwhile with Chebyshev polynomial along the wall normal. Time derivatives are approached in two different ways: Runge-Kutta 3 is used for temporal derivatives of non linear terms meanwhile Crank- Nicholson for linear terms.

OpenMP parallelization strategy on 12 processors is used in order to speed-up the computation.

5.3.1 Heat balance

In order to obtain correct statistics, variables should reach a statistical stationarity. For temperature case, a balance between heat production and heat loss has to be reached. Starting from equation 5.1 (* is neglected for a better visualization), heat production and dissipation terms can be found.

Integrating all over the volume, convective term at lhs of equation 5.1, becomes:

$$\iiint_V \mathbf{u}\cdot\nabla T dV = \iiint_V \left[\nabla\cdot(\mathbf{u}T) - \underbrace{T\nabla\cdot\mathbf{u}}_{=0 \text{ for continuity}}\right] dV \overset{Gauss-Green}{=}$$
$$= \iint_S (\mathbf{u}T)\cdot\mathbf{n}dS = \underbrace{\iint_{\Delta y,\Delta z} uTdydz}_{=0 \text{ for simmetry}} = \underbrace{\iint_{\Delta x,\Delta y} wTdxdy}_{=0 \text{ for simmetry}} =$$
$$= \underbrace{\iint_{\Delta x,\Delta z} vTdydz}_{=0 \text{ for b.c.}} = 0$$

Integrating the diffusive term on the rhs of equation 5.1 the following result is achieved:

$$\frac{1}{Re_\tau Pr}\iiint_V \nabla^2 T dV = \frac{1}{Re_\tau Pr}\iiint_V \left(\frac{\partial^2 T}{\partial y^2}+\frac{\partial^2 T}{\partial z^2}+\frac{\partial^2 T}{\partial x^2}\right)dxdydz =$$
$$= \frac{1}{Re_\tau Pr}\left[\int_x\left(\frac{\partial^2}{\partial x^2}\iint_{y,z} Tdydz\right)dx + \int_y\left(\frac{\partial^2}{\partial y^2}\iint_{x,z} Tdxdz\right)dy +\right.$$
$$\left.+\int_z\left(\frac{\partial^2}{\partial z^2}\iint_{x,y} Tdxdy\right)dz\right]$$

Dividing each term in round brackets for the corresponding surface ($LxLy$, $LxLZ$ or $LYLZ$), mean temperature on that surface is obtained thus:

$$\frac{1}{Re_\tau Pr}\left[LyLz\int_x \frac{\partial^2\overline{T}^{y,z}}{\partial x^2}dx + LxLz\int_y\frac{\partial^2\overline{T}^{x,z}}{\partial y^2}dy + LxLy\int_z\frac{\partial^2\overline{T}^{x,y}}{\partial z^2}dz\right] =$$
$$= \frac{1}{Re_\tau Pr}\left[LyLz\underbrace{\frac{\partial\overline{T}^{y,z}}{\partial x}\Big|_{x=0}^{x=4\pi}}_{=0 \text{ for symmetry}} + LxLz\frac{\partial\overline{T}^{x,z}}{\partial y}\Big|_{y=0}^{y=2} + LxLy\underbrace{\frac{\partial\overline{T}^{x,y}}{\partial z}\Big|_{z=0}^{z=2\pi}}_{=0 \text{ for symmetry}}\right] =$$
$$= \frac{LxLz}{Re_\tau Pr}\frac{\partial\overline{T}^{x,z}}{\partial y}\Big|_{y=0}^{y=2}$$

This term represent heat loss across the wall.
Heat production is given by the source term integrated all over the volume. However Q is fixed as a constant, i.e. the same heat flux in each point, thus:

$$\iiint_V QdV = QLx\,Ly\,Lz$$

Thus, if statistical stationary condition is achieved for temperature the following balance should be valid::

$$\begin{aligned} \frac{LxLz}{Re_\tau Pr}\frac{\partial \overline{T}^{x,z}}{\partial y}\Big|_{y=0}^{y=2} &= Q Lx\, Ly\, Lz \\ \frac{1}{Ly\, Re_\tau\, Pr}\frac{\partial \overline{T}^{x,z}}{\partial y}\Big|_{y=0}^{y=2} &= Q \end{aligned} \tag{5.2}$$

i.e. balance between heat loss (lhs) and heat production (rhs).

5.3.2 Dimensional and not dimensional quantities

Considering wall turbulence, e.g. turbulent flow inside a channel flow, two different dynamics are present, that characterize respectively the regions close and far from the wall, i.e. inner and outer region. In fact the presence of no-slip condition on the wall, modifies the usual turbulent flow behavior. In free wall condition, turbulence increases mixing and tends to smear out gradients, however close to the wall, viscosity forces the flow to adhere to the wall, generating a higher gradient, thus higher shear stress and drag, than laminar flow case.
Inner region is thinner than outer one and it is characterized by high anisotropic and inhomogeneity behavior, and complex turbulence structures like streaks. can be observed inside this layer.
This is the reason to use two different length scales to describe these two regions. Due to high viscosity influence, thus shear stress, the inner lengthscale is defined as $l^+ = u_\tau/\nu$ where u_τ is the viscous velocity equal to

$$u_\tau = \sqrt{\tau_w/\rho}$$

For Channel flow the outer region lengthscale is defined as the semi channel height h.
Not dimensional velocity from Simson is based on the centerline laminar velocity thus the Reynolds number defined with this velocity is equal to:

$$Re_{cl} = \frac{U_{cl} h}{\nu} = 4200$$

In order to obtain velocity output in wall/viscous units, is sufficient to use the following formulation:

$$u^+ = u^* \frac{Re_{cl}}{Re_\tau}$$

Dimensional velocity is obtained assuming several dimensional parameters. Semi-channel height is fixed to $3cm$ and kinematic viscosity to $1.53 \cdot 10^{-5}$ [1]. Real velocity is then calculated starting from a reference velocity, i.e. centerline laminar velocity, computed from the vales assumed before:

$$U_{cl} = \frac{Re\,\nu_{exp}}{h_{exp}} \longrightarrow u_{real} = u^{+}U_{cl}$$

where the Reynolds value used is $Re = Re_{cl} = 4200$.
Temperature is treated in a slightly different way. Reference temperature is set to 1, thus in order to compute viscous temperature, the only step is to divide not dimensional temperature T^* with the friction temperature T_τ:

$$T^{+} = \frac{T^*}{T_\tau} \tag{5.3}$$

where

$$T_\tau = \frac{\dot{q}|_w}{u_\tau} = \frac{\kappa \frac{dT}{dy}\big|_w}{c_p \rho u_\tau} = \left.\frac{dT}{dy}\right|_w \frac{\nu}{u_\tau}\frac{\kappa}{\nu c_p \rho} = \frac{1}{Re_\tau Pr}\left.\frac{dT}{dy}\right|_w \tag{5.4}$$

Dimensional temperature field is created fixing both wall and centerline temperature. Then

$$T^* = \frac{T - T_w}{T_{cl} - T_w} \rightarrow T = T^*(T_{cl} - T_w) + T_w \tag{5.5}$$

Ferro's experiments [Ferro, 2012] were characterized by $10K$ of temperature difference between wall and ambient temperature meanwhile $2K$ between wall and centerline. Those values are used as reference values inside this project. Here ambient temperature is fixed to 293.15 K (20 °).

5.4 Hot wire data simulation

Channel flow simulation provides velocity and temperature fields. From these data, it is aimed to reconstruct the velocity field sensed by the hot wire. Once obtained this value, it is possible to study how flow temperature influences sensed velocity, since, as it was introduced in section 5.1, wire temperature is influenced by flow temperature fluctuations.
The first step is to reconstruct hot wire output, i.e. the hot wire voltage output needed to compensate heat loss due to forced convection and flow temperature fluctuations. This goal can be satisfied through King's law 4.9, where the variables u and T_a are respectively the instantaneous velocity and instantaneous

[1] These two values are taken from Marco Ferro's experiment [Ferro, 2012]. However in that project thesis a pipe is considered instead of a channel.

flow temperature obtained from simulation.
During experiments, coefficients A, B and n are usually calculated through a calibration procedure. Here, their value is fixed following the results found inside Bruun [1975]. Wire settings R_w and T_w are also fixed by the user. Then the following values are chosen:

- $A = 0.000085$
- $B = 0.000045$
- $n = 0.5$
- $R_w = 7\Omega$
- $T_w = 503.15K(230°C)$

Calculation of wire resistance and wire temperature is a hard issue during experiments. This is the reason to convert King's law, equation 4.9, in a slightly different expression where thermal coefficient of resistivity and over heat ratio substitute wire resistance and temperature. Starting from King's law equation 4.9 and temperature correction 4.13, it is possible to obtain a new relation between voltage output and instantaneous velocity and temperature:

$$E_w^2 = (A + Bu^n)\left(1 - \frac{T - T_{ref}}{a_R/\alpha_{el}}\right) \tag{5.6}$$

where T_{ref} is the calibration reference temperature, which is considered zero in this work and T is the instantaneous temperature field from the simulation.
Overheat ratio and thermal coefficient are instead fixed to:

- $a_r = 1.1$
- $\alpha_{el} = \frac{a_R}{T_w - T_{ref}} = 4.782 \cdot 10^{-3}$

Once obtained the wire voltage output for each node of the domain, velocity sensed by hot wire has to be computed. Considering a probe with a cold and hot wire, it is possible to know experimentally velocity and temperature. However, as already stated, frequency resolution of cold wire is smaller than hot wire's one, thus it is not possible to compensate instantaneously voltage output of hot wire. The usual procedure, when a temperature correction is used, is to correct hot wire voltage output through centerline temperature or, for each wall normal position, through the averaged temperature profile. This means that

sensed velocity from hot wire is equal to:

$$u_{HW} = \left[\frac{E_w^2}{R_w B(T_w - T_c)} - \frac{A}{B} \right]^{1/n} \tag{5.7}$$

$$u_{HW} = \left[\frac{E_w^2}{B\left(1 - \frac{T_c - T_{ref}}{a_r/\alpha_{el}}\right)} - \frac{A}{B} \right]^{1/n} \tag{5.8}$$

where equation 5.7 is the velocity sensed by hot wire using King's law 4.9, meanwhile equation 5.8 is referred to equation 5.6. Temperature T_c is the correction temperature used to evaluate temperature influence: both cases, i.e. correction made with centerline temperature $T_c = T_{cl}$ and with averaged temperature $T_c = T_{av}$ are considered.
Summarizing, velocity sensed by hot wire is computes as

$$\left.\begin{matrix} u_{sim} \\ T_{sim} \end{matrix}\right\} \xrightarrow{\text{King's law}} E_W^2 \xrightarrow{\text{Rev. King's law}} u_{HW}$$
$$\uparrow$$
$$T_c$$

Chapter 6

Results

Results chapter is split in two main sections. In the first one statistical turbulence behavior of the flow is analyzed. Results from simulation are discussed and compared with other works [del Alamo and Jimenez, 2001] and with analytical results, i.e. the log law for velocity and temperature profiles (their derivation is made simultaneously with the visualization of numerical results). The second part is focused on the main topic of this thesis, i.e. temperature influence on hot wire measurements. Both King's equations 5.7, 5.8 are used:

$$u_{HW} = \left[\frac{E_w^2}{R_w B(T_w - T_c)} - \frac{A}{B} \right]^{1/n}$$

$$u_{HW} = \left[\frac{E_w^2}{B\left(\frac{T_c - T_{ref}}{a_r/\alpha_{el}}\right)} - \frac{A}{B} \right]^{1/n}$$

and also both temperature correction T_c are analyzed, i.e. centerline temperature T_{cl} and average temperature at a certain wall normal position $T_{av}(y)$.

6.1 Turbulence statistic

This section is focused on statistical turbulence analysis of a channel flow at $Re_\tau = 180$. Single point statistics and several correlations coefficients are presented in next paragraphs.

6.1.1 Velocity profile

Logarithmic velocity profile scaled in viscous units is showed in figure 6.1. Agreement with Jimenez channel flow simulation [del Alamo and Jimenez, 2001] and with log law (where coefficients values $\kappa = 0.4$, $B = 5.5$ are suggested

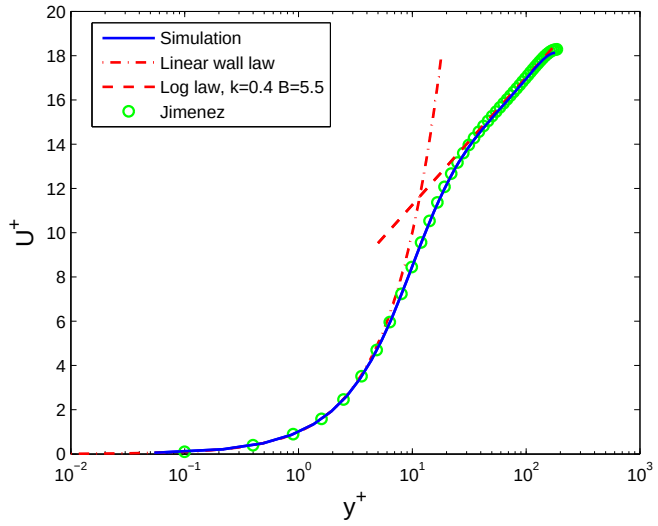

Figure 6.1: Velocity profile in viscous units. Blue solid line is the simulation case, red dot line is log law with $\kappa = 0.4$ and $B = 5.5$ and green circle are data from Jimenez.

by Kim et al. [1987]) is achieved.

This curve is characterized by high gradient close to the wall (inner region), meanwhile it decreases going closer to the centerline (outer region) thus two different dynamics are present. Mean velocity at high Reynolds numbers, is assumed to depend only to viscous scale y^+ inside the inner region [Prandtl, 1925], thus the law of the wall is established:

$$U^+ = \frac{U}{u\tau} = \Phi(y^+) \tag{6.1}$$

With no pressure gradients, in the area between the wall and $y^+ = 5$, a viscous sublayer can be defined. This region is characterized by a linear mean velocity profile with viscous units.

Outer region is scaled with semi-channel height h. Not dimensional wall normal coordinate in this layer becomes $Y = y/h$. Von Karman [1931] formulates velocity defect law, which describes deviation from free-stream behavior in the region far from the wall:

$$\frac{U_\infty - U}{u_\tau} = \Psi(Y) \tag{6.2}$$

In between inner and outer regions, Von Karman assumes the existence of a layer where both laws 6.1 and 6.2 hold simultaneously, i.e. an overlap layer. Matching their derivatives, a lengthscale independence is achieved in order to

Inner layer	$Y < 0.1$
Viscous sublayer	$y^+ < 5$
Outer layer	$y^+ > 50$
Overlap region	$y^+ > 50$ & $Y < 0.1$
Log law region	$y^+ > 30$ & $Y < 0.3$

Table 6.1: Description of region limits inside a channel flow Pope [2000]

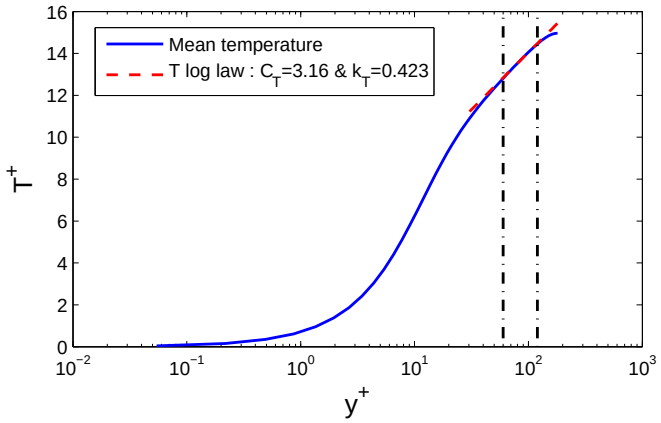

Figure 6.2: Temperature profile in viscous units. Blue solid line is the simulation case and red dash line is temperature log law with $\kappa = 0.423$ and $C_T = 3.16$

satisfy the equivalence, thus:

$$\frac{y}{u_\tau}\frac{\partial U}{\partial y} = y^+\frac{d\Phi}{dy^+} = -Y\frac{d\Psi}{dY} = const.$$

and integrated gives a logarithmic profile, known also as logarithmic law, which seems to hold for a bigger area than overlap layer:

$$\Phi(y^+) = \frac{1}{\kappa}\ln y^+ + B \tag{6.3}$$

$$\Psi(Y) = -\frac{1}{\kappa}\ln Y^+ + C \tag{6.4}$$

where κ is the Von Karman constant.
Coefficient values are still object of studies, since a not perfect agreement between different works is achieved, as for the layers bounds. Classical layer boundaries Pope [2000] are summarized into table 6.1. However these values have been criticized by several studies.

6.1.2 Temperature profile

Temperature profile is showed in figure 6.2. Assuming constant wall temper-

ature, zero mean pressure gradient on x-direction, steady flow, statistical homogeneity on x and z direction, incompressible fluid, constant fluid properties and passive behavior of the heat, a logarithmic law for heat transfer can be also established. Moreover a fully developed heat region is considered and only forced convection has a significant effect.

This law is derived for the first time by Squire 1959 [1]. Here derivation based on the articles of Kader and Yaglom [1972] and Bradshaw and Huang [1995] is followed.

In analogy with the law of the wall for the velocity profile, the temperature distribution close to the wall can be written as:

$$T_w - T(y) = T_\tau \phi(\frac{u^* y}{\nu}, \frac{\nu}{\alpha} \equiv Pr) \tag{6.5}$$

where T_τ is the friction temperature defined in equation 5.4. This law is formulated on the assumption that close to the wall outer scale does not influence the temperature value. Thus the temperature in this region depends only on the heat flux at the wall, $\dot{q}_w$, density ρ, pressure coefficient c_p, friction velocity u_τ, kinematic viscosity ν and heat molecular diffusivity α.

If Reynolds and Péclét numbers are high enough, molecular transfer is negligible compared to the turbulent heat transfer in the outer region, thus the dependance of the temperature defect from ν and α is negligible. This allows the formulation:

$$T(y) - T_1 = \Theta_\tau \phi_1(\frac{y}{L}) \tag{6.6}$$

where L is the outer length scale, e.g. semi channel height and Θ_1 is the centerline temperature.

For high enough Reynolds and Péclét numbers, the regions where the laws 6.5 and 6.6 are valid, overlap. Thus a simpler formulation can be achieved, in analogy with the velocity case:

$$\frac{T_w - T(y)}{T_\tau} = \frac{1}{\kappa_T} \ln(\frac{u_\tau y}{\nu} \equiv y^+) + C_T(Pr) \tag{6.7}$$

Following Bradshaw indications, this law should be valid for large y^+ and $y^+ Pr$ (around $y^+ Pr > 30 - 50$). The outer limit of overlap region depends on the thickness of temperature profile δ_T.

These conditions are more restrictive than the ones for the velocity profile. In fact, in the latter case, the inner boundary for log law region is $y^+ > 30 - 50$, which is more reliable for Prandtl numbers smaller than one. Moreover the

[1] The first paper where it was written about logarithmic law temperature seems to be Squire - An extended Reynolds analogy, *Proc.6th Midwestern Confer. Fluid Mech.*, pp.16-33, Univ. of Texas. Austin (1959).

layer thickness (or semi channel height) δ is larger than the thermal one. Using a least square method, simulation coefficients are fixed to $C_T = 3.16$ and $\kappa_T = 0.423$.

6.1.3 Velocity and temperature moments

As seen in paragraph 2.2.1, statistical moments are derived from probability density function. Figure 6.3 shows mean value of velocity (left) and temperature (right), together with probability density function, pdf. Temperature pdf exhibits a wide width similar to velocity pdf.

First statistical moment analyzed are root mean square for velocity, figure 6.4(a) and temperature 6.4(b). The former statistic is compared with del Alamo and Jimenez [2001]. A good agreement is achieved, with a small deviation of 0.33% on the root mean square peak, at $y^+ \approx 15$.

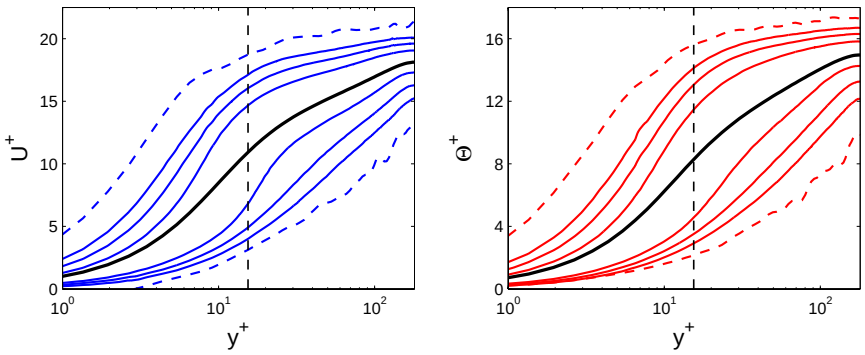

Figure 6.3: *Left* Black solid line represents inner scaled velocity profile, blue solid lines pdf of instantaneous streamwise velocity: contour levels represent confidence interval for 50, 10, 1 %, dash blue lines are the extreme values of pdf. *Right* Same as *Left* figure, however, for the passive scalar (temperature). Location of the widest pdf, i.e. $y^+ \approx 15$, is indicated through vertical dashed line

Skewness and flatness of velocity (left) and temperature (right) are represented in figure 6.5. Skewness, both for velocity and temperature, shows a positive peak around $y^+ = 6$ meanwhile a negative peak is only present on velocity skewness ($y^+ \approx 28$). However both skewness show a negative value after 12 viscous length for velocity and 16 for temperature

Flatness has a peak close to the wall, around 17 viscous length for velocity and 19 for temperature.

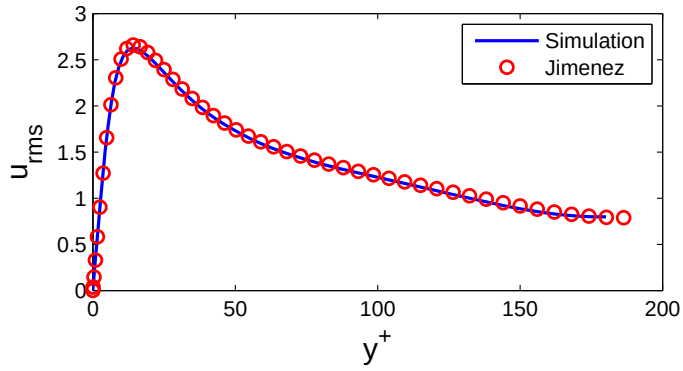

(a)

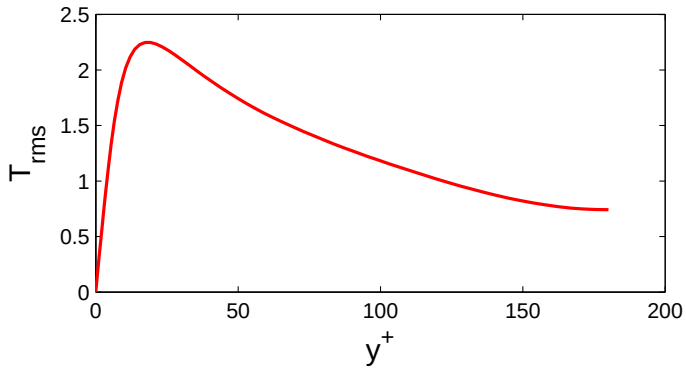

(b)

Figure 6.4: *A*: Blue line - streamwise velocity rms, red circle streamwise velocity from Jimenez; *B*: Red line - temperature rms

6.1.4 Correlation

Streamwise and spanwise correlations close to the wall ($y^+ \approx 15$) are analyzed in this section. Classical formula 6.8 is used to evaluate different correlation coefficients around the wall normal position of rms peak:

$$\zeta_{i,j}(\boldsymbol{x}, \boldsymbol{r}) = \frac{\overline{\alpha_i(\boldsymbol{x})\alpha_j(\boldsymbol{x}+\boldsymbol{r})}}{\overline{\alpha_i^2}\,\overline{\alpha_j^2}} \tag{6.8}$$

where α_i, α_j can assume the value of streamwise, spanwise, wall normal velocity fluctuation or temperature fluctuation.

Correlation of velocity quantities, $u'u'$, $u'v'$, $v'v'$ and $w'w'$ are shown in figure 6.6. Converge to zero value is not achieved by streamwise velocity correlation, thus the domain used is not large enough to solve correctly flow structures. However, this characteristic does not influence the key point of this work, i.e. temperature influence on hot wire measures.

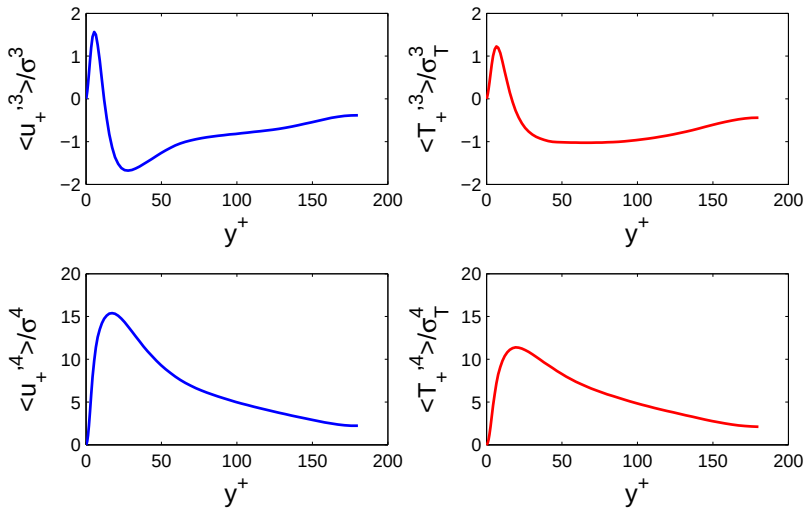

Figure 6.5: Skewness value of streamwise velocity (top left) and temperature (top right), flatness of streamwise velocity (bottom left) and temperature (bottom right)

Cross correlations between velocity and passive temperature are shown in figure 6.7. It is possible to note a high correlation between streamwise velocity and temperature. This characteristic is one of the starting point of this work. In effect velocity fluctuations generate temperature fluctuations that influence the hot wire response. Moreover a correlation between temperature and wall normal velocity is also present.
Figure 6.8 shows the similarity among correlations $T'T'$, $u'u'$ and $T'u'$. Spanwise correlations are provided in figures 6.9, 6.10 and 6.11. Information about structures span dimensions can be achieved by these kind of correlations. A similar behavior is showed in span direction, as well for streamwise one, by $u'u'$, $T'T'$ and $T'u'$ correlations.

6.2 Temperature influence on hot wire measurements

Temperature influence on the velocity sensed by hot wire is evaluated through King's law equation, applied on data obtained from simulation. Firstly equation 5.7 is used, after that eq. 5.8 is considered.
Real temperature profile are generated fixing wall temperature to 303.15 K (30° C), meanwhile centerline temperature is swept between 303.15 K and 309.15 K (30° $C \div$ 36° C), as shown in figure 6.12. This approach generates differ-

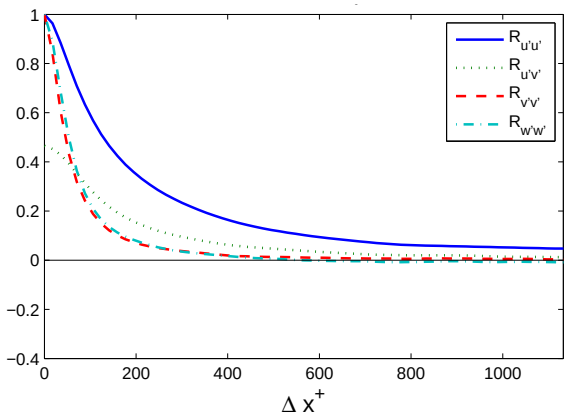

Figure 6.6: Streamwise velocity correlation: · blue solid line $u'u'$ correlation, · green dots $u'v'$, · red dashed line $v'v'$, · cyan dash dot $w'w'$

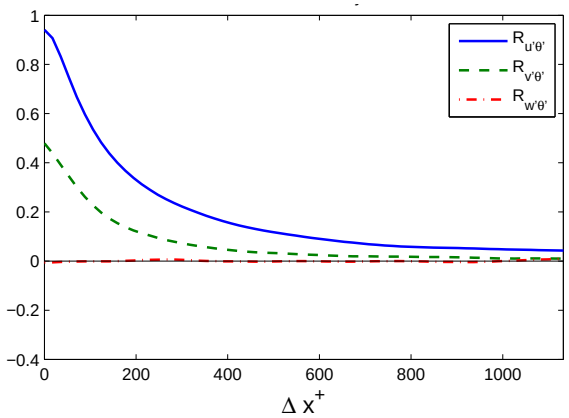

Figure 6.7: Streamwise velocity - temperature correlation: · blue solid line $u'T'$ correlation, · green dashed line $v'v'$, · red dash dot line $w'T'$

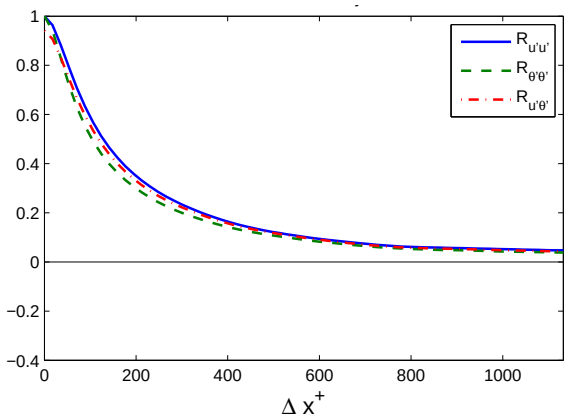

Figure 6.8: Streamwise velocity correlation: · blue solid line $u'u'$ correlation,· green dashed line $T'T'$ and · red dash dot line $u'T'$

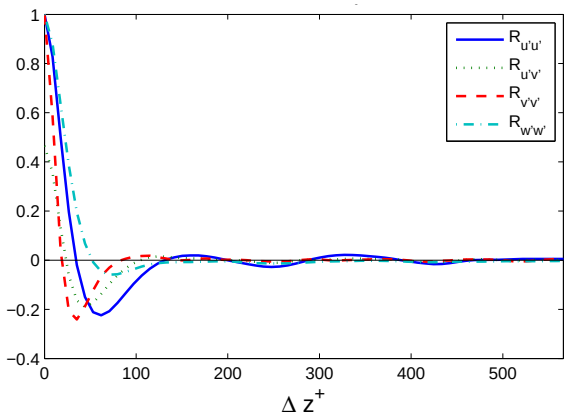

Figure 6.9: Spanwise velocity correlation: : · blue solid line $u'u'$ correlation, · green dots $u'v'$, · red dash line $v'v'$, · cyan dash dot $w'w'$

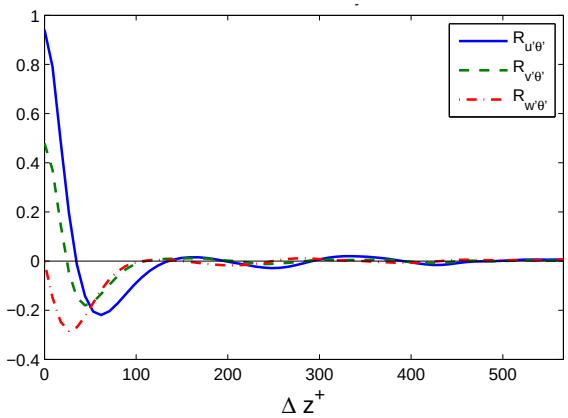

Figure 6.10: Spanwise velocity-temperature correlation: · blue solid line $u'T'$ correlation, · green dashed lined $v'v'$, · red dash dot line $w'T'$

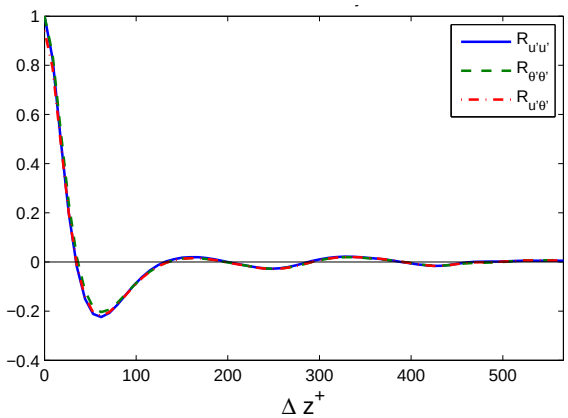

Figure 6.11: Spanwise velocity correlation: · blue solid line $u'u'$ correlation,· green dashed line $T'T'$ and · red dash dot line $u'T'$

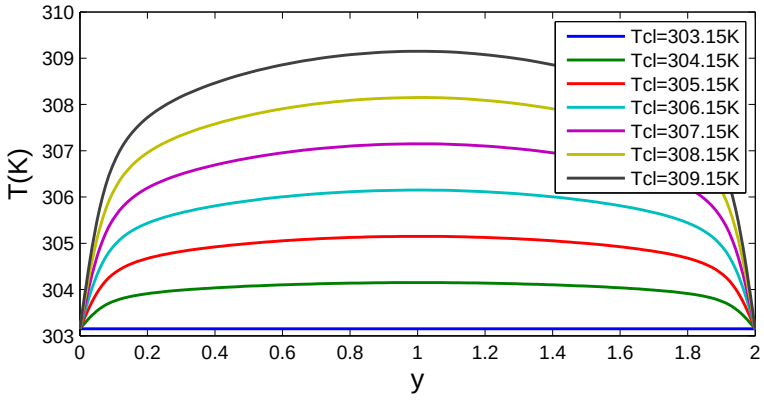

Figure 6.12: Dimensional temperature profiles for different ΔT

ent temperature profiles, characterized by a own wall - centerline temperature difference and a own heat flux at the wall. However these two quantities are directly related.
Using the linear property of derivation and not dimensional temperature expression:

$$T^* = \frac{T - T_w}{T_{cl} - T_w}$$

a relation for dimensional temperature flux can be established:

$$\frac{dT}{dy} = \frac{d(T^* \Delta T + T_w)}{dy} = \Delta T \frac{dT^*}{dy} \tag{6.9}$$

Since dT^*/dy is the same for each curve, a linear dependence between temperature flux on the wall and temperature difference between centerline and wall temperature is present.
In following analysis, terms sensed and measured velocity are referred to velocity computed after King's law is applied, meanwhile statement "from simulation" is referred to the numerical result from simulation, i.e. the "correct" value to achieve with the virtual measuring of the hot wire.

6.2.1 First method analysis

In this section hot wire's voltage is evaluated through equation 4.9 meanwhile sensed velocity through equation 5.7. Both temperature correction T_c are made, i.e. centerline temperature first and mean temperature profile after.

Centerline temperature correction Using a centerline temperature correction, averaged sensed velocity shows a certain displacement from the computed

velocity profile. Figure 6.13 represents mean velocity profile where all the curves are not dimensionalized by the same viscous unit u_τ, derived from the simulation. Obviously mean profile shows the largest percentage error close to the wall.

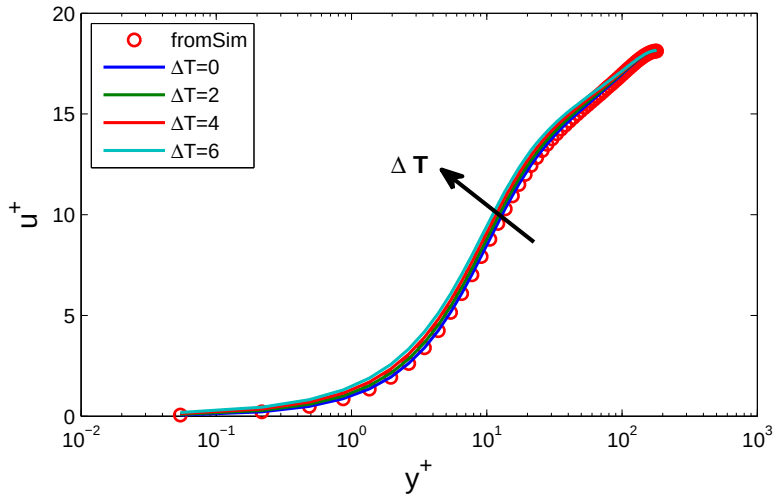

Figure 6.13: Velocity profile in viscous units for different ΔT. Temperature correction is performed through centerline temperature and u_τ from simulation is used to perform not dimensionalization

The reason is due that close to the wall, the largest temperature difference with centerline temperature is achieved. Moreover increasing the temperature difference, sensed mean velocity increases.
Considering for each curve own viscous unit, $u_{\tau,j}$ with $j = 1, ..., 7$, behavior changes. In fact, since sensed velocity has a different behavior close to the wall, friction velocity, thus Re_τ, changes due to its dependence to wall viscous stress. Figure 6.14 is obtained not dimensionalizing each curve for each own viscous velocity. Here maximum percentage error is shifted to 8 viscous lengths and behavior of sensed velocity, as temperature function, is changed. Increasing wall heat flux measured viscous velocity decreases its value due to the higher viscous stress at the wall. Moreover linear wall law is not followed by measured velocities. This can be interpreted as a consequence of how temperature correction is performed, i.e. using centerline temperature.
Root mean square analysis are also analyzed on previous cases. As for velocity profile, if velocity rms not dimensionalization is performed using simulated friction velocity, largest error is obtained close to the wall, where sensed velocity rms is increasing with larger ΔT, see figure 6.15. However, after around 1 viscous unit from the wall, this behavior is reverted and smaller rms is measured increasing ΔT. Obviously error is larger for higher temperature difference.

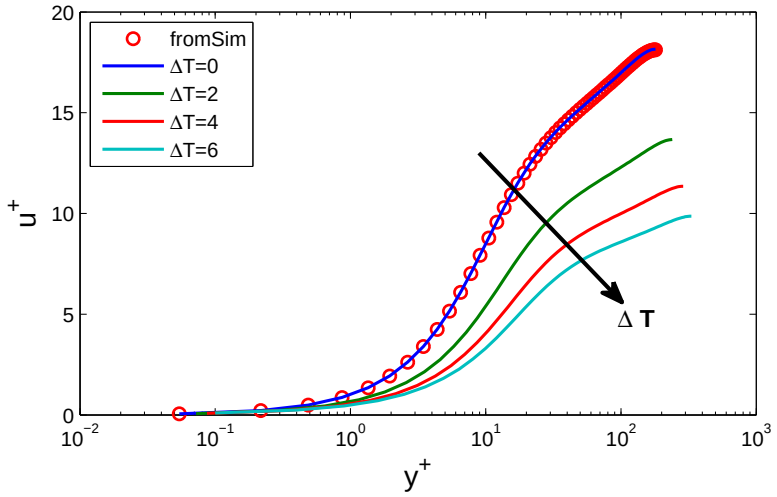

Figure 6.14: Velocity profile in viscous units for different ΔT. Temperature correction is performed through centerline temperature and adimensionalization is performed through the proper u_τ of each curve

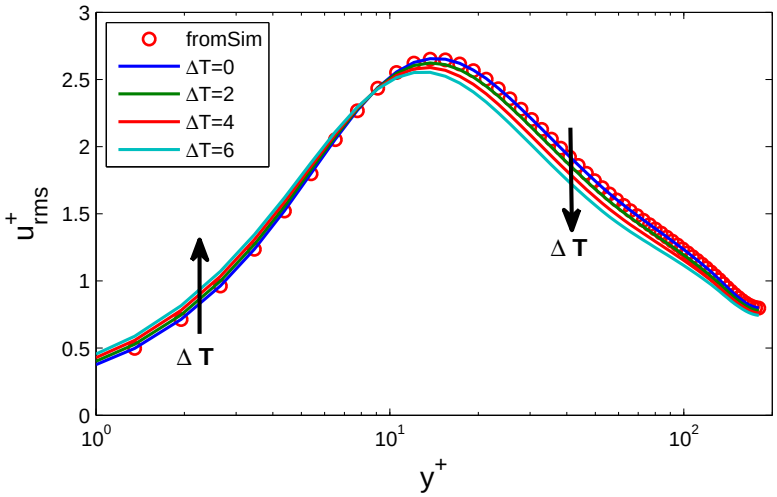

Figure 6.15: Streamwise velocity rms in viscous units for different ΔT. Temperature correction is performed through centerline temperature and u_τ from simulation is used to perform not dimensionalization

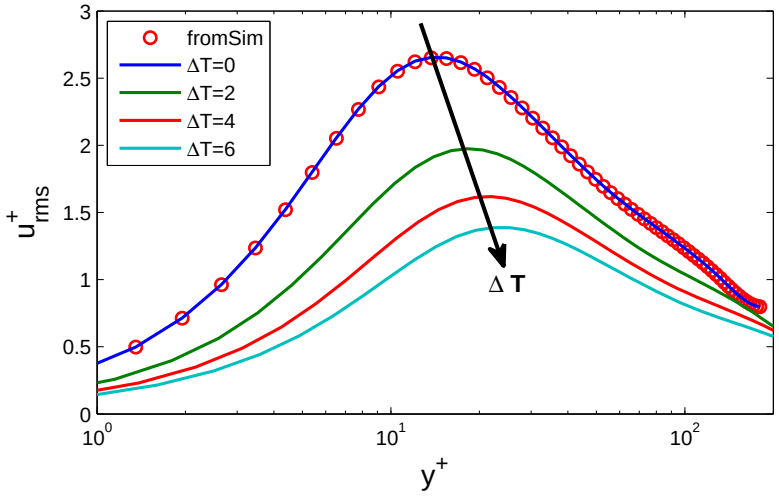

Figure 6.16: Streamwise velocity rms in viscous units for different ΔT. Temperature correction is performed through centerline temperature and adimensionalization is performed using own u_τ from each curve

Performing not dimensionalization of rms by own friction velocity on each curve, see figure 6.16, smaller rms are measured increasing temperature difference. Furthermore, rms peak moves farther from the wall, i.e. from around 15 y^+ to around 25 y^+.

Mean temperature correction Temperature correction is performed through mean temperature profile, thus each wall normal position is corrected with the proper mean temperature at that height. This correction provides good results when measured mean velocity is computed, see figure 6.17. In fact agreement is achieved for curves with different ΔT. Maximum percentage error is smaller than 1%. This mean velocity behavior yields to close values of friction velocity, thus to almost equal Re_τ, among different cases. Hence only cases with not dimensionalization performed by own friction velocity are showed.
With this temperature correction method, a good improvement on measured rms is also achieved. As shown in figure 6.18, if temperature difference between wall and centerline is increasing, rms value is decreasing. The inner plot in figure 6.18 shows the percentage error on the peak value, which increases almost linearly with ΔT.

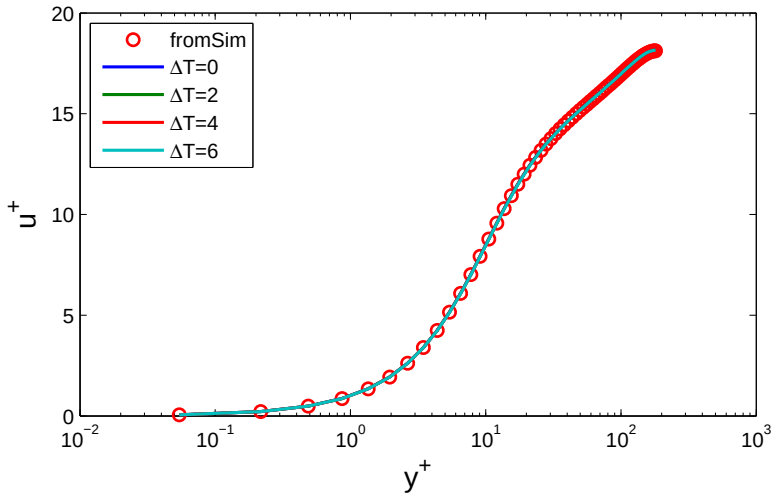

Figure 6.17: Velocity profile in viscous units for different ΔT. Temperature correction is performed through mean temperature and adimensionalization is performed through the proper u_τ of each curve

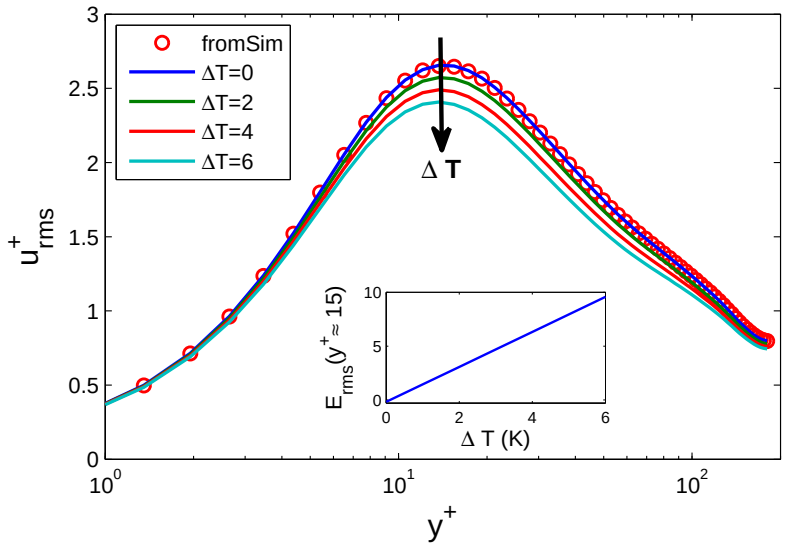

Figure 6.18: *Main* Streamwise velocity rms in viscous units: red circles from simulation, solid lines sensed velocity with a different ΔT. Correction temperature fixed to mean temperature values. *Inner* Relative streamwise velocity rms percentage error at the inner peak, $y^{+}{\approx}15$

6.2.2 Second method analysis

Here hot wire's voltage is evaluated through equation 5.6 meanwhile sensed velocity through equation 5.8. Parameters are fixed with values showed in paragraph 5.4, i.e.:

- $a_r = 1.1$
- $\alpha_{el} = 4.782 \cdot 10^{-3}$ ([2])

Here velocity not dimensionalization is performed using always the friction velocity of each curve. Results are close to the ones achieved in the previous case. The reason lie on the possibility to derive in the same way these two versions of King's law. This method is also used for analysis in next sections, since it contains experimental parameters which are already known by experimentalist. Here both temperature correction T_c are made, i.e. centerline temperature first and mean temperature profile after.

Centerline temperature correction Centerline temperature is used to correct equation 5.8. Figure 6.19 shows mean velocity profile, meanwhile figure 6.20 shows streamwise velocity rms.

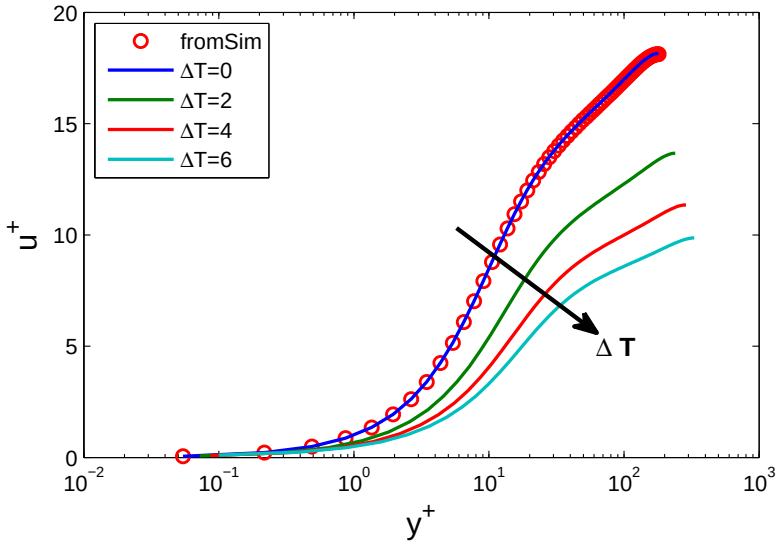

Figure 6.19: Streamwise mean velocity profile in viscous units for different ΔT. Temperature correction is performed through centerline temperature and adimensionalization is performed using own u_τ from each curve. King's equation with experimental parameters is used.

[2] $\alpha_e l$ value is computed using the relation $a_r = \alpha_{el}\ (T_w - T_{ref})$ where $T_{ref} = 0$ and $T_w = 503.15\ K\ (230\ ^\circ C)$

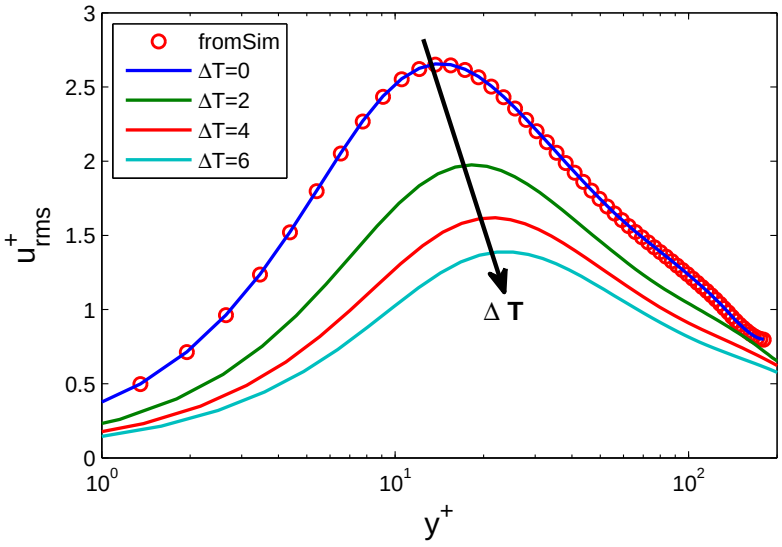

Figure 6.20: Streamwise velocity rms in viscous units for different ΔT. Temperature correction is performed through centerline temperature and adimensionalization is performed using own u_τ from each curve. King's equation with experimental parameters is used.

Mean temperature correction Mean temperature is used to correct equation 5.8. Figure 6.21 shows mean velocity profile, meanwhile figure 6.22 shows streamwise velocity rms.

6.3 Experimental parameters analysis

King's law 5.6 is used to evaluate experimental parameters effects on the measured sensed velocity. Each analysis is performed keeping constants all the other parameters. Moreover temperature difference between wall and centerline is fixed to $2K$ and mean temperature is used as temperature correction.

6.3.1 Temperature coefficient α_{el} analysis

Over heat ratio is fixed to a value of 1.1 meanwhile temperature coefficient of electrical resistivity is swept between a range of $0.0015 < \alpha_{el} < 0.005$.
Velocity profile is not affected by temperature coefficient value when mean temperature is used to correct data. Streamwise velocity rms, is influenced by the value of temperature coefficient of resistivity (figure 6.23). Rms value shows a decreasing of its value when temperature coefficient α_{el} is increased.

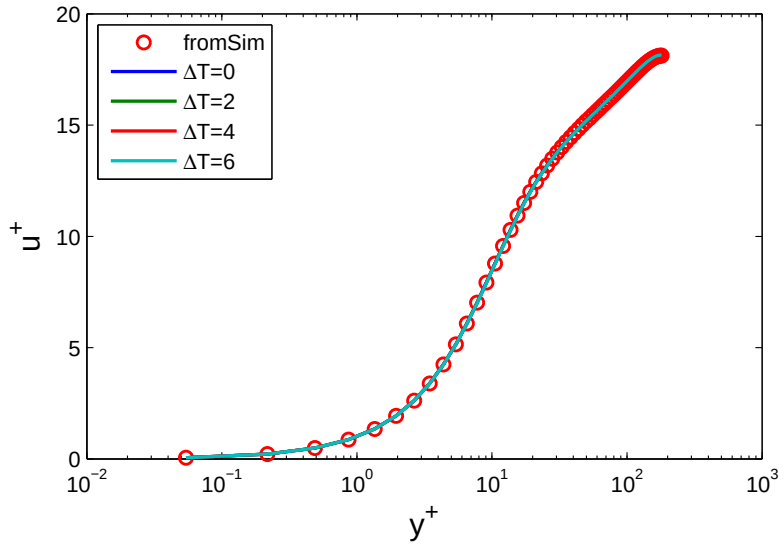

Figure 6.21: Velocity profile in viscous units for different ΔT. Temperature correction is performed through mean temperature and adimensionalization is performed using own u_τ from each curve. King's equation with experimental parameters is used.

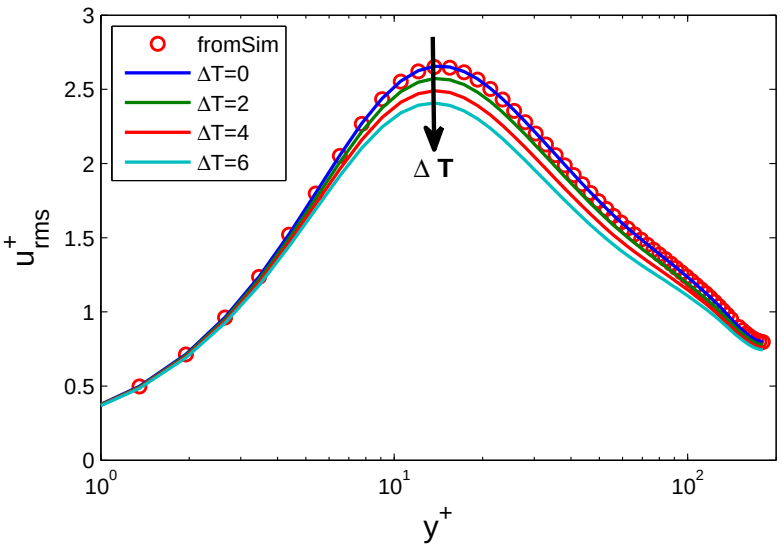

Figure 6.22: Streamwise velocity rms in viscous units for different ΔT. Temperature correction is performed through mean temperature and adimensionalization is performed using own u_τ from each curve. King's equation with experimental parameters is used.

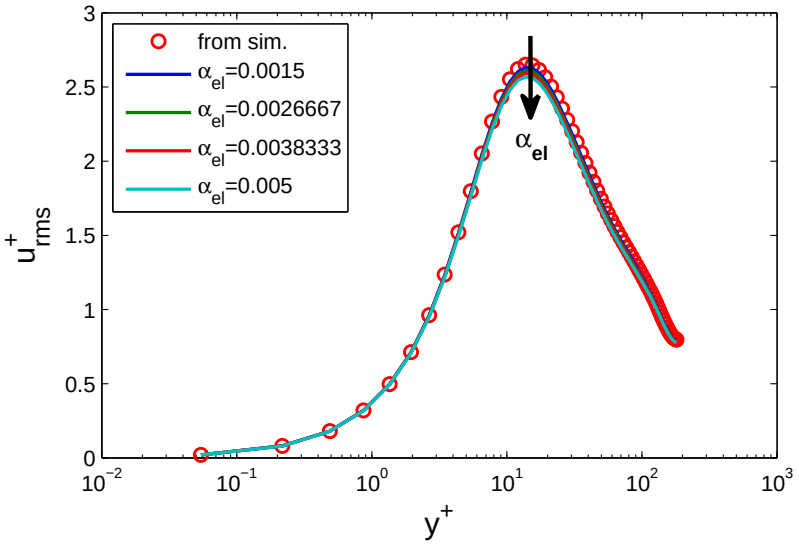

Figure 6.23: Streamwise velocity rms in viscous units

6.3.2 Over heat ratio analysis

Temperature coefficient of electrical resistivity is fixed to 0.004872, while over heat ratio varies in between $0.5 < a_r < 1.5$. Sweeping over heat ratio, like for temperature coefficient, mean sensed velocity does not show any evident modification of its profile. Root mean square of streamwise velocity, instead, shows an increasing of its value when overheat ratio has a larger value, see figure 6.24

6.4 Spatial averaging

The aim of this section is to investigate one other issue of hot wire measuring: spatial averaging. As already explained, wire is usual larger than smaller eddies that are contained in the flow. This means that different point of the wire are characterized by different velocity fluctuations. Thus the measured voltage is the result of a spatial averaging over the entire wire.

On mean velocity this phenomena does not produce any visible effect. Anyway rms are strongly affected by spatial averaging. Figure 6.25 shows rms velocity once a top hat filter is applied on streamwise velocity along spanwise direction, in order to reproduce wire effect. Moreover, percentage rms error at the rms peak value, $y^+ \approx 15$, obtained after filter is applied on data from simulation, is showed into the small box inside figure 6.25.

In order to evaluate combined effect of spatial averaging with temperature in-

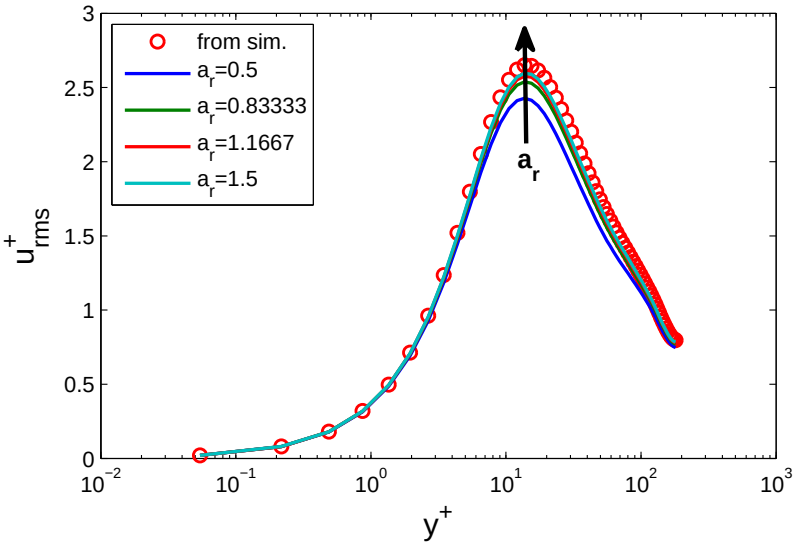

Figure 6.24: Streamwise velocity rms in viscous units

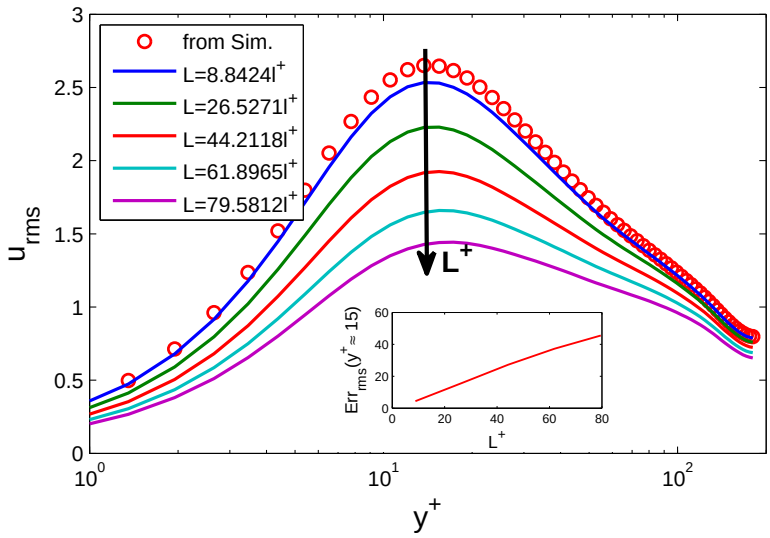

Figure 6.25: *Main* Streamwise velocity rms in viscous units: red circles from simulation, solid lines after spatial averaging with a top hat filter with length from 8.8 L^+ to 79.58 L^+. *Inner* Relative streamwise velocity rms percentage error at the inner peak, $y^{+}{\approx}15$

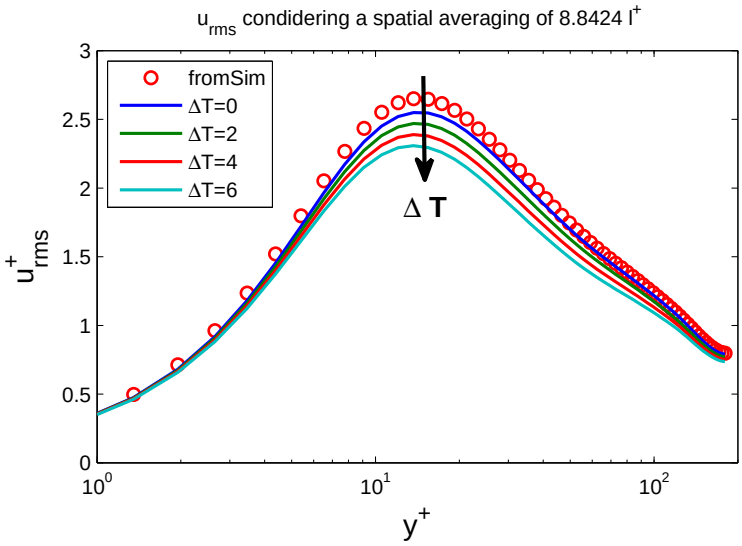

Figure 6.26: Streamwise velocity rms in viscous units: · red circles, from simulation; · solid lines, with filter L^+ =8.8 and for different ΔT

fluence on hot wire measurements, top hat filter is applied on hot wire voltage data after the latter is computed through King's law 5.6. After that streamwise velocity is computed by the use of 5.8. Results are shown in paragraph 6.4.1.

6.4.1 Combined effect of temperature and spatial averaging

Effects of both temperature fluctuations and spatial averaging are analyzed in this paragraph. Figures 6.26, 6.27, 6.28 show temperature influence on filtered data with length of the filter (thus wire length) of 8.8 L^+, 26 L^+ and 44 L^+ respectively. It is possible to note that both increasing wire length and wall - centerline temperature difference, the total error is increasing. An overview about total error and temperature influence error at rms peak is provided by figure 6.29. In the upper figure is possible to observe an almost linear total error increasing with larger wire lengths. This is achieved for all different ΔT cases. This error is made up by two contributions: spatial averaging and temperature fluctuation errors. From the bottom figure it is possible to observe the percentage of temperature fluctuations errors in relation with the total one:

$$\frac{E_{\Delta T}}{E_{tot}} = \frac{u_{rms} - u_{rms,L^+=0}}{u_{rms}} \frac{u_{rms}}{u_{rms} - u_{rms,totErr}}$$

Considering for example $\Delta T = 2K$ case, error due to temperature fluctuation is around 40% of the total error with a wire length of 10 l^+, $\approx$ 20% with a

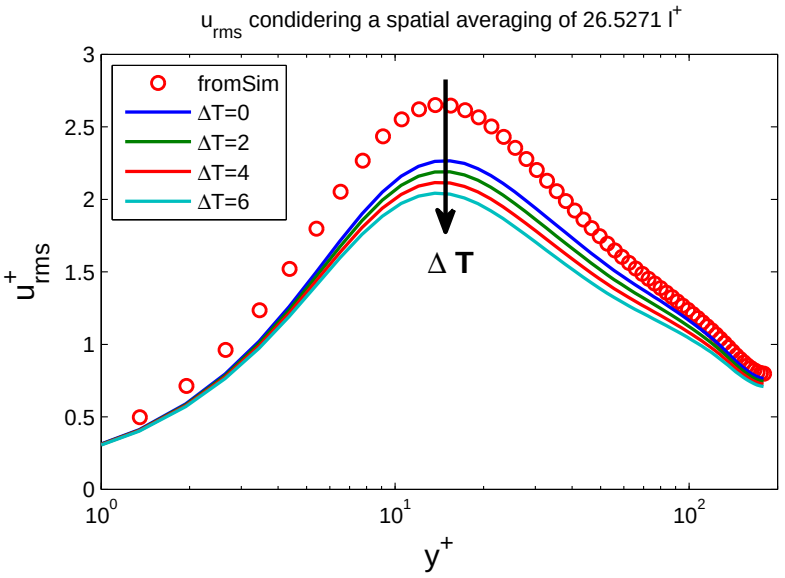

Figure 6.27: Streamwise velocity rms in viscous units: · red circles, from simulation; · solid lines, with filter L^+ =26 and for different ΔT

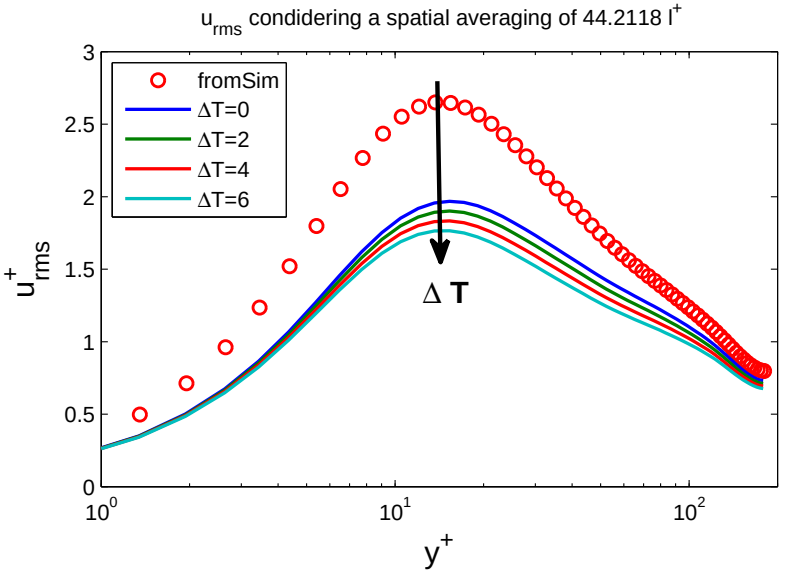

Figure 6.28: Streamwise velocity rms in viscous units: · red circles, from simulation; · solid lines, with filter L^+ =44 and for different ΔT

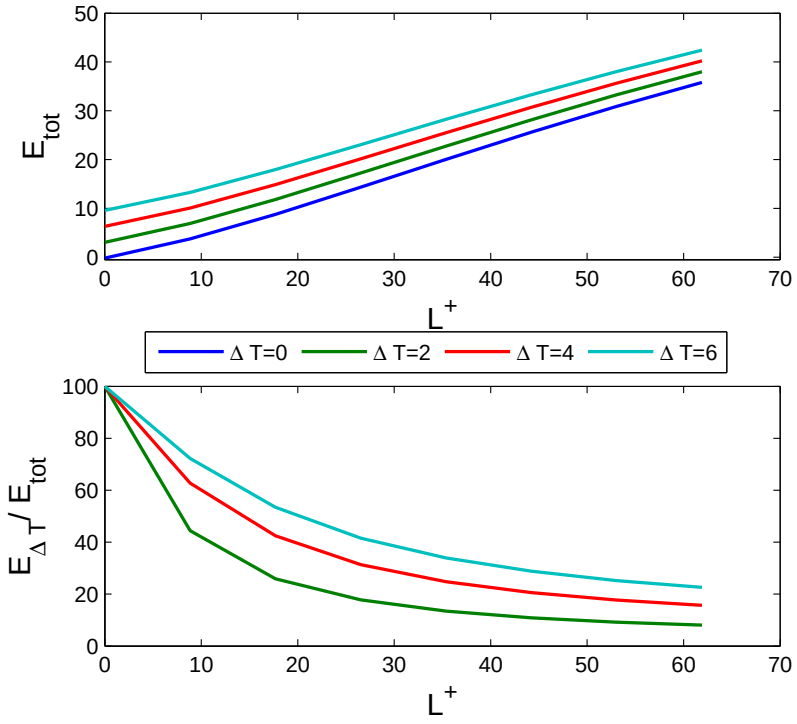

Figure 6.29: *Up*: Percentage total error (spatial averaging and temperature influence) in function of filter length for different ΔT (blue $\Delta T = 0$, green $\Delta T = 2$, red $\Delta T = 4$, cyan $\Delta T = 6$); *Down* Relative percentage error between temperature influence error and total error in function of filter length, same color as figure above.

wire length of 20 l^+ and $\approx 10\%$ of the total with a wire length of 45 l^+. These relative percentage errors increase for larger ΔT.Thus temperature influence is an important feature to take care above all when wire length is small and for high ΔT.

According to Ligrani and Bradshaw [1987], wire length should be smaller than 20 l^+ in order to reduce spatial averaging error. At these wire lengths, temperature fluctuation influence is not negligible if a correct measure is aimed.

In next chapter some methods to measure instantaneous temperature and correct velocity values are proposed.

Chapter 7

Correction methods

Considering King's equation 5.6, three variables are present: hot wire voltage E^2, streamwise velocity u and temperature T. Voltage is the output of the hot wire, thus it is known. However it is related with two variables, temperature and velocity, but only one equation is provided: this means that problem cannot be solved directly since unknowns are more than equations.
A method to overcome this issue, is to use a cold wire together with the hot wire: cold wire provides the required temperature field which is necessary to calculate velocity using the King's law equation and the output voltage from the hot wire. However cold wire is characterized by a lower frequency resolution than hot wire thus it is not possible to measure velocity and temperature simultaneously. This means that it is not possible to correct instantaneously the King's law for computing the velocity, causing a velocity error. The result is that a combination of hot and cold wire cannot be used to properly correct the temperature influence on velocity measurements [1].
This is the reason to move the focus to temperature measure and to temperature error correction in this chapter. Three methods are analyzed, i.e. two probes method, correlation between temperature and velocity fluctuation and temperature log law.

7.1 Two probes methods

Another way to solve the problem of instantaneous temperature measurements is to use two hot wires with a certain span displacement, in order to have two unknowns, velocity and temperature, and two equations, given by King's law. This method is well explained in [Bruun, 1995, chap.7].

[1] In the last chapter was showed two ways to correct King's law equation, i.e. centerline temperature and mean temperature. Best results were achieved using the latter method.

In order to have a solution, the two equations cannot be equal: this is achieved using a different over heat ratio for probes. Hence system 7.1 is obtained:

$$\begin{cases} u = \left[\frac{E_1^2}{B\left(1-\frac{T-T_{ref}}{a_{r,1}/\alpha_{el}}\right)} - \frac{A}{B} \right]^{1/n} \\ u = \left[\frac{E_2^2}{B\left(1-\frac{T-T_{ref}}{a_{r,2}/\alpha_{el}}\right)} - \frac{A}{B} \right]^{1/n} \end{cases} \tag{7.1}$$

This system is obtained making a strong hypothesis: the two probes are assumed to behave similarly, i.e. coefficients A, B, n and α_{el} are the same for both probes. This assumption is not correct in reality, however here it is made to simplify the approach and to have an idea about the results obtained with this method. In order to solve the system 7.1, another strong assumption has to be done: same velocity and same temperature is sensed by both probes despite the span displacement.
Making an equivalence between the two equation in system 7.1, the following result is obtained:

$$\frac{E_1^2 a_{r,1}}{a_{r,1} - T\alpha_{el}} = \frac{E_2^2 a_{r,2}}{a_{r,2} - T\alpha_{el}}$$

which solved for temperature gives:

$$T = \frac{\left(E_1^2 - E_2^2\right) a_{r,1} a_{r,2}}{\alpha_{el}\left(a_{r,1} E_1^2 - a_{r,2} E_2^2\right)} \tag{7.2}$$

meanwhile velocity can be computed from one of the equation of system 7.1.
The two probes are placed at zero distance firstly, meanwhile span displacement is increased in the next analysis.

7.1.1 Zero displacement results

Zero displacement between the probes is fixed. This choose is not reliable in reality since it is not possible to overlap the two probes. Anyway this choice is made in order to check the formula used.
Following parameters are chosen for this analysis:

- $A = 0.000085$
- $B = 0.000045$
- $n = 0.5$
- $\alpha_{el} = 4.782 * 10^{-3}$
- $\Delta T = 2\ K$

- $T_{wall} = 30\ K$
- $T_{w,1} = 150 \longrightarrow a_{r,1} = 0.7173$
- $T_{w,2} = 270 \longrightarrow a_{r,2} = 1.2911$

High difference between wire temperatures is chosen in order to avoid numerical errors.
From figure 7.1 it is possible to observe velocity and rms profile, for both velocity and temperature. Matching between results from simulation and the two probes method is perfectly achieved when the two probes are placed in the same point.

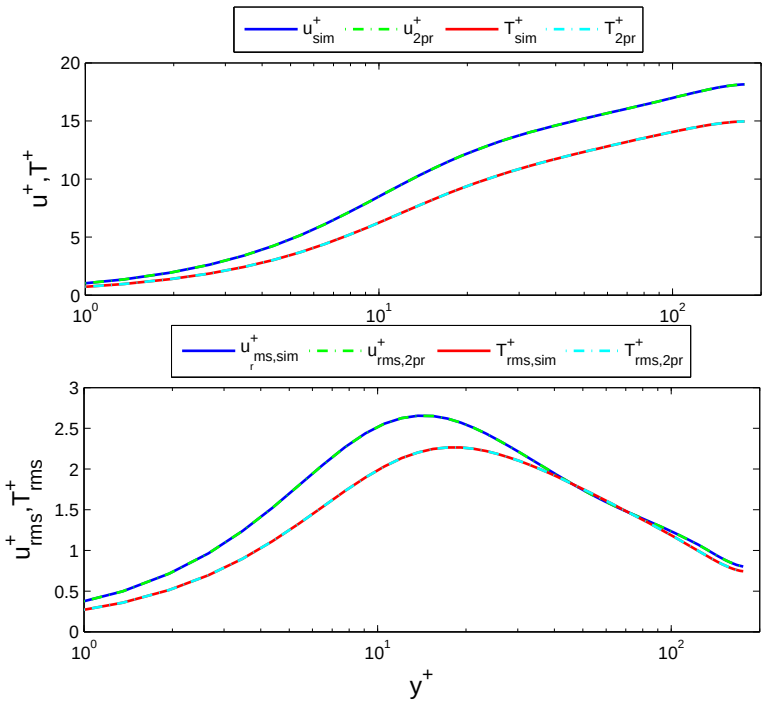

Figure 7.1: *Up*: Mean streamwise velocity profile from simulation (blue solid line) and from two probes evaluation (dash dot green line) and mean temperature profile from simulation (red solid line) and from two probes evaluation (dash dot cyan line); *Down*: Rms profiles, line colors referred to the same quantity as before

7.1.2 Results with span displacement between probes

Same formulation as before is now used to compute velocity and temperature for the case when the two probes are placed with a certain span displacement. Figure 7.2 shows mean velocity profiles, considering $\Delta z = 0$, 8.8 L^+ and 88 L^+.

Errors on velocity profiles are achieved already for span displacement equals to 8.8 l^+, meanwhile for a large displacement, 88.8 y^+, after the near wall peak this method fails to reproduce the flow dynamic, with a smaller velocity measured. Velocity rms can be observed in figure 7.3. Formulation used to solve sys-

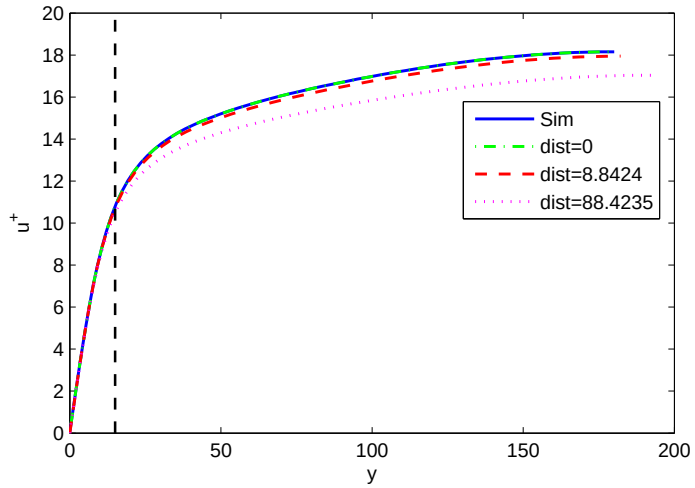

Figure 7.2: Mean velocity profile: - blue solid line, from numerical simulation; - green dash dot, from two probes evaluation at 0 distance; - dash red line, from two probes evaluation at 8.8 l^+ distance; - dots magenta, from two probes evaluation at 88.4 l^+ distance. Black dash line indicates near wall peak at ≈ 15 l^+

tem 7.1, lacks to capture the dynamics of the flow. Even larger errors are obtained for temperature profile and rms.
These errors are due to the small size of structures that breaks the strong assumption made: same velocity and temperature sensed by the two hot wires.

7.1.3 Future ideas about two probes method

Further investigations has to be performed in order to find a correction term that take in account the instantaneous difference of velocity and temperature between the probes.
A possible way to solve this problem, is to average the two equations in system 7.1. In fact the system 7.3 obtained, is characterized by same mean velocity

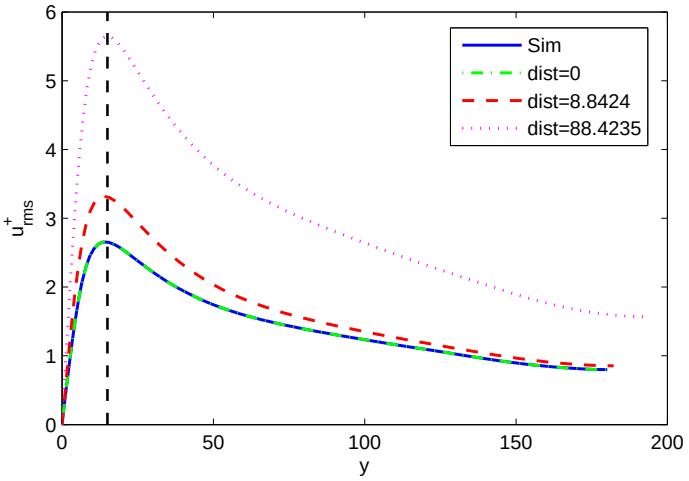

Figure 7.3: Streamwise velocity rms: - blue solid line, from numerical simulation; - green dash dot, from two probes evaluation at 0 distance; - dash red line, from two probes evaluation at 8.8 l^+ distance; - dots magenta, from two probes evaluation at 88.4 l^+ distance. Black dash line indicates near wall peak at ≈ 15 l^+

and mean temperature.

$$\begin{cases} \overline{u_1} = U = \overline{\left[\frac{E_1^2}{B\left(1-\frac{T_1-T_{ref}}{a_{r,1}/\alpha_{el}}\right)} - \frac{A}{B}\right]^{1/n}} \\ \overline{u_2} = U = \left[\frac{E_2^2}{B\left(1-\frac{T_2-T_{ref}}{a_{r,2}/\alpha_{el}}\right)} - \frac{A}{B}\right]^{1/n} \end{cases} \tag{7.3}$$

A satisfactory mathematical solution for the system 7.3 was not possible to be achieved by the author.

7.2 Velocity - temperature correlation

Temperature and velocity are characterized by high correlation. This result is used in this chapter to reconstruct the temperature signal. Experimentally a hot wire probe with a thermocouple can be used to perform this method, or a combined hot and cold wire works as well.

The idea is to use velocity fluctuations in substitution of temperature ones. However from figure 5.1, it is possible to observe that correlation between velocity and temperature decreases going farther from the wall, meanwhile is higher close to it. The following temperature correction is proposed in order to evaluate the

efficacy of the previous reasoning:

$$T_c = T_m + \Delta T * u' * \frac{< u'T' >}{\sqrt{u'^2}\sqrt{T'^2}} \tag{7.4}$$

Results are showed in figure 7.4 for velocity profile, and figure 7.5, for rms. Ve-

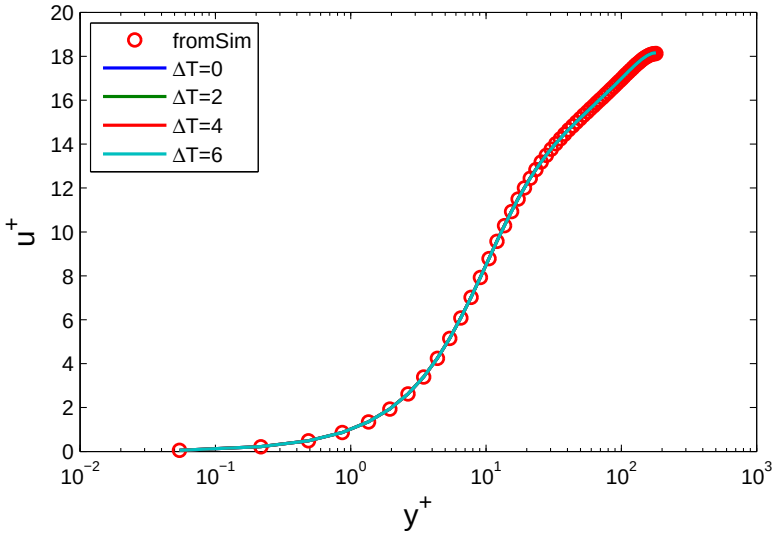

Figure 7.4: Mean velocity profile with temperature correction made by the summation of average temperature and scaled velocity fluctuation. - Red circles, from simulation; - blue line, sensed velocity from hot wire with $\Delta T = 0$; - green line, sensed velocity from hot wire with $\Delta T = 2$; - red line, sensed velocity from hot wire with $\Delta T = 4$; - cyan line, sensed velocity from hot wire with $\Delta T = 6$

locity profile is not affected by this correction type, keeping the matching with the real curve that was already achieved using the only average temperature. Rms shows instead a great improvement in comparison with average temperature correction case, see inner plot inside 7.5. A maximum error of around 2.18% at $y^+ \approx 15$ is obtained with a $\Delta T = 6$.

However this correction is performed using two quantities that are not known a priori, i.e. real streamwise velocity fluctuations and cross moment coefficient between velocity and temperature fluctuations.

The idea to overcome the impasse, is to solve twice the reversed King's law equation 5.8. As first step King's law is solved using mean temperature for correction. This step is required in order to obtain a streamwise velocity field, from which is possible to compute velocity fluctuations. In the second step, temperature correction is built by the summation of the mean temperature profile and

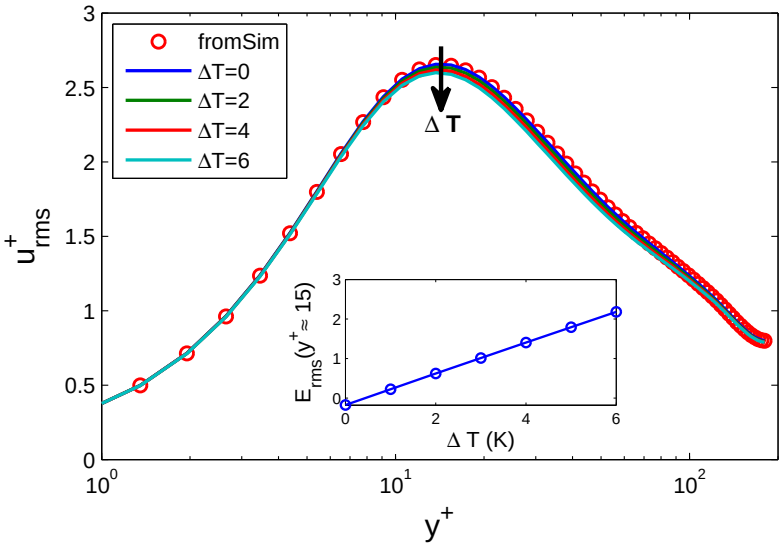

Figure 7.5: *Main* Velocity rms with temperature correction made by the summation of average temperature and scaled velocity fluctuation. - Red circles, from simulation; - blue line, sensed velocity from hot wire with $\Delta T = 0$; - green line, sensed velocity from hot wire with $\Delta T = 2$; - red line, sensed velocity from hot wire with $\Delta T = 4$; - cyan line, sensed velocity from hot wire with $\Delta T = 6$. *Inner* Percentage error between sensed and simulated velocity, at $y^+ = 15$

a proper scaled velocity fluctuation [2], derived from the previous application of King's law.

Summarizing, the steps performed are:

- Computing the output voltage from the wire, using King's law, eq. 5.6, with real temperature and velocity field
- Computing sensed velocity, through eq. 5.8, with output voltage and mean temperature as temperature correction T_c
- Calculating Re_τ and streamwise velocity fluctuation from the sensed velocity field, and T_τ from the mean temperature
- Create the new correction temperature:

$$T_c = \overline{T} + \frac{u'}{Re_\tau \nu} T_\tau \tag{7.5}$$

- Computing sensed velocity, through eq. 5.8, with output voltage and the new correction temperature from eq. 7.5

[2] Sensed velocity fluctuations become smaller increasing the heat flux at the wall, i.e. the temperature difference ΔT.

Results are showed in figures 7.6 and 7.7. The velocity profile is not affected by the new correction temperature meanwhile the streamwise velocity rms shows a remarkable improving on the near wall peak, decreasing the percentage error (see figure 7.8, left one). This case is characterized by a new behavior, i.e. the rms is overestimated and not anymore underestimated. The most negative feature

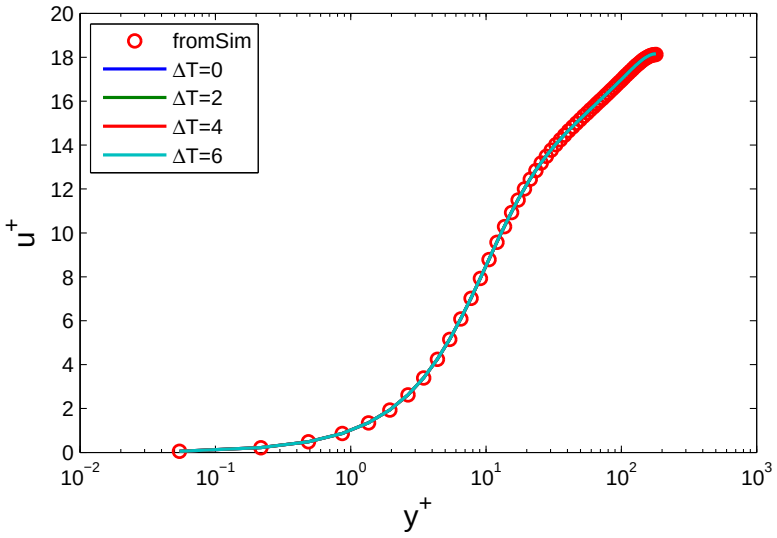

Figure 7.6: Mean velocity profile with temperature correction in equation 7.5. - Red circles, from simulation; - blue line, sensed velocity from hot wire with $\Delta T = 0$; - green line, sensed velocity from hot wire with $\Delta T = 2$; - red line, sensed velocity from hot wire with $\Delta T = 4$; - cyan line, sensed velocity from hot wire with $\Delta T = 6$

of this correction method is the increasing of the error close to the centerline, (see figure 7.8 on the right), in effect velocity and temperature are less correlated going farther from the wall, thus the idea to use velocity fluctuations instead temperature ones becomes less efficient close to the centerline. Since it is not possible to measure properly the cross moment coefficient, a linear coefficient C_L with value 0.9 at wall and 0.5 at the centerline [3], is multiplied to the fluctuation velocity term into the previous correction temperature, equation 7.5, giving the following correction temperature:

$$T_c = \overline{T} + \frac{u'}{u_\tau} T_\tau C_L = \overline{T} + \frac{u'}{Re_\tau \nu} T_\tau C_L \tag{7.6}$$

where C_L is equal to:

$$C_L = [(1 - y) \cdot 0.4] + 0.5$$

[3] These values are chosen to have an agreement with the cross moment coefficient.

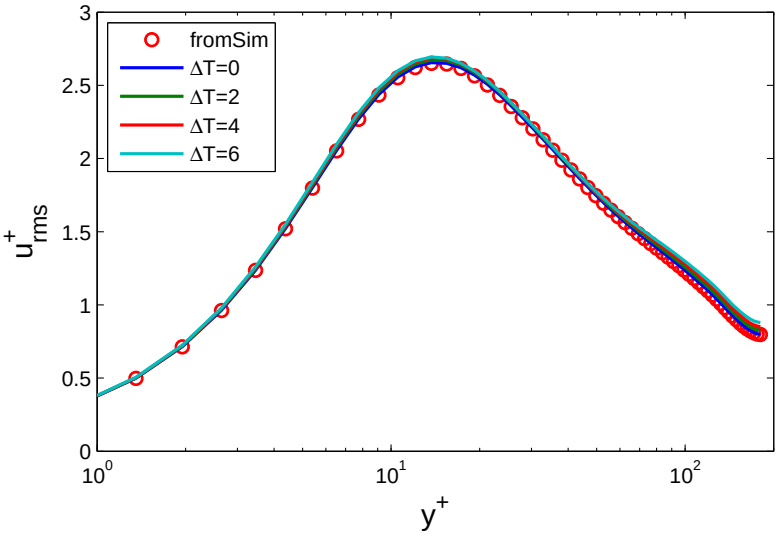

Figure 7.7: Velocity rms with temperature correction in equation 7.5. - Red circles, from simulation; - blue line, sensed velocity from hot wire with $\Delta T = 0$; - green line, sensed velocity from hot wire with $\Delta T = 2$; - red line, sensed velocity from hot wire with $\Delta T = 4$; - cyan line, sensed velocity from hot wire with $\Delta T = 6$

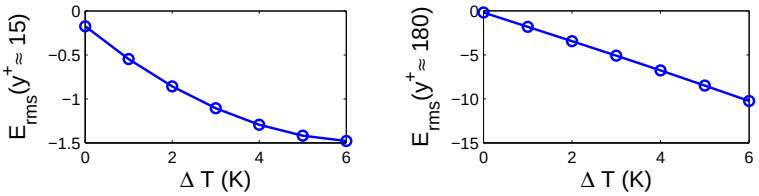

Figure 7.8: Percentage error between sensed and simulated velocity, at $y^+ = 15$ (*Left*) and at $y^+ = 180$ (*Right*)

This modification of the correction temperature gives the rms curve [4] in figure 7.9. Curves have an analogous shape, and from figure 7.10 the error behavior can be observed. Curves oscillated several times around the result for $\Delta T = 0$.

The weakness of this approach is the linear coefficient used: its validity has to be verified for other Re and Pr numbers.

[4] As for the cases before, streamwise velocity profile matches the profile from the simulation, thus it is not showed.

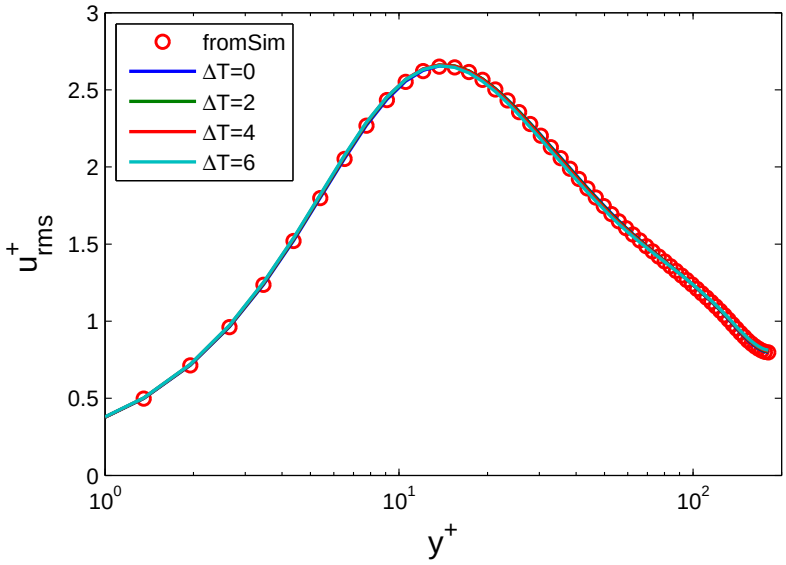

Figure 7.9: Velocity rms with temperature correction made by equation 7.6 with a linear coefficient that multiplies the fluctuating term. - Red circles, from simulation; - blue line, sensed velocity from hot wire with $\Delta T = 0$; - green line, sensed velocity from hot wire with $\Delta T = 2$; - red line, sensed velocity from hot wire with $\Delta T = 4$; - cyan line, sensed velocity from hot wire with $\Delta T = 6$

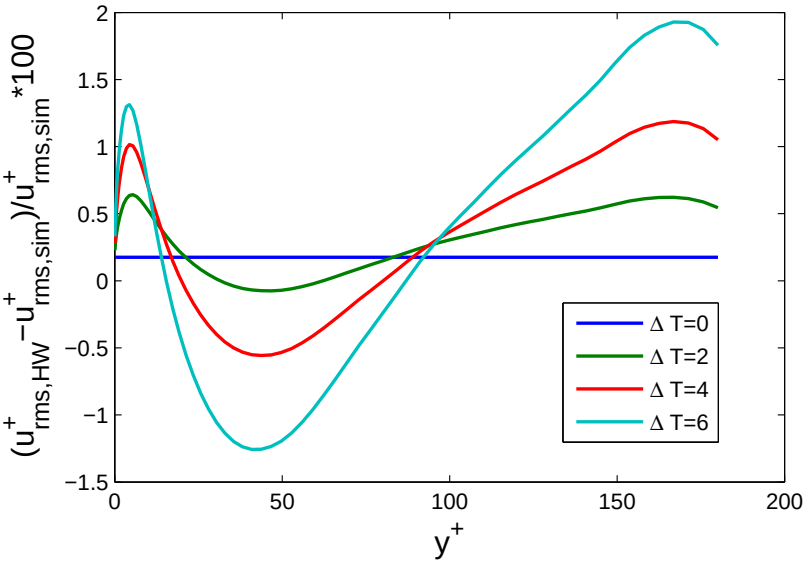

Figure 7.10: Percentage error between curves obtained in figure 7.9 and simulated curve.

7.2.1 Iteration method

An evolution on the procedure explained in the previous paragraph, is to iterate the application of the reversed King's law 5.8. In fact, what was performed in the last chapter was to guess a first velocity field correcting the temperature with the mean temperature. After that the fluctuation velocity field created was used together with the mean temperature in order to find a second velocity field, where velocity rms shows a remarkable improvement.
The new idea is to use this second velocity field to guess another velocity field, theoretically improving the convergence towards the real data.
However this analysis is not provided here.

7.2.2 Two probes method for cross moment evaluation

In this paragraph an analytical derivation for a similar term to the cross moment is provided. Here different temperature and velocity for the two probes are considered. However, mean temperature and mean velocity are equals, thus:

$$\overline{T1} = \overline{T_2} = \overline{T}$$
$$\overline{u1} = \overline{u_2} = \overline{u}$$

Starting from system 7.1, first equation can be developed as:

$$E_1^2 = A - AT_1\frac{\alpha}{a_{r,1}} + Bu_1^n - \frac{B\alpha}{a_{r,1}}u_1^nT_1 \tag{7.7}$$

Equation 7.7 is then averaged:

$$\overline{E_1^2} = A - A\overline{T}\frac{\alpha}{a_{r,1}} + B\overline{u^n} - \frac{B\alpha}{a_{r,1}}\overline{u^nT} \tag{7.8}$$

Subtracting to this equation the one constructed in the same way but referred to the second probe (thus $a_{r,2}$ instead of $a_{r,1}$), the following result is obtained:

$$\overline{E_1^2} - \overline{E_2^2} = -A\overline{T}\alpha\left(\frac{1}{a_{r,1}} - \frac{1}{a_{r,2}}\right) - B\alpha\overline{u^nT}\left(\frac{1}{a_{r,1}} - \frac{1}{a_{r,2}}\right)$$

which solved for $\overline{u^nT}$ gives:

$$\overline{u^nT} = \frac{\overline{E_2^2} - \overline{E_1^2}}{B\alpha}\left(\frac{a_{r,1}a_{r,2}}{a_{r,2} - a_{r,1}}\right) - \frac{A}{B}\overline{T} \tag{7.9}$$

The critical point is the knowledge of mean temperature value, which can be measured through the use of a thermocouple or a cold wire.

7.3 Temperature log law correction

Measure of the entire temperature profile can be an issue during experiments. Here a simplification of this measure procedure is made using the temperature log law expressed in 6.7 combined with few mean temperature measurements. However in order to get the two unknowns coefficients, κ_T and C_T, at least two mean temperature measurements are needed,in order to make solvable the following system:

$$\begin{cases} T_1^+(y_1^+) = \frac{1}{\kappa_T}\ln(y_1^+) + C_T(Pr) \\ T_2^+(y_2^+) = \frac{1}{\kappa_T}\ln(y_2^+) + C_T(Pr) \end{cases} \tag{7.10}$$

The idea is to extend the use of this formulation to a range going from the near wall peak to the centerline. This is going to cause a measurement error, but also a great reduction of experimental time needed for mean temperature profile measurement is achieved.
Two cases are analyzed now:

- Case A: Linear law from the wall to near wall peak, log law from near wall peak to centerline
- Case B: Linear law from the wall to $y^+ \approx 10$, log law from $y^+ \approx 35$ to centerline, and a fitting between these two regions made with another logarithmic profile

This means that case A needs two measurements meanwhile case B three in order to get the viscous temperature profile [5]. However another measurement, temperature at the wall, is needed if the real temperature profile is required. The mean temperature profiles obtained for the two cases are showed in figure 7.11. A general agreement between these curves and the real mean temperature profile can be observed, above all for the case B curve. Future step is to analyze the velocity profile and rms obtained with the assumptions made on mean temperature profile behavior and the errors introduced by this method.

[5] Assuming to know friction temperature T_τ.

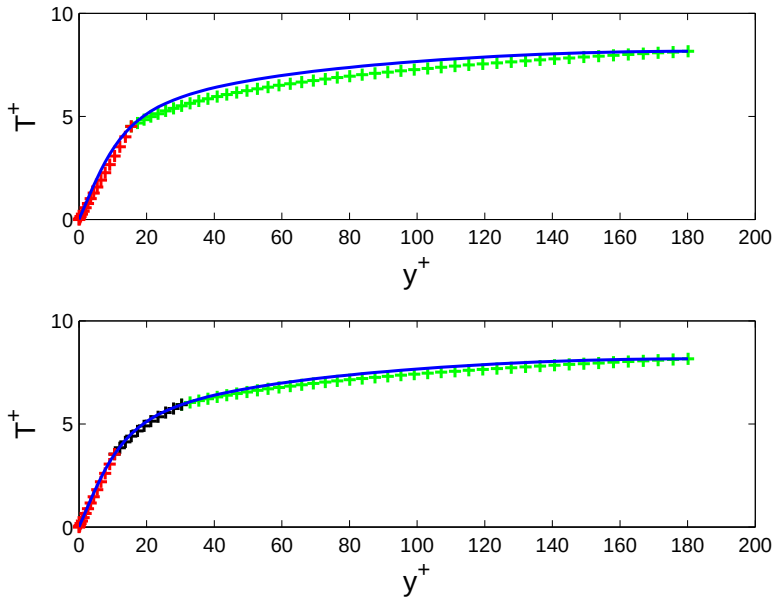

Figure 7.11: Mean temperature profiles made with linear wall law and log laws. *Up* Using three mean temperature virtual measurements; *Down* Using four mean temperature virtual measurements

Chapter 8

Channel flow at $\mathbf{Re}_\tau = 590$

This chapter focuses on the results obtained from a simulation at $Re_\tau = 590$. Similar statistics and analysis of previous case are performed.

8.1 Simulation details

Numerical simulation of a channel flow at $Re_\tau = 590$ is described in this paragraph. Parameters are fixed following the work of Moser et al. [1999] and summarized into table 8.1. No slip condition is reproduced at wall fixing the velocity boundary condition with a zero value. Temperature parameters are set as for $Re_\tau = 180$ numerical simulation, described in paragraph 5.3. Thus:

- Dirichlet b.c. at walls temperature, with a value set to 0
- $Pr = 0.71$

Numerical simulation is performed at department of Mechanics of KTH.

Direction	Box size	#Nodes/Modes	Grid spacing
x	2π	384	9.65 l^+
y	2	257	min: 0.044 l^+
z	π	384	4.83 l^+

Table 8.1: Number of nodes/modes of channel domain and spacing in viscous units $l^+ = \nu/u_\tau = Re_\tau$ since the semi channel height h is equal to 1. Note that wall normal nodes distribution is made using Chebyshev polynomial then spacing is smaller close to walls and larger far from it.

8.2 Turbulence statistics

Firstly, general turbulence statistics are showed in order to see the behavior at this Re_τ and compare the results with MKM [1]. Velocity and temperature profile are shown in figure 8.1, where it is possible to observe agreement with data from MKM for streamwise velocity profile. Velocity and temperature rms are showed

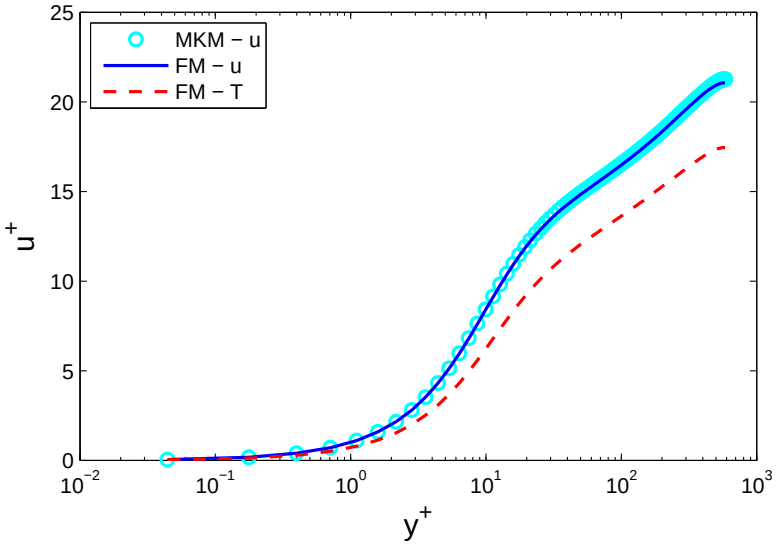

Figure 8.1: Solid blue line, mean streamwise velocity from simulation, cyan circles mean streamwise velocity from MKM, red dot line mean mean temperature

in figure 8.2. Last statistic showed in this section, see figure 8.3, is the cross moment coefficient between streamwise velocity fluctuation and temperature one, for both numerical simulation performed, i.e. $Re_\tau = 180$ and $Re_\tau = 590$. Numerical results for the simulation at higher Reynolds, shows a similar cross moment to the one at $Re_\tau = 180$. This is an useful information regarding the linear coefficient used for the correction method explained in section 7.2.

8.3 Hot wire measuring and correction

First step of this section is to evaluate the velocity measured by a hot wire using the King's law in equation 5.8 together with a mean temperature correction. Mean velocity profile, as for $Re_\tau = 180$ case, is correctly measured for each ΔT as it is shown in figure 8.4. Streamwise velocity rms, shows instead a certain displacement once ΔT is increasing, as is possible to observe in figure 8.5. This

[1] MKM is used to refer to Moser et al. [1999], meanwhile "FM" to refer to the simulation performed during this thesis work.

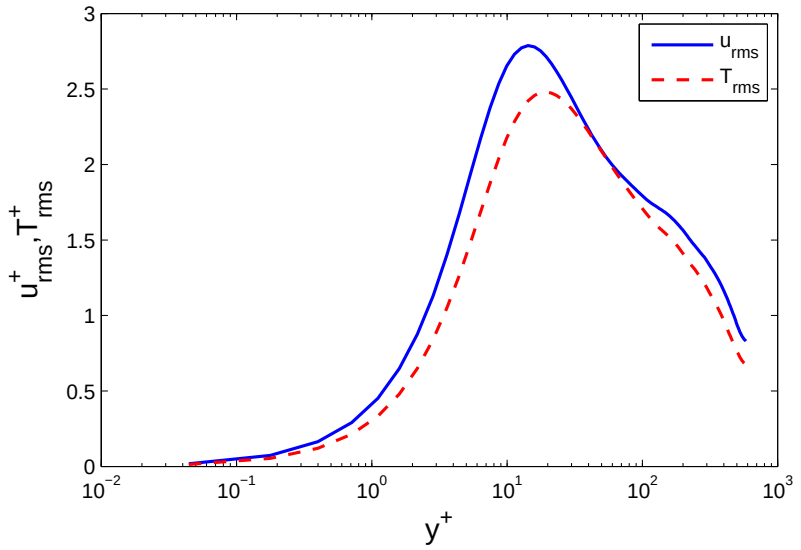

Figure 8.2: Solid blue line, mean streamwise velocity from simulation, red dot line mean mean temperature

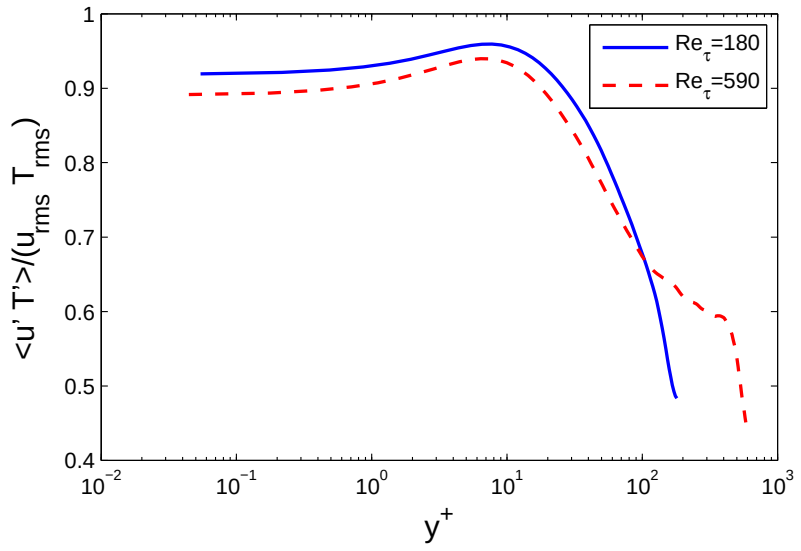

Figure 8.3: Cross moment between u' and T', not dimensionalized for velocity and temperature rms. Solid blue line is the value for numerical simulation at $Re_\tau = 180$, red dash line for $Re_\tau = 590$.

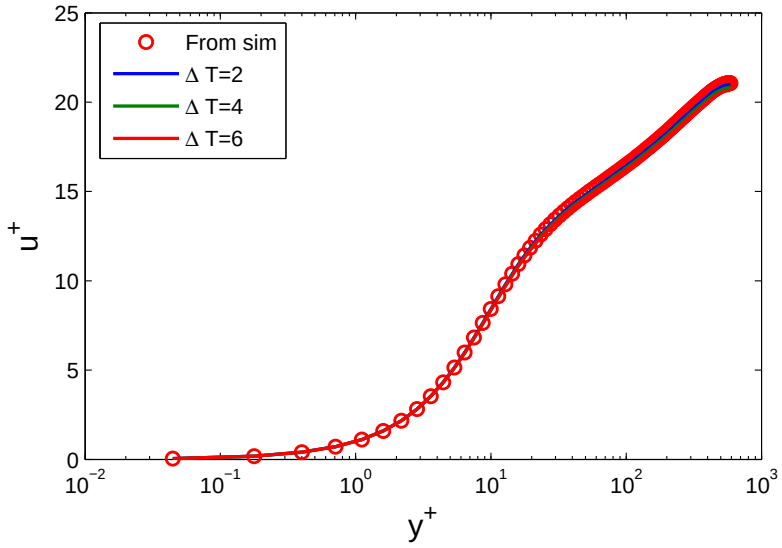

Figure 8.4: Mean streamwise velocity profile, red circles for numerical results, meanwhile blue, green and red solid lines are the sensed velocity by the virtual HW, respectively with $\Delta T = 2$, $\Delta T = 4$ and $\Delta T = 6$

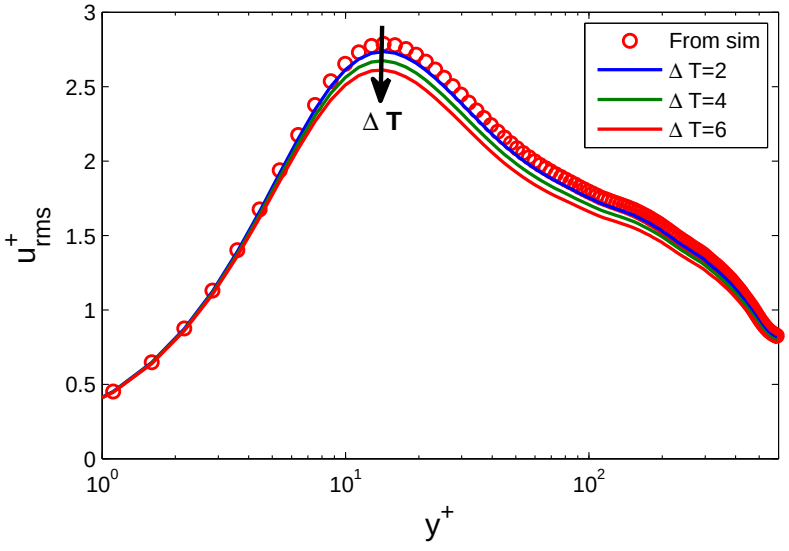

Figure 8.5: Mean streamwise velocity rms, red circles for numerical results, meanwhile blue, green and red solid lines are the sensed velocity by the virtual HW, respectively with $\Delta T = 2$, $\Delta T = 4$ and $\Delta T = 6$

result confirms the results achieved in section 6.2.2, for the homologous case at $Re_\tau = 180$, i.e. data correction performed with mean temperature introduces an error on streamwise velocity rms results.
Applying the correction expressed in equation 7.6, i.e. using a scaled velocity fluctuation and linear coefficient, errors in streamwise rms are remarkably reduced, as shown in figure 8.6, where the inner plot focuses on the error at the mean peak value for both corrections' method analyzed: blue line is the case with mean temperature correction meanwhile the green one is referred to temperature correction with equation 7.6.

Error behavior all over the curve, in figure 8.7, shows a percentage error higher

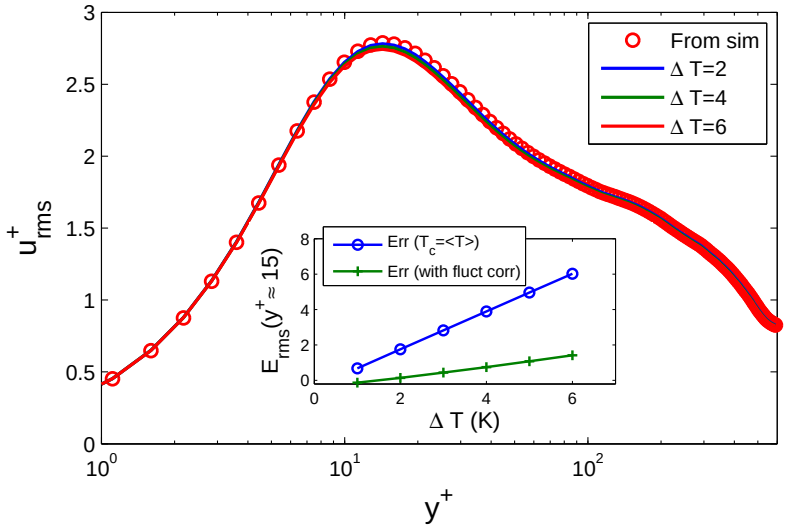

Figure 8.6: *Main* Velocity rms with temperature correction made by the summation of average temperature and scaled velocity fluctuation multiplied by a linear coefficient. - Red circles, from simulation; - blue, green and red line sensed velocity from hot wire respectively with $\Delta T = 2$, $\Delta T = 4$ and $\Delta T = 6$. *Inner* Percentage error, at $y^+ = 15$, between sensed and simulated velocity with mean temperature correction, blue line, and with equation 7.6 (green line).

close to the wall, with values bounded to an error of 0.5% for $\Delta T = 2$, of 1.5% for $\Delta T = 4$ and of 2.5% for $\Delta T = 6$.

Last analysis performed about this correction method, is spectra analysis. Measures with hot wires allows to temporal spectra analysis [2]. However, using Taylor's frozen flow hypothesis on numerical data obtained with the simulation, one dimensional streamwise spatial spectra are considered. Worst case, at $\Delta T = 6$ is considered.
Firstly is analyzed spectra close to the wall, $y^+ \approx 14.3$, see figure 8.8. Improv-

[2] Spatial spectra can be obtained using combination of hot wires

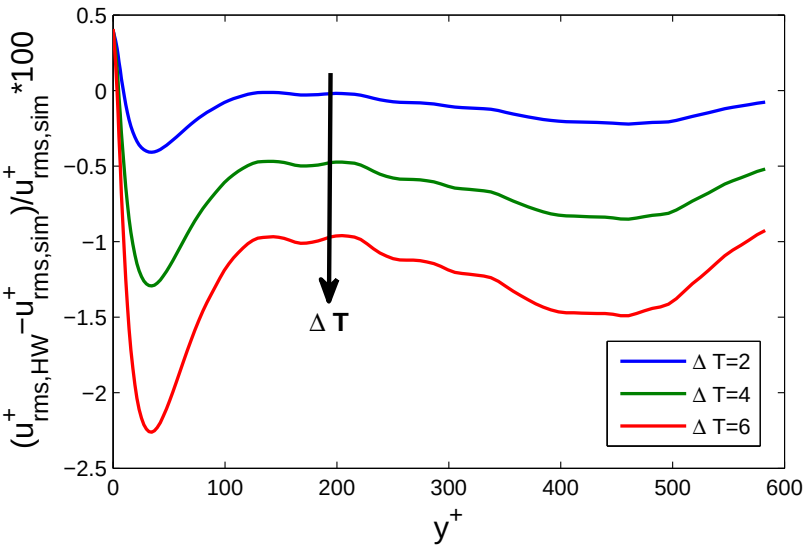

Figure 8.7: Mean streamwise velocity rms percentage error. Blue, green and red solid lines are errors between sensed velocity rms and the one from the simulation, respectively with $\Delta T = 2$, $\Delta T = 4$ and $\Delta T = 6$

ing of the error is achieved when fluctuation correction method, explained into equation 7.6, is used, as it is possible to observe in figure 8.9. Error is decreased of about three times, from around 10 - 12% for mean temperature correction case to around 0-3 % of fluctuation correction case.

Spectra far from the wall, at $y^+ \approx 99.4$, is showed in figure 8.10. Here fluctuation correction method presents a non optimal behavior. Indeed from figure 8.11 is possible to note that for small wavenumbers, fluctuation correction method improves the spectrum quality. However, for large wavenumbers an overestimation of the spectra is achieved with fluctuation correction method, meanwhile mean temperature correction shows a good agreement with the numerical data.

This is an important conclusion, since far from the wall, considering viscous units, mean temperature correction gives a good estimation of large wavenumbers energy spectra, meanwhile fluctuation correction gives better results for small ones.

Few ideas can be followed theoretically [3] to improve the results far from the wall:

- Use the iterative approach explained in section 7.2.1
- Use a different linear coefficient C_L. An idea is to split the coefficient into two curves: value from 0.9 to 0.5 in the range between zero and the

[3] Quantitative evaluation of the error estimation using these ideas is not performed yet.

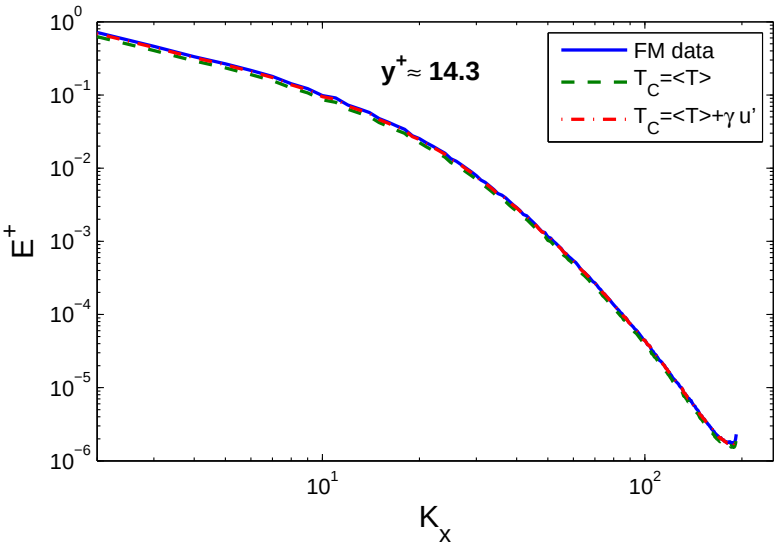

Figure 8.8: Streamwise velocity spectra on longitudinal wavenumbers for a $\Delta T = 6$. Blue solid line from numerical simulation, dash green line sensed velocity using mean temperature correction, red dash dot sensed velocity using temperature correction made with equation 7.6. $y^+ \approx 14.3$

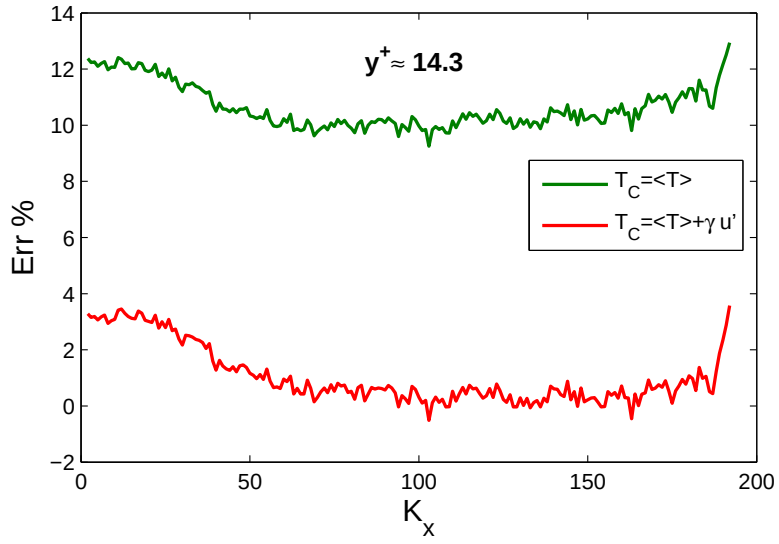

Figure 8.9: Error between longitudinal spectra of streamwise velocity between numerical simulation and sensed velocity, with $\Delta T = 6$. Green line considering mean temperature correction, red line considering temperature correction made with equation 7.6. $y^+ \approx 14.3$

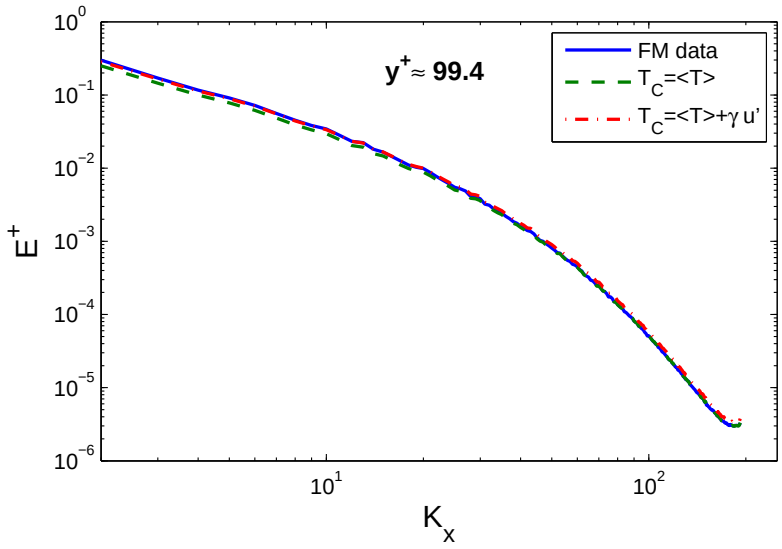

Figure 8.10: Streamwise velocity spectra on longitudinal wavenumbers for a $\Delta T = 6$. Blue solid line from numerical simulation, dash green line sensed velocity using mean temperature correction, red dash dot sensed velocity using temperature correction made with equation 7.6. $y^+ \approx 99.4$

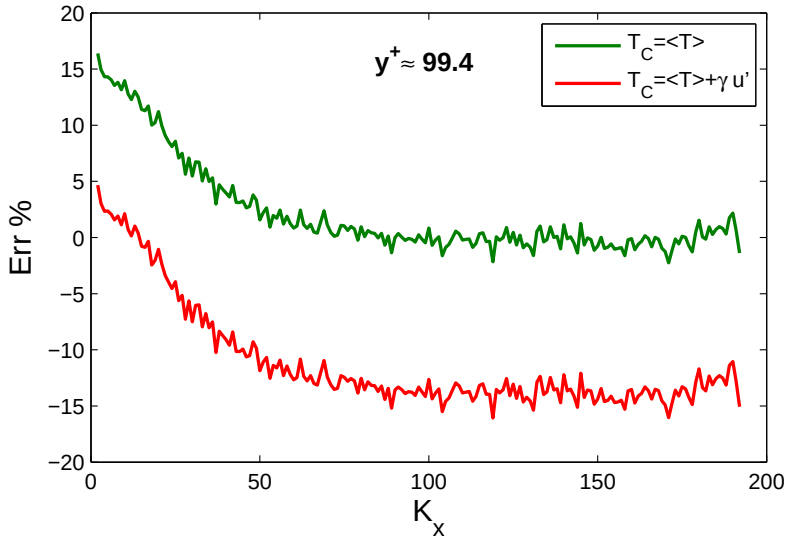

Figure 8.11: Error between longitudinal spectra of streamwise velocity between numerical simulation and sensed velocity, with $\Delta T = 6$. Green line considering mean temperature correction, red line considering temperature correction made with equation 7.6. $y^+ \approx 99.4$

beginning of the log layer; value from 0.5 to 0 in the remain range of the wall normal coordinate.

In fact, close to the wall, fluctuation correction is needed in order to improve measurements' quality and achieve correct rms and energy spectra for all wave numbers.

Chapter 9

Conclusions

Numerical simulations of a turbulent channel flow at $Re_\tau = 180$ and 590 were performed in order to evaluate temperature gradient influence on hot wire measurements. Temperature was considered as a passive scalar and its dynamic solved using a scalar equation with $Pr = 0.71$.

As a first step, temperature - velocity correlation was verified. This correlation is higher close to the wall and smaller far from it. This is an important result, since it gives a physics explanation to how the presence of a temperature gradient influences the hot wire measurements: positive fluctuations of streamwise velocities are in correspondence with positive fluctuations of temperature, which increases hot wire temperature. This yields to a less heat generated by the electrical system of hot wire to compensate the real effect of the forced convection on the wire. This means that hot wire operates underestimating flow velocity, due to temperature effect. Vice-versa, negative streamwise velocity fluctuation transports negative temperature fluctuations: wire temperature becomes smaller than the one expected considering the only forced convection on the wire. In this case, streamwise velocity is overestimated: summarizing, sensed streamwise velocity fluctuations by the hot wire are damped down due to temperature influence.

Hot wire measurement was reproduced from numerical data applying two versions of King's law, which provide same results if properly related. These equations were applied together to real streamwise velocity and real temperature from the numerical simulation to firstly estimate hot wire voltage output. From this value, it is possible to measure streamwise velocity reverting the King's law and using the voltage computed and a proper temperature correction: in fact experimentally is not possible to have an instantaneous measure of the temperature. In the first case centerline temperature was chosen, meanwhile in the second case mean temperature for each wall normal position was set.

The first temperature correction used shows different kind of errors, mainly due to a wrong mean streamwise velocity profile sensed above all close to the wall, where difference between real temperature and centerline correction temperature is highest. This generates a wrong friction velocity sensed which effects the Re_τ measured. A strong underestimation of the root mean square is achieved, which increases for higher temperature difference between wall and centerline, ΔT, or equivalently for higher temperature gradient at the wall.
The second case, i.e. mean temperature profile used as correction temperature, is characterized by a perfect match of mean streamwise velocity profile for any ΔT. However, root mean square is underestimated above all close to the wall peak value. This error increases for larger ΔT. All the following analysis were performed using this method.
King's law experimental coefficients are swept into a range of values in order to observe their effect on the sensed velocity: increasing the overheat ratio, streamwise velocity rms increases, meanwhile increasing the temperature coefficient of resistivity streamwise velocity rms is decreasing. Mean streamwise velocity profile is not affected by their value.
The next step was to compare temperature effect with the most known problem in hot wire measurements: spatial averaging. Firstly only the spatial average effect was considered: increasing the wire's length, small scale turbulence is filtered. This leads to an underestimation of the root mean square. Combining the two measurement's errors, it is possible to note that temperature influence gives a not negligible contribution to the total error when small wires are considered and mainly if high temperature difference between wall and centerline is present inside the flow. For instance, with ΔT =2 and wire length $L^+ \approx$20, temperature influence error is around 20% of the total error at the near wall peak.
Estimation of temperature influence's error, allows to formulate some correction methods, in order to generate the correct streamwise velocity root mean square starting from the one affected by temperature gradient.
The first method proposed is the two probes method: measuring flow velocity with two probes with a different overheat ratio and placed at different span positions, it is theoretically possible to know instantaneously temperature and velocity. However the results achieved are perfect only with a zero distance between the probes, meanwhile the error quickly increases for larger span displacement.
The second method has been developed using the high streamwise velocity - temperature correlation result: the idea is to use streamwise velocity fluctuations instead of temperature ones, inside the instantaneous temperature correction, i.e. the temperature correction inside the King's law equation is made up the

sum of mean temperature and a proper scaled velocity fluctuation. Best results are achieved scaling the velocity fluctuation with friction temperature and friction velocity, and multiplying the modified temperature fluctuation with a linear coefficient which decreases its value going farther from the wall, since a smaller velocity - temperature correlation is present far from the wall. The velocity fluctuations were measured by a first iteration using mean temperature profile as correction temperature.

The aim of the last method proposed is to estimate the mean temperature profile using only few temperature measurements, and interpolating the points obtained with a linear law close to the wall and the logarithmic law in the rest of the domain. The temperature profile obtained is similar to the real one. However some errors can be introduced for the measuring of the friction temperature.

All these results were obtained considering a numerical simulation at $Re_\tau = 180$, but same results are achieved considering a $Re_\tau = 590$ channel flow numerical simulation, which is described in the last chapter. Temperature fluctuation correction method is also verified and an improvement of this method is proposed.

Acknowledgments

First of all I would like to thank my Italian supervisor, Prof. A. Talamelli, who gave me the opportunity to perform this master thesis both at the University of Bologna and at the Department of Mechanics of KTH, Stockholm. Moreover he introduced me into the field of fluid mechanics and supported me during this work. He also showed a lot of courage to accept my request to participate to the exchange program LLP/Erasmus at KTH in 2010 [1].
Moreover I would like to thank Dr. R. Örlü and Dr. P. Schlatter for guiding my work at KTH and giving me answers and suggestions about the issues I encountered during my Swedish period of the thesis and also for giving me the opportunity to publish a proceedings of my work.
Last but not the least, I would like to express my sincere gratitude to Dr. A. Cimarelli, for his useful and stimulating comments and suggestions about this thesis and mainly because he manages to transfer his passion for science and turbulence to me.

Moreover I would like to acknowledge all the people that help me directly and not directly during these months of my work. At the department of Mechanics, Enrico and Onofrio were really patience, helping me with the code and giving answers to my silly questions. I hoped that they liked the way I thanked them, i.e. paying them by nature, with "Focaccia" (nothing ambiguous, I just baked a total amount of around 22 kg of flour in 5 months!!!). Moreover, I am waiting the answer of Onofrio about to the proposal of open a "rosticceria": just say where and when!!!.

[1] A funny story happen in 2010, during the course of "Experimental Aerodynamic". The group I was working with, sent him the final report about our project work; Talamelli replied us in English by email: "Dear students, except for some English mistakes [...] the report is fine.". With my wonderful English, I replied him: "[...] We are pleased that you enjoyed our relationship. [...]". The problem is that in Italian there is just one word for report and relationship: "Relazione", and even if I wrote firstly report, when I checked on google translator I modified the word in relationship. Prof. Talamelli accepted two months later my request to participate to the exchange program LLP/Erasmus at KTH. I still thank him for the courage he showed to let me go there!

Talking about Focaccia how I could not cite my colleague Stefano, for all the fruitful discussion (starting from heat transfer and ending up with eat transfer), and also all the other Italians at KTH, Marco (who replied to my email during his USA journey, only for this he deserves all the best), Luca Bi., Nicolò, Francesco, Gaetano, Antonio and Prof. Luca Brandt: it was nice enjoy coffee breaks (in Swedish "fika") and playing football with you.
I do not have so much space left but I want also to thank my office colleagues, Naser, Jyothish, Yuli and Yue; Carolina and Hanno who tried to teach me some Swedish words during lunchtime, unfortunately without so many results; Armin, Iman, Nima and all the others people in the department.
Out of the department, special thanks go to Matt for his friendship, Laura for hes cheering up, my dancing class, my running group "Runday", my corridormates, LBG Stockholm and all the people I met and I spent nice time with: you made my exchange period.
At the end of Stockholm side, I want also to thank the people I met during my previous exchange, firstly all the lovely people I was lucky to meet in my corridor: DKV 73, second floor is going to be always in my hearth; after that all the others people I met: it is a long list and I hope you will be not angry with me if I do not it write here.

Italian side Innanzitutto voglio ringraziare i Caterina Sforza 41 boys, Adriano e Fabione, abbiamo trascorso dei gran anni all together e spero che la nostra amicizia rimanga uno dei capisaldi della nostra vita: sia per quanto riguarda i momenti di felicità che condivideremo ancora insieme, sia come porto sicuro per i momenti meno belli della vita, un molo dal quale ripartire con rinnovata forza. Vi ho dedicato poche righe ma con il cuore.
A Forlì ho avuto poi la fortuna di incontrare molte altre persone fantastiche, dai ragazzi di via Merenda, alla Miss, Clara, Veronica Whitewool, dalle persone con cui ho condiviso pranzi della domenica, della modica durata di 10 ore, e cene, di non molta inferiore durata, fino a tutti quelli con cui ho trascorso dei piacevoli momenti.
Certo che poi questi anni non sarebbero stati lo stesso senza tutti i miei colleghi. Ricordarsi tutte le cose che abbiamo fatto e scriverle in poche righe non è facile. Esenzialmente, spero che non mi odiate per tutte le volte che parlavo troppo!!!. Con un po' di tristezza nel non poter citare tutti voi spero che possiate perdonare questa mia piccola lista: Ale Esty, Ale Romolo, Ale Zarco, Ale New Jersey Roberto, Ale Epson Paolo, Daniele (mi dispiace sei ancora matricola), Maria Pia, Eurosia, Alberto, i miei nuovi coinquilini e tutti, tutti gli altri.
A San Benedetto, dove ho trascorso gran parte della mia vita, ho avuto anche li la fortuna di avere dei grandi amici... con il tempo son diminuiti un poco

ma spero di poter sempre contare su tutti gli altri, nonostante la vita mi abbia portato spesso ad esser via da li e forse continuerà a farlo. Il primo nome è senza dubbio Marco, so che ci sarai sempre, sei un amico anche se hai il tuo caratterino e hai un po' la testa fra le nuvole, daje Roma. Poi Elena, Alessandro, Simone, Serena, Marino, Cristian e Mark... quasi tutti che bazzicavamo il campo di atletica, che nel bene o nel male è stata la nostra culla di gioventù. Spero che si riesca a rimanere tutti uniti nonostante tutti noi abbiamo caratteri diversi e a volte non si riesce ad esser d'accordo su tutto. Poi vorrei ringraziare Cristina per la nostra amicizia, che sebbene perda punti per non esser qui alla mia laurea li recupererà per ospitarmi alle Canarie fra qualche giorno. Grazie anche a Maria Elena, per le nostre chiacchierate vicino ad una tazza di thé.
Per tutti coloro che mi son scordato perché fra qualche minuto devo mandare in stampa la tesi e a causa del mio cervello in rottamazione, vi ringrazio.

Infine vorrei ringraziare la mia famiglia, per aver fatto sacrifici per permettermi di esser qui a scrivere queste pagine di tesi, per essersi dimenticati di cosa significa la parola vacanza per dare l'opportunità a me di farne, per aver sopportato i miei sfoghi dovuti alla tensione pre-esami e per la tristezza dovuta alla nostalgia. Grazie Ivo, grazie Marcella.
Grazie poi a mio fratello Raniero e a sua moglie Antonella, per i consigli di vita che mi son stati dati e per essermi stati vicini nei momenti di bisogno.
Grazie a mia zia Lia, perché anche se sei un po' strana alla fine mi vuoi bene, grazie poi ai miei nonni, sia quelli che sfortunatamente non ci son più e sia a nonna Anita, perché so che tutti mi avete voluto e vorrete bene; ed infine grazie a tutti gli altri familiari.

Bibliography

J. D. Anderson. *A History of Aerodynamics: And Its Impact on Flying Machines*. Cambridge University Press, 1999.

G.K. Batchelor. *The theory of homogeneous turbulence*. Cambridge University Press, 1959.

U. Bordoni. Un procedimento per la misura della velocità dei gas. *Il nuovo Cimento*, 6:241–283, 1912.

J.N. Bracewell. *The Fourier transform and its applications*. McGraw-Hill, 2000.

P. Bradshaw and G. P. Huang. The law of the wall in turbulent flow. In *Proceedings: Mathematical and Physical Sciences*, volume 451, pages 165–188, 1995.

H. H. Bruun. On the temperature dependence of constant temperature hotwire probes with small wire aspect ratio. *J. Phys. E: Sci. Instrum.*, 8(942), 1975.

H.H. Bruun. *Hot Wire Anemometry-Principal and Signal Analysis*. Oxford University Press, 1995.

S. Carnot. Réflexions sur la puissance motrice du feu et sur les machines propres à développer cette puissance. In *Annales scientifiques de l'É.N.S.*, volume I of *2*, pages 393–457. 1872.

Mattias Chevalier, Philipp Schlatter, Anders Lundbladh, and Dan S. Henningson. Simson : A pseudo-spectral solver for incompressible boundary layer flows. Technical Report 2007:07, KTH, Mechanics, 2007. QC 20120306.

C.C. Chin, N. Hutchins, A.S.H. Ooi, and I. Marusic. Use of direct numerical simulation (dns) data to investigate spatial resolution issues in measurements of wall-bounded turbulence. *Meas. Sci. Technol.*, 20:115401, 2009.

C.C. Chin, N. Hutchins, A.S.H. Ooi, and I. Marusic. Spatial resolution correction for hot-wire anemometry in wall turbulence. *Exp. Fluids*, 50:1443–1453, 2011. Issue 5.

R. Clausius. Ueber die bewegende kraft der wärme und die gesetze, welche sich daraus für die wärmelehre selbst ableiten lassen. *Annalen der Physik*, 79:368–397, 500–524, 1850. Translated work: R. Clausius, *On the Moving Force of Heat, and the Laws regardingthe Nature of Heat itself which are deducible therefrom*, London, Edinburgh and Dublin Philosophical Magazine and Journal of Science. 4th 2 (VIII): 1-21; 102-119 (July 1851).

R. Clausius. Ueber eine veränderte form des zweiten hauptsatzes der mechanischen wärmetheoriein. *Annalen der Physik und Chemie, 93*, 12:481–506, 1854. Translated work: R. Clausius, *On a Modified Form of the Second Fundamental Theorem in the Mechanical Theory of Heat*, Philos. Mag. 4 12 (77): 81-98 (1856).

Juan C. del Alamo and J. Jimenez. Direct numerical simulation of the very large anisotropic scales in a turbulent channel. Annual research briefs., Center for Turbulence Research, Stanford University, 2001.

A. Van Dijk and F.T.M. Nieuwstadt. The calibration of (multi-)hot-wire probes. 1. velocity-calibration. *Experiments in Fluids*, 36:550–564, 2004. Issue 4.

H.L. Dryden, G.B. Schubauer, W.C.Jr. Mock, and H.K. Skramstad. Measurements of intensity and scale of wind tunnel turbulence and their relation to the critical reynolds number of spheres. Technical report, National advisory committee for aeronautics, 1936.

J.S. Dugdale. *Entropy and its physical meaning.* Taylor & Francis Group, 1996.

E. Fermi. *Thermodynamics.* Courier Dover Publications, 1956.

M. Ferro. Experimental study on turbulent pipe flow. Master's thesis, KTH, Mechanics, Stockholm, 2012.

R.P. Feynman, B.R. Leighton, and M. Sands. *The Feynman Lectures on Physics.* Addison-Wesley, 1966.

J.B.J. Fourier. Mémoire sur la propagation de la chaleur dans les corps solides. In *Nouveau Bulletin des sciences par la Société philomatique de Paris*, pages 112–116. 1808.

F.N. Frenkiel. The influence of length of a hot wire on the measurements of turbulence. *Phys. Rev.*, 75(8):1263–1264, 1949.

J.O. Hinze. *Turbulence.* McGraw-Hill, 1975.

N. Hutchins, I. Marusic, M.S. Chong, and T.B. Nickels. Hot-wire spatial resolution issues in wall-bounded turbulence. *J. Fluid Mech.*, 635:103–136, 2009.

A.V. Johansson and P.H. Alfredsson. Effects of imperfect spatial resolution on measurements of wall-bounded turbulent shear flows. *Journal of Fluid Mechanics*, 137:409–421, 1983.

R. W. Johnson. *The Handbook Fluid Dynamics*. Springer, 1998.

B. A. Kader and A. Yaglom. Heat and mass transfer laws for fully turbulent wall flows. *International Journal of Heat and Mass Transfer*, 15(12):2329–2351, 1972.

T. V. Von Karman. Mechanical similitude and turbulence. NACA Technical Memorandum 611, NASA, Washington, 1931.

J.M. Kay and R.M. Nedderman. *An Introduction to Fluid Mechanics and Heat Transfer*. Cambridge university press, 3rd edition, 1974.

W. Thomson (Lord Kelvin). On the dynamical theory of heat, with numerical results deduced from mr joule's equivalent of a thermal unit, and m. regnault's observations on steam. *Transactions of the Royal Society of Edinburgh*, XX (part 2):261–268, 289–298, 1851. Or also published at: W. Thomson, *On the Dynamical Theory of Heat, with numerical results deduced from Mr Joule's equivalent of a Thermal Unit, and M. Regnault's Observations on Steam* Philos. Mag. 4 IV (22): 8-21 (December 1852).

A.E. Kennelly, C.A. Wright, and J.S. Van Bylevelt. The convection of heat from small copper wires. *Trans. A.I.E.E.*, 28:363–396, 1909.

J. Kim, P. Moin, and R. Moser. Turbulence statistics in fully developed channel flow at low reynolds number. *J. Fluid Mech*, 177:133–166, 1987.

L.V. King. On the convection of heat from small cylinders in a stream of fluid: determination of the convection constants of small platinum wires with applications to hot wire anemometry. *Phil. Trans. Roy. Soc.*, 214:373–432, 1914.

L.V. King. On the precision measurement of air velocity by means of the linear hot-wire anemometer. *Phil. Mag.*, 29(172):566–577, 1915.

B. Kirby. *Micro- and Nanoscale Fluid Mechanics, Transport in Microfluidic Devices*. Cornell Unuversity, New York, 2010.

A.N. Kolmogorov. The local structure of turbulence in incompressible viscous fluid for very large reynolds numbers. volume 434 of *A*, pages 9–13, London, 1991. Translation.

P.M. Ligrani and P. Bradshaw. Spatial resolution and measurement of turbulence in the viscous sublayer using subminiature hot-wire probes. *Experiments in Fluids*, 5(6):407–417, 1987.

E.N. Lorenz. Deterministic nonperiodic flow. *Journal of the Atmospheric Sciences*, 20:130–141, 1973.

P.A. Monkewitz, K.A. Chauhan, and H.M. Nagib. Comparison of mean flow similarity laws in zero pressure gradient turbulent boundary layers. *Physics of fluids*, 20:105102, 2008.

J.T. Morris. The electrical measurement of wind velocity. *Engineering*, 94: 892–894, 1912.

R.D. Moser, J. Kim, and N.N. Mansour. Dns of turbulent channel flow up to $re_\tau = 590$. *Phys. Fluids*, 11:943–945, 1999.

R. Örlü. *Experimental studies in jet flows and zero pressure-gradient turbulent boundary layers*. PhD thesis, KTH mechanics, Stockholm, Sweden, 2009.

S.B. Pope. *Turbulent Flows*. Cambridge University press, 2000.

L. Prandtl. Bericht über untersuchungen zur ausgebildeten turbulenz. *Z. Angew. Math, Meth.*, 5:136–139, 1925.

O. Reynolds. An experimental investigation of the circumstances which determine whether the motion of water shall be direct or sinuous, and of the law of resistance in parallel channels. *Philosophical Transactions of the Royal Society*, 174:935–982, 1883.

O. Reynolds. *Papers on mechanical and physical subjects-the sub-mechanics of the Universe*, volume III. Cambridge University Press, 1903. Collected work.

L.F. Richardson. *Weather prediction by numerical process*. Cambridge University press, 1922.

I.A. Richter. *The notebooks of Leonardo da Vinci*. Oxford University Press, USA, 1883. ed.1999.

S. S. Sattarzadeh, M. Ferro, R. Örlü, and P. H. Alfredsson. Revisiting the near-wall scaling of streamwise variance in turbulent pipe flows. In *Progress in turbulence V, Proc. iTi Conf. Turbulence*, Bertinoro (Italy), 2013.

A. Segalini, A. Cimarelli, J.D. Ruedi, E. De Angelis, and A. Talamelli. Effect of the spatial filtering and alignment error of hot-wire probes in a wall-bounded turbulent flow. *Measurements Science and Technology*, 22:105408, 2011a.

A. Segalini, R. Örlü, P. Schlatter, P.H. Alfredsson, J.D. Rüedi, and A. Talamelli. A method to estimate turbulence intensity and transverse taylor microscale in turbulent flows from spatially averaged hot-wire data. *Exp.Fluids*, 51:693–700, 2011b.

A.J. Smits, J. Monty, M. Hultmark, S.C.C. Bailey, N. Hutchins, and I. Marusic. Spatial resolution correction for wall-bounded turbulence measurements. *J. Fluid Mech.*, 676:41–53, 2011.

A. Sommerfeld. Ein beitrag zur hydrodynamischen erklärung der turbulenten flüssigkeitsbewegung. In *Proceedings of the 4th International Congress of Mathematicians*, volume III, pages 116–124, Rome, 1908.

Alessandro Talamelli, Franco Persiani, Jens H. M. Fransson, P. Henrik Alfredsson, Arne V. Johansson, Hassan M. Nagib, Jean-Daniel Rueedi, Katepalli R. Sreenivasan, and Peter A. Monkewitz. CICLoPE-a response to the need for high Reynolds number experiments. *Fluid Dynamics Research*, 41, 2009.

G.I. Taylor. Statistical theory of turbulence. volume 151 of *A*, pages 421–444, 1935.

G.I. Taylor. The spectrum of turbulence. volume 164 of *A*, pages 476–490, 1938.

H. Tennekes and J.K. Lumley. *A First Course in Turbulence*. MIT Press, 1972.

R. Verzicco. Appunti di turbolenza. 2002.

S. Zuccher. Note di fluidodinamica. 2012.